Politecnico
di Torino

Politecnico di Torino

Master of Science in Aerospace Engineering

Master's Degree Thesis

Random Vibration Fatigue

Abaqus plug-in tool based on spectral methods

Supervisor:
Marco Gherlone

Candidate:
Moreno Dal Borgo

Co-Tutors:
Zuheir Barsoum
Fredrik Ivarsson

October 2024

Random Vibration Fatigue

Abaqus Plug-in tool based on Spectral Methods

MORENO DAL BORGO

Date: October 2024

Supervisors: Zuheir Barsoum, Fredrik Ivarsson, Marco Gherlone
Examiner: Zuheir Barsoum
School of Engineering Sciences
Host company: Sigma Industry Development AB

Abstract

Fatigue life calculation is crucial for those structures that are applied into a severe dynamic environment, also characterized by high level of randomness. Some commercial software, as Ansys and Comsol, have already built-in tools for random vibration fatigue calculation but Abaqus CAE does not. Hence, this thesis fills this gap, developing a plug-in tool integrated into Abaqus CAE to perform multi-axial fatigue analysis of metal components subjected to random vibration loading.

Since this loading is characteristic of high cycle fatigue, first a random stress analysis is perform in Abaqus CAE and then the tool is applied as a post-processor. The literary review suggests some frequency domain methods extremely more efficient compared to time-domain approaches. Thus, they are implemented by Python scripting and incorporated into an Abaqus's Graphic User Interface.

The tool, which can be applied to study random vibration with Gaussian distribution and zero mean, was first validated studying a simple L-plate. The hotspot identification and the maximum damage accumulated were compared against the results obtained with the commercial software Simulia Fe-Safe. Then, a real application case was analyzed and the fatigue effect of the background random vibrations were studied for a cable connectors bracket mounted on a helicopter. Satisfying results were obtained for both cases and they allowed to explore the accuracy and limitations of the tool developed.

Moreover, the study permitted to give some suggestion of future works on this field which include non-isotropic materials, critical plane methods, transient random vibration loading and non-Gaussian processes.

The tool showed promising results on the hot-spot identification and damage calculation especially for in-phase loading. Hence, it can be an useful tool for the analysis of random vibration fatigue in Abaqus CAE but further improvements are required in case of out-of-phase loading.

Keywords

Abaqus, Fatigue, Random Vibrations, Python, Spectral Methods

Sommario

Il calcolo della vita a fatica è cruciale per quelle struttire che si trovano a operare in ambienti dinamici severi, sopprattutto se cratterizzati da sollecitazioni casuali. Alcuni software commerciali, come Ansys e Comsol, possiedono già dei specifici tool per il calcolo della vita a fatica dovuta alle vibrazioni random. Tuttavia, Abaqus CAE ne è spovvisto. Questa tesi cerca quindi di colmare questa mancanza, sviluppando un tool, integarto in Abaqus CAE, che fornisca analisi a fatica multiassiali, per componenti metallici soggetti a vibrazioni random. Questo tipo di sollecitazione è tipico della fatica ad alto numero di cicli e quindi, inizialmente, un' analisi degli stress random viene eseguita in Abaqus CAE. Successivamente il tool viene utilizzato per post-processare gli stress ricavati. L'analisi letteraria ha suggerito alcuni metodi nel dominio delle frequenze necessari al calcolo del danno accumulato. Questi metodi sono stati implementati nel tool per mezzo di codici Python e poi incorporati all'interno dell'interfaccia grafica di Abaqus.

Il tool, applicato allo studio di vibrazioni random con distribuzione gaussiana e media nulla, è statao inizialmente validato studuiando una pista ad L. L'identificazione dell' hot-spot ed il massimo danno accumulato sono stati quindi confrontati con i risultati ottenuti tramite il software commerciale Simulia Fe-Safe. In fine, un'applicazione reale è satata analizzata. In particolare, gli effetti della fatica, dovuta alle vibrazini random di fondo, sono stati studati per un supporto montato su un elicottero. Soddisfacenti risultati sono stati ottenuti per entrambi i casi e hanno permesso quindi di studiare l'accuratezza e le limitazioni del tool.

Lo studio ha permesso poi di fornire alcuni suggerimenti per lavori futuri in questo campo. Questi spaziano dai materiali non isotropici ai metodi basati sul piano critico oppure dalle vibrazioni random transitirie ai processi non Gaussiani.

Per qaunto riguarda l'identificazione dell' hot-spot ed il calcolo del danno, il tool sviluppato ha mostrato risultati promettenti, specialmente nel caso di sollecitazioni in fase. Si dimostra quindi essere uno strumento utile per l'analisi della vita a fatica con l'impiego di Abaqus CAE. Tuttavia, esso necessita di ulteriori miglioramenti per lo studio di sollecitazioni fuori fase.

Parole chiave

Abaqus, Fatica, Vibrazioni Random, Python, Metodi Spettrali

Acknowledgments

This report is a master thesis in structural dynamics and fatigue as final project of Master of Science in Aerospace engineering at Politecnico di Torino. The master thesis, through the Erasmus+ program at KTH Royal Institute of Technology, has been executed at Sigma Industry Development AB in Stockholm from January to August 2024.

I would like to thank my academic supervisor and examiner at KTH, Zuheir Barsoum, for his fundamental guidance during the project. His expertise and constructive feedback were invaluable.

I also wish to acknowledge my supervisor at Sigma, Fredrik Ivarsson, and all the calculation team for the opportunity and the experience. It has significantly contributed to my professional growth.

I am also grateful to my academic advisor at Politecnico di Torino, Marco Gherlone, for his generous support.

And at last a great thanks to my family, relatives and friends who always supported and encouraged me during the years. Your belief in me has been precious.

Stockholm, October 2024
Moreno Dal Borgo

Contents

1 Introduction **1**
1.1 Context . . . 3
1.2 Purpose and Goals . . . 7
1.3 Delimitations . . . 8
1.4 Structure of the thesis . . . 9

2 Background **11**
2.1 Random processes . . . 11
2.1.1 Random Vibration Properties in the Frequency Domain 16
2.1.2 Statistical properties of random process . . . 22
2.2 Finite Element Model . . . 28
2.2.1 Modal Analysis . . . 31
2.2.2 Dynamic Analysis for random vibrations . . . 33
2.2.2.1 Frequency Response Functions . . . 34
2.2.2.2 Random Analysis . . . 35
2.3 Multi-axial Criteria for Fatigue Analysis . . . 35
2.3.1 Fatigue-limit criteria . . . 37
2.3.1.1 Equivalent Von Mieses . . . 37
2.3.1.2 Equivalent Lemaitre . . . 38
2.3.2 Infinite-life criteria . . . 40
2.3.3 Sterss-invariant criteria . . . 40
2.3.3.1 Projection by Projection . . . 42
2.3.3.2 Crossland . . . 44
2.3.3.3 Matsubara . . . 45
2.3.3.4 Sines . . . 47
2.3.4 Critical plane criteria . . . 49
2.3.4.1 Matake . . . 50
2.3.4.2 Carpinteri-Spagnoli . . . 51
2.4 Rain-flow counting and Probability Density Function . . . 53

2.4.1 Rainflow counting method . . . 54
2.4.2 Narrow-band method . . . 56
2.4.3 Wide-band methods . . . 57
2.4.3.1 Dirlik method . . . 57
2.4.3.2 Tovo-Benasciutti method . . . 59
2.5 Material Properties and S-N curve . . . 60
2.5.1 Modified S-N curve . . . 62

3 Method 65
3.1 Abaqus CAE . . . 65
3.2 Analysis with Fe-Safe . . . 66
3.3 Analysis with Abaqus CAE Plug-in tool . . . 67
3.3.1 Abaqus CAE RSG . . . 69
3.3.2 Fatigue plug-in tool . . . 70

4 Application 81
4.1 Case study I: L-plate . . . 81
4.2 Case study II: Bracket . . . 84

5 Results 89
5.1 Comparison between the Fatigue Tool and Fe-Safe . . . 89
5.1.1 L-Plate . . . 89
5.1.2 Bracket . . . 101

6 Discussions 105
6.1 Conclusions . . . 105
6.2 Future works . . . 107

References 109

A Supporting material 115
A.1 Gaussian and Rayleigh distribution . . . 115
A.2 Auto-correlation and Cross-correlation functions . . . 115
A.3 Power spectral density . . . 117
A.4 Wiener-Khinchine relations . . . 118
A.5 Transfer functions . . . 119

List of Figures

1.1 Fatigue within the product development process 2
1.2 Classification of deterministic and random processes [1] . . . 3
1.3 Time domain approach[2] 5
1.4 Frequency domain approaches [2] 5

2.1 Sample of random process [19] 12
2.2 Probability densities with non-zero skewness [19] 13
2.3 Kurtosis influence on probability density [19] 14
2.4 Examples of autocorrelation functions [19] 14
2.5 Example of Sine signal at 3 Hz 16
2.6 Examples of sum of Sine signals at 3 Hz and 5 Hz. First one with in-phase signals and second one with $45°$ of phase shift . 16
2.7 Example of random signal 17
2.8 Examples of Power Spectral Density (PSD) and Cross-Spectral Density (CSD) of the signals in Fig. 2.5, 2.6 and 2.7 21
2.9 Probability distribution of peaks by varying the regularity factor r [21] 27
2.10 Transfer Function 34
2.11 Representation of the safe and unsafe regions for the safe-life criteria 41
2.12 Example of random loading path Ψ in two-dimensional deviatoric space and its projections Ψ_1 and Ψ_2 [7] 43
2.13 Example of Minimum Circumscribed Circle (MCC) and Minimum Circumscribed Ellipse (MCE) definitions for a random loading path. The Expected Minimum Circumscribed Circle (EMCC) and Expected Minimum Circumscribed Ellipse (EMCE) refer to the statistical definition in the frequency domain [28] 45

2.14 Critical plane definition for the Carpinteri-Spagnoli criterion [29] . . . 52
2.15 Examples of rain-flow counting applied to the signal in Fig. 2.5 55
2.16 Examples of rain-flow counting applied to the signal in Fig. 2.7 55
2.17 Examples of rain-flow counting applied to the PSD in Fig. 2.8c 56
2.18 Regions of S-N curve [11] . . . 61
2.19 Reference S-N lines determined as modified S-N curves [7] . . 62
2.20 Bi-linear S-N fatigue-life curve with the Haibach assumptions [13] . . . 63

3.1 Random Vibration Fatigue analysis by Fe-Safe . . . 67
3.2 Random Vibration Fatigue analysis by plug-in tool in Abaqus CAE . . . 68
3.3 Graphical User Interface (GUI) of Random Vibration Fatigue plug-in tool in Abaqus CAE . . . 70

4.1 L-Plate Geometry [33] . . . 82
4.2 L-Plate - Case study I . . . 82
4.3 Normal modes . . . 83
4.4 Stress PSDs of the element in the middle of the notched area . 84
4.5 Bracket Geometry . . . 85
4.6 Acceleration PSD representing the helicopter vibration environment [16] . . . 85
4.7 Bracket's model . . . 86
4.8 Normal modes . . . 88

5.1 Equivalent Von Mises - Case study I . . . 90
5.2 Equivalent Lemaitre - Case study I . . . 91
5.3 Projection by Projection - Case study I . . . 91
5.4 Crossland - Case study I . . . 92
5.5 Matsubara - Case study I . . . 93
5.6 Sines - Case study I . . . 94
5.7 Projection by Projection with Tovo-Benasciutti's Probability Density Function (PDF) - Case study I . . . 94
5.8 Projection by Projection with Narrow-band PDF - Case study I 95
5.9 Multi-axial criteria with extended S-N curve . . . 96
5.10 Multi-axial criteria with modified S-N curve . . . 97
5.11 Fe-Safe result with Equivalent Von Mises multiaxial criteria and Dirlik's PDF - Case study I . . . 98

5.12 Fe-Safe result with Equivalent Von Mises multiaxial criteria and Tovo-Benasciutti's PDF - Case study I 98
5.13 Damage map obtained with the Crossland criterion [34] - Case study I 99
5.14 Fe-Safe's results with Critical Plane criteria 100
5.15 Projection by Projection - Case study II 102
5.16 Crossland - Case study II 102
5.17 Fe-Safe result with Equivalent Von Mises multiaxial criteria and Dirlik's PDF - Case study II 103

List of Tables

3.1 Random Vibration Fatigue Tool - Main Function 74
3.2 Random Vibration Fatigue Tool - Equivalent Von Mises Function 75
3.3 Random Vibration Fatigue Tool - Equivalent Lemaitre Function 75
3.4 Random Vibration Fatigue Tool - Projection bu Projection Function 76
3.5 Random Vibration Fatigue Tool - Crossland Function 76
3.6 Random Vibration Fatigue Tool - Matsubara Function 77
3.7 Random Vibration Fatigue Tool - Sines Function 78
3.8 Random Vibration Fatigue Tool - SpectralMoments Function . 78
3.9 Random Vibration Fatigue Tool - Parameters Function 79
3.10 Random Vibration Fatigue Tool - Narrow-band Function . . . 79
3.11 Random Vibration Fatigue Tool - Dirlik Function 79
3.12 Random Vibration Fatigue Tool - Tovo-Benasciuti Function . . 79
3.13 Random Vibration Fatigue Tool - Damage Function 80
3.14 Random Vibration Fatigue Tool - Contourplot Function 80

4.1 Material properties of L-plate 81
4.2 Material properties of bracket 84
4.3 First ten natural frequencies of the bracket 87

5.1 Fatigue Material Properties - Case Study I 90
5.2 Fatigue Material Properties - Case Study II 101

List of acronyms and abbreviations

ASD	Auto-Spectral Density
CAE	Computer-aided Engineering
CSD	Cross-Spectral Density
FE	Finite Element
FEM	Finite Element Method
FFT	Fast Fourier Transform
FRF	Frequency Response Function
FT	Fourier Transform
GUI	Graphical User Interface
HCF	High-Cycle Fatigue
LCC	Level-Crossing Counting
LCF	Low-Cycle Fatigue
MCC	Minimum Circumscribed Circle
MCE	Minimum Circumscribed Ellipse
MDOF	Multi-Degree-Of-Freedom
ODB	Output DataBase
PbP	Projection by Projection
PDF	Probability Density Function
PSD	Power Spectral Density
RC	Range Counting
RMS	Root Mean Squared
RSG	Really Simple GUI
SSD	Steady-State Dynamics
TF	Transfer Function

List of Symbols Used

The following symbols will be later used within the body of the thesis.

$G_{eq}(\cdot)$ Equivalent PSD , see equation (2.68), ... page 38

$L(\cdot)$ Fourier Transform of the signal l , see equation (2.10), ... page 17

ϵ Euler's constant , see equation (2.44), ... page 26

$\Gamma(\cdot)$ Gamma function , see equation (2.106), ... page 56

μ'_3 Skewness of the signal , see equation (2.7), ... page 13

μ'_4 Kurtosis of the signal , see equation (2.8), ... page 13

μ_n Centered Moment of order n in time domain , see equation (2.5), page 13

ν_a the average number the maxima in the time interval t - $t + dt$, see equation (2.39), ... page 25

ν_{eq} Peak factor , see equation (2.80), ... page 44

ω Pulsation , see equation (2.50), ... page 29

$\overline{u_0}$ Expected maximum peak value , see equation (2.44), ... page 26

Φ Displacement modal shape matrix , see equation (2.48), ... page 28

Φ^s Stress modal shape matrix , see equation (2.53), ... page 29

Ψ Stress path , see equation (2.73), ... page 41

ρ Reference stress ratio , see equation (2.72), ... page 39

σ_m Hydrostatic stress , see equation (2.69), ... page 39

$\sigma_s(\cdot)$ Stress vector process , see equation (2.53), ... page 29

σ_{eq} Equivalent uni-axial stress , see equation (2.69), ... page 39

$\sqrt{J_{2,a}}$ Maximum amplitude of the second invariant of the stress deviator , see equation (2.80), ... page 44

$\sqrt{J_{2a\rho=-1}}$ Fatigue limit under uni-axial loading , see equation (2.102), page 52

$\sqrt{J_{2a\rho=0}}$ Fatigue limit under torsional loading , see equation (2.102), page 52

a Vector defining the critical plane criterion , see equation (2.99), page 50

b Basquin's slope of the S-N curve, see equation (2.111), ... page 61

C Basquin's constant of the S-N curve, see equation (2.111), . . . page 61

C Damping matrix , see equation (2.47), ... page 28

C' Stress invariant covariance matrix , see equation (2.77), ... page 42

C'_0 Diagonal stress invariant covariance matrix , see equation (2.77), page 42

C_a Shear stress amplitude , see equation (2.72), ... page 40

c_r Modal damping , see equation (2.51), ... page 29

C_v Stress covariance matrix , see equation (2.58), ... page 31

D Damage , see equation (2.104), ... page 53

D_{NB} Damage given by the Narrow-band method, see equation (2.107), page 59

D_{RCF} Damage given by the rain-flow counting method, see equation (2.107), page 59

D_{RC} Damage given by the range-mean counting method, see equation (2.107), ... page 59

$E[\cdot]$ Mathematical expectation , see equation (A.3), ... page 115

$erf(\cdot)$ Error function , see equation (2.44), ... page 26

$F(\cdot)$ function for amplitude extremes according to Davenport formula , see equation (2.83), ... page 45

$F(t)$ Force excitation vector , see equation (2.47), ... page 28

f_1 Axial fatigue limit , see equation (2.83), ... page 45

f_m True fracture strength , see equation (2.83), ... page 46

f_r Modal force excitation , see equation (2.51), ... page 29

$G(\cdot)$ PSD of a random signal , see equation (2.12), ... page 18

$G_a(\cdot)$ Random excitation PSD matrix , see equation (2.57), ... page 30

$G_I(\cdot)$ PSD of the first stress tensor invariant , see equation (2.76), . page 42

$G_s(\cdot)$ Response stress PSD matrix , see equation (2.57), ... page 30

$G_{eqH}(\cdot)$ PSD of the Hydrostatic pressure , see equation (2.75), ... page 42

$G_{sd}(\cdot)$ PSD of the stress deviator , see equation (2.74), ... page 41

$H(\cdot)$ Transfer Function of a linear system , see equation (2.22), . . . page 22

$H_d(\cdot)$ Displacement Frequency Response Functions (FRFs) matrix , see equation (2.52), ... page 29

$H_s(\cdot)$ Stress FRFs matrix , see equation (2.54), ... page 30

$H_s(\cdot)$ Stress FRFs matrix with acceleration random base excitation , see equation (2.56), ... page 30

K Stiffness matrix , see equation (2.47), ... page 28

k_r Modal stiffness , see equation (2.51), ... page 29

$l(t)$ Random signal in the time domain , see equation (2.9), ... page 15

M Mass matrix , see equation (2.47), ... page 28

m Mean of the signal , see equation (2.9), ... page 15

M_0 Spectral moment of order 0 in the frequency domain , see equation (2.31), ... page 24

M_2 Spectral moment of order 2 in the frequency domain , see equation (2.33), ... page 24

M_4 Spectral moment of order 4 in the frequency domain , see equation (2.35), ... page 24

M_n Spectral moment of order n in the frequency domain , see equation (2.30), ... page 24

m_r Modal mass , see equation (2.51), ... page 29

$Max[\cdot]$ Maximum value over the period $[0, T]$, see equation (2.80), page 44

N Normal stress , see equation (2.72), ... page 40

$N(T)$ Total number of cycles , see equation (2.104), ... page 53

n_0 Average total number of zero crossings per unit time, , see equation (2.25), ... page 23

n_0^+ Average total number of zero crossings with positive slope, per unit time , see equation (2.25), ... page 23

n_a Average total number of crossings of a threshold, per unit time, , see equation (2.23), ... page 23

N_a^+ Expected value of the number of threshold crossings with positive slope over the duration T , see equation (2.28), ... page 24

n_a^+ Average total number of crossings of a threshold with positive slope, per unit time, , see equation (2.23), ... page 23

N_e Number of cycles of fatigue limit , see equation (2.72), ... page 40

N_i Number the cycles to failure with amplitude s_i , see equation (2.104), page 53

n_i Number the cycles with amplitude s_i , see equation (2.104), . page 53

n_p^+ the average number the maxima per second , see equation (2.43), page 26

n_{rfc} Number of rain-flow cycles counted in the period T , see equation (2.105), ... page 54

$p(\cdot)$ Probability Density Function , see equation (2.1), ... page 12

$p(t)$ Hydrostatic pressure , see equation (2.80), ... page 44

P_m Mean power of an excitation , see equation (2.12), ... page 18

$q(\cdot)$ Probability density of maxima per unit time , see equation (2.44), page 26

Q^* Matrix of coefficients for the Lemaitre method , see equation (2.71), page 39

Q_h Matrix of coefficients for the hydrostatic pressure , see equation (2.76), page 42

Q_M Matrix of coefficients for the Huber-Mises-Hencky equivalent stress , see equation (2.65), ... page 37

r Irregularity factor , see equation (2.42), ... page 26

$R_l(\cdot)$ Auto-correlation function of the signal , see equation (2.8), . . page 14

R_m Tensile strength , see equation (2.83), ... page 46

$r_{corr,}$ Correlation coefficient , see equation (2.61), ... page 31

$R_{lu}(\cdot)$ Cross-correlation function of the signal , see equation (2.8), . page 14

s_l Standard deviation of the signal in time domain , see equation (2.6), page 13

s_l^2 Variance of the signal in time domain , see equation (2.6), . . . page 13

S_{inv} Stress invarinat PSDs in the Euclidean space , see equation (2.97), page 49

T Constant Transfer Function (TF) matrix , see equation (2.55), page 30

t_1 Torsional fatigue limit , see equation (2.83), ... page 45

$tr\{\dots\}$ Trace operator , see equation (2.65), ... page 37

U Eigenvectors matrix of the covariance matrix , see equation (2.77), page 42

$u(t)$ Displacement vector , see equation (2.47), ... page 28

$v(\cdot)$ Relative displacement vector , see equation (2.55), ... page 30

$w(\cdot)$ Acceleration random base excitation vector , see equation (2.55), page 30

w_{TB} Weight factor of Tovo-Benasciutti method, see equation (2.108), page 59

Chapter 1

Introduction

Fatigue is one of the main criteria that engineers have to face when high level of structural reliability has to be guarantee. In different fields of engineering as aerospace, automotive, offshore, marine, wind or railway, many components are subjected to complex fatigue loading during in-service conditions. Examples can be the loads inducted by a rough road on vehicles traveling at different speeds, the loads generated by the wind on wind turbines due to meteorological variations, the loads experienced by aircraft due to jet noise, the white noise on helicopters, or the wave loads in offshore platforms under different sea states. Mostly when the environment excites the resonant frequencies of the structure through a random input, the study of the dynamic response of the structure becomes essential. Moreover, a good prediction on the damage accumulation due to the environmental loading permits to detect the weak spots and achieve a good structural reliability. For these reasons, the random excitation could significantly decrease the life span of the structure and hence is important to prevent possible catastrophic consequences. In order to achieve a high level of structural confidence, fatigue life calculations must be made at several stages, from the design to the development process, as shown by figure 1.1. It is well known that fatigue test are exceptionally time consuming and when it comes to random vibrations, the variable amplitude and multiaxiality of the loading make them more complex. Thus, cumulative damage calculations are helpful for structural integrity assessment of metallic components, preventing unexpected failures and reducing the amount of test needed.

Especially in the last decades, computer-aided design and analysis became essential on the design of components in all the engineering fields. During

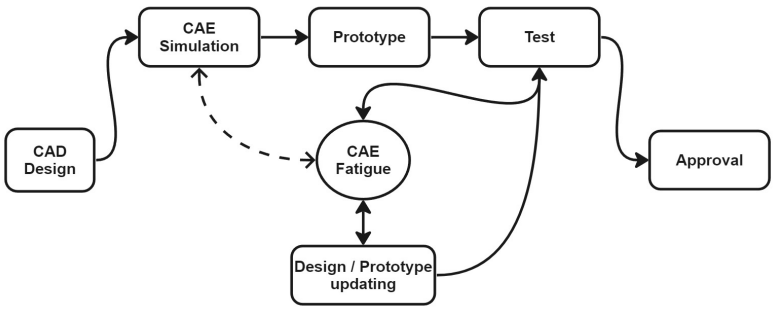

Figure 1.1: Fatigue within the product development process

the years there has been an increasing growth in the use of advanced simulation and calculation approaches using Finite Elements Analysis. So, also fatigue damage calculations of structures subjected to random vibrations are addressed trough Finite Element Method (FEM) analysis. In particular, for linear systems, frequency domain approach are preferred to time domain approach, when they deal with random vibrations, because they can shorten the computation time considerably. Therefore, fatigue life calculation methods based on frequency domain information of a random loading are now well established and available in many commercial software as nCode DesignLife, Simulia Fe-Safe, CAE fatigue, LS-DYNA, FEMFAT or Ansys Random Vibration Fatigue.

Abaqus CAE is a well-known and largely used commercial software for FEM Analysis, used by many industries. It permits numerous different types of simulation and analysis, by incorporating also pre and post processing tools. However, Abaqus CAE lack in the fatigue field and a tool for random vibration fatigue is completely missing. However, it is sometimes preferred to other software for its capability on supporting scripted operation and Graphical User Interface (GUI) customization. For this reason, this thesis takes advantage of this and it fills the gap on random vibration fatigue by developing a plug-in tool in Abaqus CAE for multi-axial random fatigue analysis of metal components. In particular, a python script has been written and used as kernel for a custom application realised using the Abaqus' Really Simple GUI (RSG) dialog builder. It permitted to create a GUI dialog box connected to the script which can be used as post-processing tool.

This research will delve into how fatigue due to multi-axial random

vibrations can be treated and analysed on metal components, with main focus on spectral methods. A literary review on research articles about spectral methods for multi-axial random vibration fatigue and detailed documentation of available software for random vibration analysis permitted to gain insight about methods that are already well establish. The study allowed to understand the methods suitable and consistent with the random vibration analysis in Abaqus CAE. Once the tool has been developed and validated against the Simulia Fe-Safe, a real component has been studied. The thesis will explain the challenges to address the problem with an Abaqus CAE plug-in tool and finally, it will give some insight on future works on this filed.

1.1 Context

Fatigue is a failure mechanism of particular interest in many fields of engineering. It is unpredictable and can take place at stress levels significantly below the ultimate strength of the material. Repetitive cycle loads move locally the dislocations contained in the material which cause the formation and grow of small fatigue cracks. The merging of these cracks leads to the fatigue failure of the component. Thus, understand how the damage is accumulated during the operational life of the structure is of primary importance to prevent unexpected failure and guarantee sufficient structural reliability.

There are many different way to classify all the different type of loads that engineering components experience during their life. Since this research deal with random loading, a convenient way to classify a process is shown in Fig. 1.2.

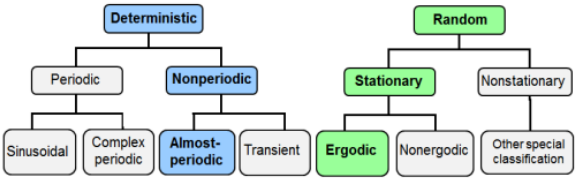

Figure 1.2: Classification of deterministic and random processes [1]

This classification may appear quite general but actually, it differentiates two completely different type of analysis. Deterministic loads are well known

and defined, so they can be simulated in a model or replicated in a test. Random processes, instead, are more easily defined in a statistical sense, since the structure's response can not be predicted in advance. Moreover, the randomness is typical of the excitation, not of the structure which is known and it is not subjected to random variations of its properties. Therefore, the loading behaviour is more clearly defined through statistical parameters. This changes substantially the prospective of analysis, through the introduction of the probability theory. Hence, mathematical theory of random vibration becomes essential to achieve realistic modeling of the structural dynamic.

Lifetime prediction and reliability assessment for engineering components under in-service conditions, where the external load shows an invariably irregular and random nature, are obviously a critical issue. A careful analysis is inevitably needed in order to avoid unexpected failure during in-service condition and to predict the lifetime. These goals can be achieved in different ways. One way is by testing in a lab, replicating the loading by the use of shakers. However, intensive test campaigns could be expensive and time consuming, hence they are avoided or limited to validation/certification purposes. A preferred way to study components subjected to random vibration is by simulations. In particular, several commercial Computer-aided Engineering (CAE) software are capable of handling random vibration fatigue calculation. Through a finite element model of the structure it is possible to calculate the dynamic response and considering the stress-life approach, from the stress at each node it is possible to perform the fatigue analysis. However, all of them can accomplish this analysis in two ways: the time domain approach or the spectral method based on the Power Spectral Density (PSD) of the load inputs, as shown in Fig. 1.3 and 1.4.

Even if the first one is the straightforward method that can be easily implemented, the second one has demonstrated to have exceptional features in terms of computational time, especially when it comes to complex models with large number of elements. For this reason, spectral methods are widely used by many industries to address the problem of random vibration fatigue calculation.

Considering a linear response of the structure, if the load is random also the stress response is random and hence the probability theory can be used to estimate the fatigue damage accumulated in the component. This is the principle underlying the spectral methods for random vibration fatigue.

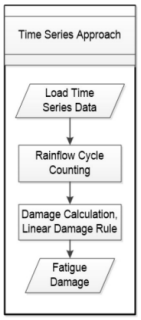

Figure 1.3: Time domain approach[2]

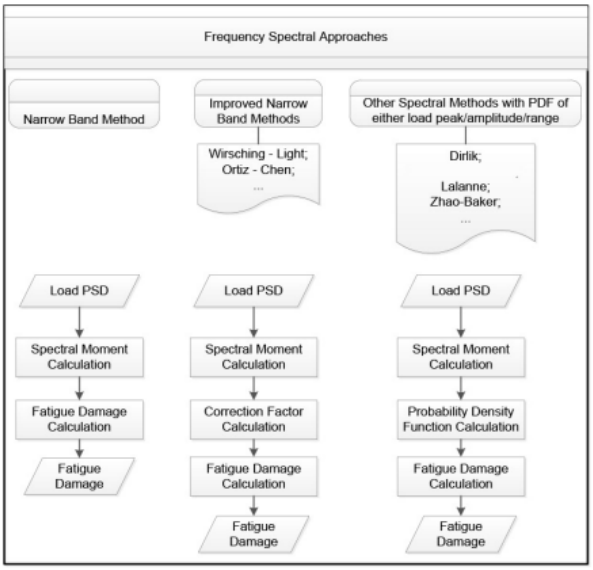

Figure 1.4: Frequency domain approaches [2]

They use statistical parameters resulting from the stress PSDs to calculate the probability distribution of the stress history. Even if in the case of narrow band excitation, there is an exact formulation of the PSD proposed by Bendat [3]. In the case of wide-band excitation, an exact formulation of the Probability Density Function (PDF) of the stress history does not exist and a wide range of spectral methods can be found in literature. They differ in the correction factor to the Bendat's narrow-band PDFs of the stress history. Many other empirical formulations of the PDF has been proposed by different authors during the years [2]. The best results have been obtained by Dirlik and Tovo-Benasciutti [4]. These two methods have demonstrated to reach better results for both, narrow-band and broad-band excitation, compared to the others methods. Thus, they are widely used in all commercial software that use spectral methods. For this reason, this project will focus on these three methods for the probability distribution of the stress history: Bendat, Dirlik and Tovo-Benasciutti.

However, engineering components under in-service conditions often experience complex multi-axial stress with random amplitudes. The project wants to investigate, in particular, the effect of multi-axial random vibrations and the methods described above are defined only for the uni-axial stress state (one PSD not a matrix of PSDs and Cross-Spectral Densitys (CSDs)). Hence, there is a need for some criteria to translate the multi-axial stress state to an

equivalent uni-axial. In particular, two criteria have been implemented and studied. The first was the Equivalent Von Mises proposed by Preumont [5] and the second was the Equivalent Laimatre [6]. These two methods, developed exactly to address this problem, are widely used due to the simplicity of their formulation. In fact, a typical assumption for the PDF is that the stress distribution has to be Gaussian. In the uni-axial case, this is achieved by considering a Gaussian distributed random load and linear behaviour of the structure. Consequently, both methods are based on a linear combination of the stress PSD to maintain the propriety of Gaussian distribution also on the equivalent PSD. Moreover, a third method based on stress-invariant, called Projection by Projection [7], has been introduced. Instead of a linear combination of the PSDs, it projects them into uncorrelated spaces, it uses the uni-axial methods and then sum the effect of each projected stress.

In addition, a wide range of multi-axial criteria in the time-domain are available in literature for fatigue life estimation. However, only a few of them were specifically reformulated in the frequency-domain, due to the complexity to translate them in statistical parameters based on spectral quantities. These methods based on stress-invariant (*e.g.,* Sines, Crossland, Matsubara) [8] [9] [10] are substantially different from the others, since they do not require any formulations of PDF of the stress history. Instead, the necessary statistical parameters are directly formulated from the matrix of PSDs.

Fatigue strength assessment in metallic structures can be carried out with reference to infinite life (fatigue limit) or finite life (fatigue strength as a function of the number of loading cycles, and S-N curves described by either Basquin equation in the High-Cycle Fatigue (HCF)) [11]. This is the main difference between the two categories of methods developed. The firsts, which make use of PDFs, are finite life criteria and belong to the damage tolerant fatigue philosophy. The second type, instead, are infinite life criteria and belong to the safe life fatigue philosophy. The firsts are used to determine the life of the components, so they assumes that the stress levels experienced by the structure can be above the Fatigue limit. The seconds are used to understand how far (below) the stress levels are from the fatigue limit.

Many commercial software adopt also critical plane criteria suitable for multi-axial random vibration to determine the equivalent uni-axial PSD. In particular two methods have been studied, the Matake [9] criteria for the infinite life and the Carpinteri-Sapgnoli [12] for the finite life. However, they

are known to be computationally expensive, hence their implementation will be left as future work and they will be only presented for completeness.

With regard to finite life approach, in other to reduce the complexity of the study, it was adopted the linear damage rule (Miner's rule) and the S-N curve of the material is represented by the Basquin equation. In order to consider also stress levels under the fatigue limit, which can contribute to the propagation of the crack, an extended 2-slope S-N curve following the Haibach criteria [13] was adopted as suggested by recommendations [14] Moreover, the standardized test used to determine the Basquin constants representing the Wöhler curve of the material are uni-axial and usually they are characterized by only axial or only torsional stress. To consider the coupling between the two stress, the modified S-N curve following the Susmel [15] model has been implemented.

A simple L-plate subjected to random vibration, found on literature, was used to validated of the different criteria against the results obtained by the commercial software Fe-Safe. Moreover, It permitted to compare the different methods in terms of hot-spot identification and in terms of accuracy. Then the Projection by Projection method and the Crossland method have been chosen to study the damage on a bracket mounted on a helicopter and subjected to the background random vibrations. The vibration spectrum in a helicopter is characterized by the combination of a random low-level background and strong peaks superimposed representing the rotors harmonics and hence, for this reason, it is usually called Sine-on-Random spectrum. Thus, the damage caused on the bracket by the random variation is analyzed considering the acceleration PSD defined by the standard MIL-STD-810F [16].

Finally, the usage of the RSG dialog builder to create the plug-in developed as post-processor to Abaqus CAE is discussed and the developed GUI dialog box is presented. In particular, Python codes are used to integrate and develop the methods into the plug-in tool in Abaqus CAE. Thus, a GUI into Abaqus CAE which performs mutli-axial random vibration analysis was created.

1.2 Purpose and Goals

The main focus of the thesis is on spectral methods for random vibration fatigue of metal structures. As mentioned previously, Abaqus CAE can handle

a lot of simulations and is largely used by many industries. Unfortunately, it lack in a fatigue calculation tool and especially for random vibration loading. However, it permits to address random analysis and to calculate the resulting stress PSDs, hence a plug-in tool that works as post-processor seems to be a valid option to fill this gap. Therefore, the purpose of the thesis is to develop a plug-in tool for Abaqus CAE which calculates the damage, and hence the fatigue life, of components subjected to multi-axial random vibration, by using the frequency-domain approach. The aim of the tool is to handle the calculation totally on Abaqus CAE, without the need of other software, which may involve problem in the files compatibility or the need of other licenses.

The goal of developing a plug-in tool for random vibration fatigue in Abaqus CAE has been divided into the following four sub-goals:

1. Overview on random processes and structural dynamics for random vibration
2. Overview on existing multi-axial criteria in frequency domain for fatigue purposes
3. Development of the tool by Python scripting and validation against Fe-Safe results
4. Study of a real application

Through these goals, the thesis aims to achieve an appropriate knowledge on random loading in the field of structural dynamics. Moreover, it has the purpose to delve into suitable multi-axial fatigue criteria and spectral methods. Finally, it will explore the possibility of fulfill the gap of Abaqus CAE in fatigue simulation by Python scripting and it will discuss the manage of large database of results created by Abaqus CAE.

1.3 Delimitations

Some simplifications are needed in order to reduce the complexity of the problem. These assumptions limit the project and mainly can affect the result of the study. In particular, the structure is considered to have a linear behaviour (small deformations) and the material is considered isotropic and homogeneous. In order to consider only the HCF region and adopt the stress-life approach, the loading is considered relatively small and not

reaching the yield stress of the material. Effects of temperature, corrosion, inclusions or defects are neglect, as the surface roughness is not taken into account. Notch factors, stress concentration factors and critical distance are not considered in this study. As well as fracture mechanics is not considered. Most of the existing spectral methods assume, as a simplifying hypothesis, that the design random loadings are Gaussian, hence, also this study is limited to random stationary ergodic processes with zero mean and Gaussian distribution. Hence, mid stress correction are not considered. Moreover, only equivalent uni-axial stress and stress-invariant criteria are implemented. The critical-plane criteria are presented but not developed, due to the long computational time that they require.

1.4 Structure of the thesis

Chapter 2 presents relevant analytical information about Random Vibration Fatigue using spectral methods. The chapter is divided into different sections. Firstly, the random processes and their statistical proprieties will be treated, then the FEM modal analysis and its application simulate the dynamic response of the structure subjected to random vibrations will be discussed in 2.2. The different multi-axial criteria for fatigue assessment adopted will be presented in section 2.3. The section 2.4 will treat the PDFs and their connection to the rain-flow counting method in the time domain. Finally, a section 2.5 is dedicated to the material properties definition and in particular to the S-N curve necessary for the fatigue calculation.
Chapter 3 presents the method used to develop the plug-in in Abaqus CAE. In particular, an overview on Abaqus CAE is reported in 3.1. Section 3.2 is dedicated to the study of random vibration fatigue with Fe-Safe and section 3.3 presents the development of the fatigue tool, focusing on the python scripting and the data handling.
Chapter 4 will present the two case studies used to validate the tool. The first one, in section 4.1, is L-plate which is described and analyzed with all the methods integrated. Then, in section 4.2, a real application of the plug-in is studied and a bracket is presented and analysed considering the Projection by Projection and the Crossland methods.
Chapter 5 presents a comparison between the fatigue calculation obtained with the fatigue tool in Abaqus CAE and the results obtained with Fe-Safe. In particular, the section 5.1.1 concerns the L-plate of the first case study and section 5.1.2 concerns the bracket.
Finally, the last chapter 6 will present some conclusion on the results obtained

with the tool and its application in section 6.1. Some further comments are presented in section 6.2 which contains some suggestion for future works on this field.

Chapter 2

Background

This chapter intends to give some insight on the basic knowledge necessary to understand the work done more easily. It will present the main topics treated by the project. In particular, it will cover the properties of random processes and their statistical features. It will go through the FEM modeling for random vibrations with a focus on modal superposition method. Then, the properties of the fatigue criteria implemented will be presented. A special section is dedicated to the rain-flow counting methods and the PDF. Finally, the material properties will be described in terms of fatigue behaviours necessary to address the random vibration fatigue calculation.

2.1 Random processes

A random variable is defined as a quantity whose instantaneous value cannot be predicted. The first mathematical analysis of random vibrations was carried out by A.Einstein studying the Brownian movement [17] in 1905 but only the works of S.O. Rice [18], in the 1940s, founded the basis for many studies in different fields of engineering.

The aim of a random process analysis is to define the probability of finding certain events within the process signal itself. These events are, for examples, peak values or the time that the signal exceeds a defined value.

By considering Fig. 2.1, the probability that the function l is in the interval Δl is expressed mathematically as:

$$Prob[l < l(t) < \Delta l] = \sum_i \frac{t_i}{T} = p(l)\Delta l \tag{2.1}$$

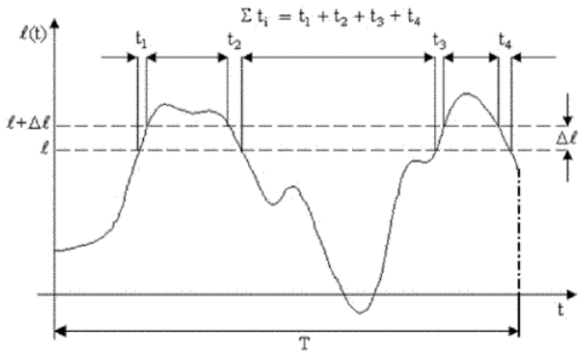

Figure 2.1: Sample of random process [19]

Where, if Δl is sufficiently small, the PDF $p(\cdot)$ is defined by:

$$p(l) = \lim_{\Delta l \to 0} \left[\lim_{T \to \infty} \left(\frac{1}{T} \frac{\sum t_i}{\Delta l} \right) \right] \tag{2.2}$$

The majority of random vibrations encountered in the real environments, thanks to the central limit theorem, can be represented by the Gaussian law. The Rayleigh law, instead, is used especially to represent the properties of a narrow-band Gaussian process. These two PDFs, largely deployed to study random vibrations, are reported in the "supporting material" chapter A.1.

In general, vibrations are oscillations of the mechanical system around its equilibrium position. Since the arithmetic mean does not carry many information, the mean value of the absolute value of the signal (Eq. 2.3) and the Root Mean Squared (RMS) value (Eq. 2.4, where $\overline{l^2(t)}$ is defined in Eq. A.6) are preferred.

$$\overline{|l(t)|} = \frac{1}{T} \int_0^T |l(t)| \, dt \tag{2.3}$$

$$l_{rms} = \sqrt{\overline{l^2(t)}} \tag{2.4}$$

The project deals with vibratory signals with zero mean called centered which is a typical feature in measured vibrations. This condition can be verified by comparing the standard deviation and the RMS of the signal. In case of centered vibrations, they should be the same. The RMS is the simplest statistical property to obtain and it provides useful insight on the global severity of the vibration. However, it is not enough since it does not indicate the energy distribution over the frequency domain. To overcome this,

it is possible to look at centered moments of order n as defined by Eq. 2.5

$$\mu_n = E[l(t) - \overline{l(t)}]^n = \lim_{T\to\infty} \frac{1}{2T} \int_{-T}^{T} [l(t) - \overline{l(t)}]^n \, dt \tag{2.5}$$

In particular, the centered moment of order 2 is the variance, denoted by s_l^2 and defined by Eq. 2.6

$$s_l^2 = E[(l - \bar{l})^n] = \overline{l^2(t)} - \overline{l(t)}^2 \tag{2.6}$$

where s_l is called the standard deviation. The centered moment of order 3, denoted by μ_3, can be reduced by division by s_l^3 defining μ_3' as Eq. 2.7

$$\mu_3' = \frac{E\{[l(t) - \overline{l(t)}]^3\}}{s_l^3} \tag{2.7}$$

μ_3' is a measure of the symmetry of the probability density law $p(l)$ with regard to the mean $\overline{l(t)}$ and for this it is called skewness. As shown by Fig. 2.2, a Gaussian process has $\mu_3' = 0$. Instead, the curve presents a peak towards the left if for $\mu_3' < 0$ and for $\mu_3' > 0$, the peak of the curve is shifted towards the right.

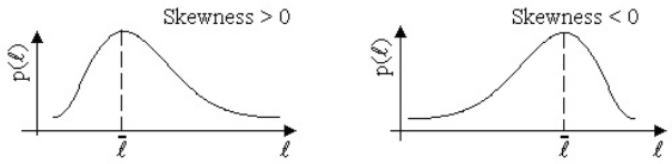

Figure 2.2: Probability densities with non-zero skewness [19]

The same can be done for the moment of order 4, defining the kurtosis by Eq. 2.8.

$$\mu_4' = \frac{E\{[l(t) - \overline{l(t)}]^4\}}{s_l^4} \tag{2.8}$$

In particular, the kurtosis permits to determine the flatness of the PDF and measures the relevance of the distribution of values. $\mu_4' = 3$ is characteristic of a normal process, $\mu_4' < 3$ characterizes a truncated signal or existence of a sinusoidal component and $\mu_4' > 3$ defines the presence of peaks of high value as shown by Fig. 2.3

Therefore, the skewness equals to zero and the kurtosis equals to three permit to verifying that the signal follows a Gaussian value distribution.

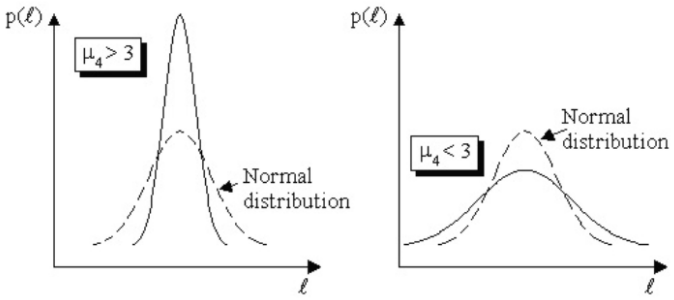

Figure 2.3: Kurtosis influence on probability density [19]

A strong variation of these parameters enables to detect the presence of mechanical shocks or signal problems and in particular, kurtosis is very sensitive to “abnormal” signal values.

Another fundamental parameter for random signals is the correlation. It is a measure of the degree of similarity between two functions of the same parameter, time generally. In the ”supporting material” chapter A.2 the auto-correlation function $R_l(\tau)$ and cross-correlation function $R_{lu}(\tau)$ are defined in the time domain. The following Fig. 2.4 shows some examples of signals and their auto-correlation functions. As can be seen, if $R_l(\tau)$ tends slowly towards zero, the changes in the random function are very slow and it might does not converge at all as for the sinusoidal signal. Thus, $R_l(\tau)$ is a measurement of the degree of randomness of the process.

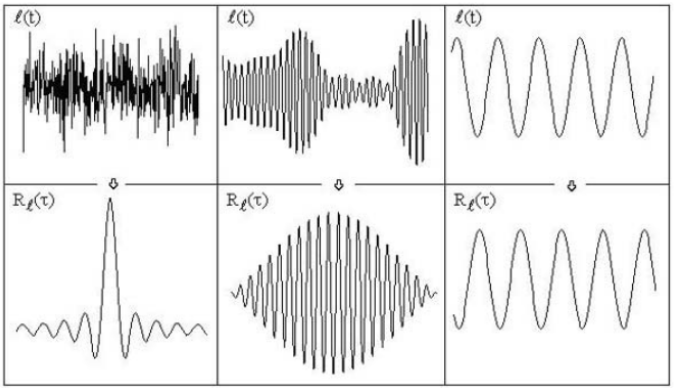

Figure 2.4: Examples of autocorrelation functions [19]

Consequently, a random phenomenon is defined stationary if every moment of all orders and all the correlations are invariable with time t. The

benefit of this feature is that it is not necessary to record the signals for a long period of time but, however, it must be long enough to subsequently enable a significant frequency analysis.

A process is defined as ergodic if all the temporal averages exist and have the same value as the corresponding ensemble averages calculated at an arbitrary given moment. An ergodic process is thus necessarily stationary. Typically, only few records are available from real tests and thus the temporal averages are calculated with the assumption that the process is stationary and ergodic. This makes it possible to perform the frequency analysis of a short sample chosen over one signal record. Then, the statistical properties are extended to the entire ensemble. A necessary and sufficient condition such that a stationary random vibration $l(t)$ is ergodic is that its correlation function satisfies the condition in the following Eq. 2.9 where $R_l(\tau)$ is the auto-correlation function calculated from the centered variable $l(t) - m$.

$$\lim_{T\to\infty} \frac{1}{T} \int_0^T \left(1 - \frac{\tau}{T}\right) R_l(\tau)\, d\tau \; = 0 \tag{2.9}$$

Stationarity and ergodicity should be checked before any analysis by verifying that, in the time sample considered, the RMS value calculated using a sliding mean varies little as a function of time. Anyway, due to experimental records deficiency or to save time, these assumptions usually are made without checking. However, the decision of the analysis method to use (frequency or time domain) is based on the stationary or non-stationary behaviour of the process and in particular, the calculation of the PSD only has meaning if the signal is stationary. For example, as reported by [19], if several instrumented flights are carried out, probably not the same RMS value will be obtained for each sequence. All the conditions would have to be perfectly the same in order for the process to be ergodic. In practice, the RMS value over the time is evaluated for each record, as well as the skewness and kurtosis. By looking at the first one, it is possible to define the temporal ranges in which the RMS value does not change much and hence, where the process can be considered as stationary. Each signal is then separated into sections representing a specific phase of the flight, generating a particular vibratory environment and with common characteristics from one flight to another. However, the RMS value of these phases is often different from one flight to another (slightly different weather conditions, *etc.*) and this represents the non-ergodicity of the process. This variation can be considered: (i) by calculating the statistical PSD; (ii) by applying an uncertainty's coefficient.

2.1.1 Random Vibration Properties in the Frequency Domain

Fig. 2.5 shows an example of sine signal with constant amplitude and frequency. How can be seen, all the properties of the signal in terms of peak amplitude, number of cycle, zero cross, *etc.*, result easy to determine for this type of signal.

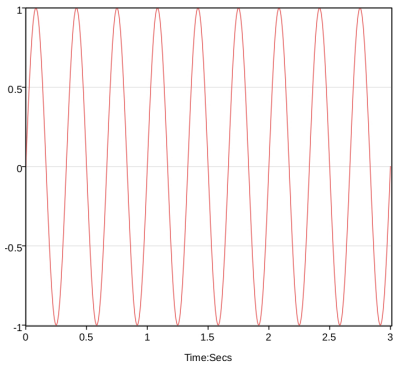

Figure 2.5: Example of Sine signal at 3 Hz

However, it can be more complex when the signal is composed by the sum of more signals. As, for example, shown by Fig. 2.6 which shows the signal resulting from the sum of two sine waves, one at 5 Hz and one at 3 Hz, characterized by the same amplitude. The first one considers in-phase signals and in the second one a delay of $45°$ is applied.

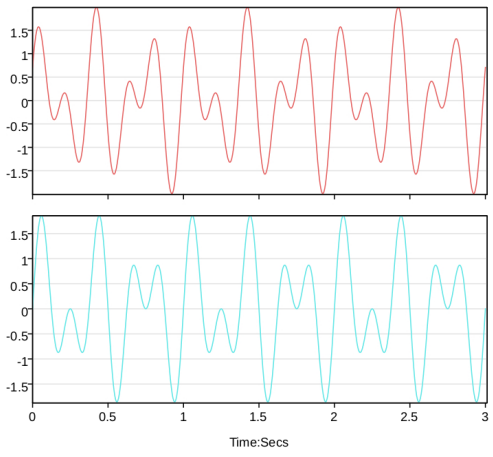

Figure 2.6: Examples of sum of Sine signals at 3 Hz and 5 Hz. First one with in-phase signals and second one with $45°$ of phase shift

Moreover, the calculation of the signal feature could be even more complex in the case of random signal as in Fig. 2.7. In fact, all the periodic properties are lost in this case and hence, studying the process by means of the frequency domain and statistical properties is a convenient way, widely used, to address this problem.

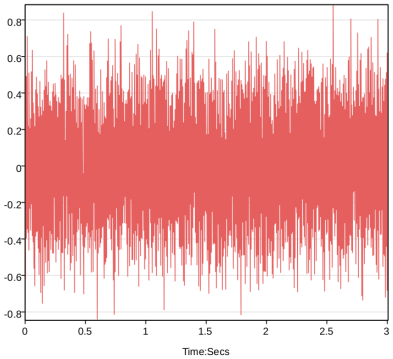

Figure 2.7: Example of random signal

The definition of PSDs and their properties provide a powerful tool to enable the description of random vibrations and have many applications. In this study, their use mainly concerns the definition of the excitation and the calculation the statistical properties of the vibrations.

The Fourier transform of a non-periodic $l(t)$ signal, having a finite total energy,is given by the relationship Eq.2.10:

$$L(\Omega) = \int_{-\infty}^{\infty} l(t) e^{-i\Omega t}\, dt \tag{2.10}$$

It is a complex quantity, hence, in order to represent it graphically, it is necessary to plot: (i) either the real and the imaginary part versus the frequency; (ii) the amplitude and the phase versus the frequency. The curve thus obtained is called the Fourier spectrum. In an indirect way, the Fourier transform is thus used very often in the analysis of random vibrations. However, the random signals are not of finite energy and hence, only the Fourier transform of a sample of signal of duration T can be calculated by assuming that this sample is representative of the whole phenomenon. Starting from $L(\Omega)$, it is possible to return to the time domain signal by using the inverse transform Eq. 2.11 .

$$l(t) = \frac{1}{2\pi} \int_{-\infty}^{\infty} L(\Omega) e^{i\Omega t}\, d\Omega \tag{2.11}$$

The idea behind the PSD is to proceed with an average of the squares of the amplitudes of Fourier transforms calculated for several signal samples. As said before, the RMS value is often used as a severity criterion of the vibrations but it has the disadvantage that it does not give any information of the distribution over the frequencies, which is nevertheless very important. A solution to this was proposed by Weiner: filtering the signal $l(t)$ using a series of rectangular filters of central frequency f and bandwidth Δf and calculating the RMS value L_{rms} of the signal collected at the output of each filter. The curve obtained represents L_{rms} with respect to f which is a description of the spectrum of signal $l(t)$ but the problem is that the spectrum so defined is not unique. In fact, depending on the width Δf the result will be different. Thus, to solve this problem, the variations of $\frac{L_{rms}^2}{\Delta f}$ with f is considered instead.

From the definition of the mean power of an excitation in vibration mechanics reported in the "supporting material" chapter A.3, according to Parseval's equality and with the Fourier transform it yields to:

$$P_m = \lim_{T\to\infty} \frac{2}{T} \int_0^{+\infty} |L_T(f)|^2 \, df \tag{2.12}$$

The above Eq. 2.12 gives the mean power contained in $l(t)$ when all the frequencies are considered. Considering a linear system and following the equations reported in chapter A.3, the PSD is hence defined as the quantity $G(f) = \lim_{\Delta f\to\infty} \frac{P(f,\Delta f)}{\Delta f}$.

The PSD $G(f)$ can be written by Eq. 2.13 where $l_T(t, \Delta f)$ is the part of the signal ranging between the frequencies $f - \Delta f/2$ and $f + \Delta f/2$.

$$G(f) = \lim_{\Delta f\to 0} \lim_{T\to\infty} \frac{1}{T\Delta f} \int_0^T l_T^2(t, \Delta f) \, dt \tag{2.13}$$

The function $G(f)$ is always positive or zero whatever the frequency f. The PSD defined by Eq. 2.13 ranges frequencies between 0 and ∞, which is the practical case. Anyway, the most general definition is $S(f)$ between $-\infty$ and $+\infty$ with $S(-f) = S(f)$. The following Eq. 2.14 shows the relations between these various definitions and it turns out that $G(f) = 2S(f)$ and $G(f) = 2\pi G_\Omega(\Omega)$:

$$l_{rms}^2 = \int_{-\infty}^{+\infty} S(f)\,df \;= \int_{0}^{+\infty} G(f)\,df \;= \int_{0}^{+\infty} G_\Omega(\Omega)\,d\Omega \;= \int_{-\infty}^{+\infty} S_\Omega(\Omega)\,d\Omega \tag{2.14}$$

The PSD of a vibration signal has for dimension the square of an acceleration divided by a frequency, so it is expressed in $(m/s^2)^2/Hz$ or in g^2/Hz. However, not only the Weiner method exist to address the definition of the PSD of a stationary and ergodic process. The Shannon's theorem helps to determine the minimum sampling frequency to correctly represent the signal. In fact, if the higher frequency is f_{max} Hz, the signal is completely determined by its values at a series of points spaced $\frac{1}{2f_{max}}$ seconds apart. This criteria is sufficient to correctly calculate the RMS value of the signal and its PSD where $f_{Nyquist} = f_{samp.}/2$ is called Nyquist frequency. Three methods are mainly used to calculate a PSD: (i) by using the auto-correlation function; (ii) by signal filtering with Δf wide filters and calculation of the RMS value of the filtered signals as defined by Weiner; (iii) by using the Fourier transforms, which is the most widely used method.

(i) The first method make use of the auto-correlation function. The PSD is calculated by evaluating the correlation in the time domain and by carrying out a Fourier transformation (Wiener-Khintchine method) Eq. 2.15

$$G(\tau) = 4\int_{0}^{+\infty} R(f)cos(2\pi f\tau)\,df \tag{2.15}$$

(ii) In the second method the the PSD is determined from the RMS value of a filtered signal. Theoretical relation reported in the "supporting material" chapter **??** which assumes an infinite duration T and a zero analysis bandwidth Δf , is replaced by the approximate relation 2.16 where $\overline{l_{\Delta f}^2}$ is the mean square value of the sample of finite duration T, calculated at the output of a filter of central frequency f and non-zero width Δf

$$G(\tau) = \frac{1}{T\Delta f}\int_{0}^{T} R(f)l_{\Delta f}^2(f,t)\,dt \;= \frac{\overline{l_{\Delta f}^2}}{\Delta f} \tag{2.16}$$

(iii) The third method carries out the calculation of PSD starting from the Fourier transform and considering the expressions above, it leads to Eq. 2.17:

$$G_{ll}(f) = \lim_{T\to\infty}\frac{2}{T}E[|L(f,T)|^2] \tag{2.17}$$

Considering that the discrete Fourier Transform (FT) can be written as $L(m,T) = \frac{T}{N}\sum_{j=0}^{N-1} l_j\ exp(-i\frac{2\pi jm}{N})$, hence the PSD becomes as stated in Eq. 2.18 where $0 < m < M$ and $l_j = j\delta t$

$$G(m,\Delta f) = \frac{2}{N} \mid \sum_{j=0}^{N-1} l_j\ exp(-i\frac{2\pi jm}{N}) \mid^2 \tag{2.18}$$

Eq. 2.13 theoretically defines the PSD which is the method use for analog calculations. However, in practice, this relation cannot be respected exactly since the calculation of $G(f)$ would require an infinite integration time and an infinitely narrow bandwidth. Thus, the PSD is ususally defined in a Fourier series $G(f) = \lim_{T\to\infty} \frac{a_i^2}{2\Delta f}$. The PSD expression of a signal l_1 is hence written as Eq. 2.19

$$G_{l_1l_1}(f) = \lim_{T\to\infty} \frac{2|L_1(f)|^2}{T} = \lim_{T\to\infty} \frac{2L_1^*(f)L_1(f)}{T} \tag{2.19}$$

$G_{l_1l_1}(f)$ is called the Auto-Spectral Density (ASD) and $L_1^*(f)$ is the complex conjugate of $L_1(f)$, the FT of l_1. Similarly, the CSD of two vibrations $l_1(t)$ and $l_2(t)$ is defined as the products $L_1^*(f)L_2(f)$, where L_1 and L_2 are the FTs of $l_1(t)$ and $l_2(t)$ calculated between 0 and T over K blocks of points of the two signals and thus by Eq. 2.20:

$$G_{l_1l_2}(f) = \lim_{T\to\infty} \frac{2L_1^*(f)L_2(f)}{T} \tag{2.20}$$

Some examples of ASD and CSD of the singlas in Fig. 2.5, 2.6 and 2.7 are reported in the following Fig. 2.8

Differently from the ASD, which has real values, the CSD is a complex quantity. As stated before, considering a stationary and ergodic random process, the PSD can be determined from several samples of only one record. A sample of this signal of duration T will be denoted by ${}^il_T(t)$ and its FT ${}^iL_T(f)$ Its PSD is ${}^iG_T(f) = \frac{2|{}^iL_T(f)|^2}{T}$. By definition, the PSD of the random process is, over time T, equal to Eq. 2.21

$$G_T(f) = \frac{\sum_{i=1}^{n} {}^iG_T(f)}{n} \tag{2.21}$$

n being the number of functions ${}^il(t)$, for T infinite, $G(f) = \lim_{T\to\infty} G_T(f)$

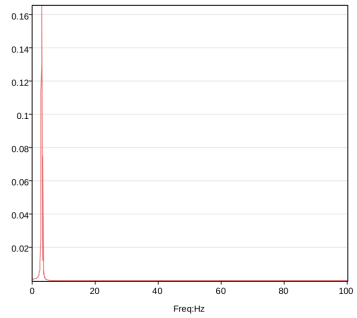

(a) Example of PSD of sine signal in Fig. 2.5

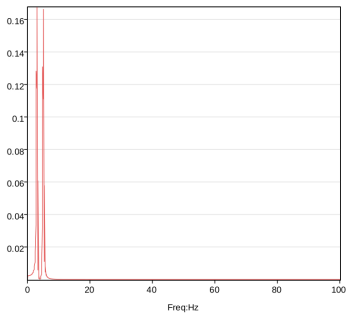

(b) Example of PSD of the first signal in Fig. 2.6

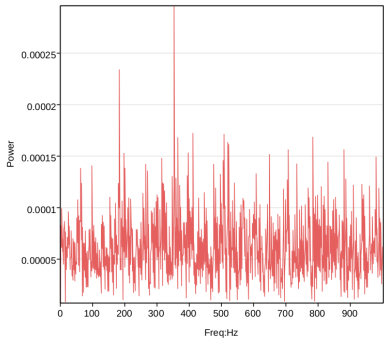

(c) Example of PSD of the first signal in Fig. 2.7

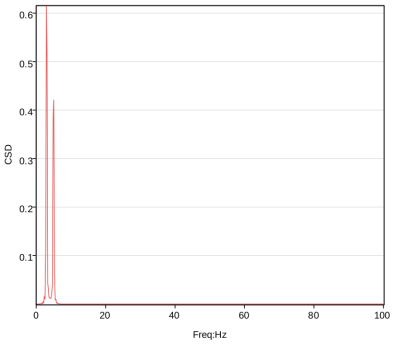

(d) Example of amplitude CSD of the two signals in Fig. 2.7

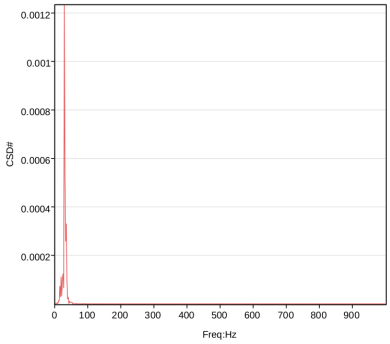

(e) Example of amplitude CSD of the sine signal in Fig. 2.5 and the white noise in Fig. 2.7

Figure 2.8: Examples of PSD and CSD of the signals in Fig. 2.5, 2.6 and 2.7

In particular, the response of a linear system is itself stationary and ergodic if the excitation is itself a random stationary ergodic process. The "Wiener-Khinchine relations" define the connection between the PSD and correlation

function of a process and are reported in the "supporting material" chapter A.4. With these assumptions and relations, it is possible to obtain the PSD of the response as Eq. 2.22:

$$G_u(f) = H^*(f)H(f)G_l(f) = |H(f)|^2 G_l(f) \tag{2.22}$$

The same procedure is also applied to the cross-spectral densities CSDs. This method is a useful tool applied to measure the Transfer Function (TF) $H(f)$ of a structure excited by random vibration. By applying a white noise excitation of duration T to the component and measuring the response at a point it is possible to determine the TF defined by the term to term ratio of the input and output coefficients of the Fourier series. In chapter A.5, three different definition of the TF are presented with different applications.

Finally, the FT method is the most used to determine the PSDs. In 1965, J.W. Cooley and J. Tukey [20] developed a method called the Fast Fourier Transform (FFT), making it possible to reduce considerably the calculation time of the FT. Calculations of PSD are done today primarily using the FFT.

2.1.2 Statistical properties of random process

The works of S.O. Rice [18] and of S.H. Crandall founded the basis for the analysis of the statistical properties of a random signal $l(t)$. A broad-band process is a random stationary process whose PSD $G(f)$ has significant values in a frequency band. A uniform PSD $G(f) = G_0$ representing the wide-band process is specifically called white noise and it assumes to have a uniform density over all frequencies. However, it is a theoretical concept, physically unrealizable (area under the curve would be infinite and hence infinite RMS value). Furthermore, a model widely used in the calculations are the band-limited white noises spectra which approximate many natural random processes. A narrow-band process, instead, is a random stationary process whose PSD has significant values only in one frequency band. In this case, the signal has a function of time $l(t)$ similar to a sine function of frequency f_0 , with amplitude and phase varying randomly. Anyway, this second type of vibratory signals are characterized by only one peak between two zero crossings. The distribution of the instantaneous values for the majority of random vibrations encountered in the real environment can be represented by the Gaussian law. With the assumption of Gaussian process, it is possible to calculate from $G(f)$ many statistical properties using the theory of probability. Defined t_a the time spent in the interval d_a, between a and $a+da$ with $\dot{l}(t) = b$

is: $\frac{p(a,b)dadb}{t_a} = \mid b \mid p(a,b)da$. The average total number of crossings of the threshold a, per unit time, for all the possible values of $\dot{l}(t)$ is written by Eq. 2.23 called "Rice formula", where $n_a^+ = \mid \int_0^{+\infty} p(l,\dot{l}),\ dld\dot{l} \mid_{l=a}$

$$n_a = \int_{-\infty}^{+\infty} \mid b \mid p(a,b)\ db\ = 2n_a^+ \tag{2.23}$$

The only assumption made is of stationary process. Obviously for $a = 0$ $n_0 = 2n_0^+ = \int_{-\infty}^{+\infty} \mid b \mid p(a,b)\ db$ In the case of Gaussian distributed acceleration (0, l_{rms}), the parameters are defined by Eq. 2.24 and 2.25:

$$n_a = \frac{1}{\pi}\frac{\dot{l}_{rms}}{l_{rms}} e^{-\frac{a^2}{2l_{rms}^2}} \tag{2.24}$$

$$n_0 = \frac{1}{\pi}\frac{\dot{l}_{rms}}{l_{rms}} \tag{2.25}$$

Since $l_{rms}^2 = \int_0^{+\infty} G(\Omega),\ d\Omega\ = R(0)$ and $\dot{l}_{rms}^2 = \int_0^{+\infty} \Omega^2 G(\Omega),\ d\Omega\ = -R''(0)[-R^2(0)]$ this results in Eq. 2.26

$$n_a = 2n_a^+ = \frac{1}{\pi}\left[\frac{\int_0^{+\infty} \Omega^2 G(\Omega),\ d\Omega}{\int_0^{+\infty} G(\Omega),\ d\Omega}\right]^{\frac{1}{2}} e^{-\frac{a^2}{2l_{rms}^2}} \tag{2.26}$$

Instead, the quantity n_0^+ is the expected frequency *i.e.,* the frequency at which energy is most concentrated in the spectrum.

$$n_0 = 2n_0^+ = 2\left[\frac{\int_0^{+\infty} f^2 G(f),\ df}{\int_0^{+\infty} G(f),\ df}\right]^{\frac{1}{2}} \tag{2.27}$$

Threshold level crossing curves give, depending on the threshold a, the number of crossings of this threshold with positive slope. These curves can be plotted:(i) either from the time history signal by effective counting of the crossings with positive slope over a duration T. For a given signal, the result is deterministic;(ii) or from the PSD of the vibration, by supposing that the distribution of the instantaneous values of the signal follows a Gaussian law with zero mean. The expected value of the number of threshold crossings a over the duration T is hence determined by Eq. 2.28.

$$N_a^+ = n_a^+ T = n_0^+ T e^{-\frac{a^2}{2l_{rms}^2}} \tag{2.28}$$

The knowledge of $G(f)$ makes it possible to calculate n_0^+ and l_{rms} and then to plot N_a^+ as a function of the threshold value a. In practice, a is generally represented with respect to N_a^+. For $N_a^+ = 1$ a_0 is, on average, the strongest value of the signal observed over a duration T is Eq. 2.29

$$n_0 = l_{rms}\sqrt{2ln(n_0^+)T} \tag{2.29}$$

As demonstrated, many important statistical properties of the signal considered, either excitation or response, can be obtained directly from the PSD $G(\Omega)$ and in particular the from their spectral moments. Defined the random signal $l(t)$, the moment of order n is the quantity determined by Eq. 2.30

$$M_n = E\left\{\left[\frac{d^{n/2}l(t)}{dt^{n/2}}\right]^2\right\} = \lim_{T\to\infty}\frac{1}{2T}\int_{-T}^{+T}\left[\frac{d^{n/2}l(t)}{dt^{n/2}}\right]^2 dt \tag{2.30}$$

The moment of order zero is the square of the RMS value l_{rms} Eq. 2.31 and 2.32

$$M_0 = E[l(t)^2] = \lim_{T\to\infty}\frac{1}{2T}\int_{-T}^{+T} l(t)^2\,dt \;= \overline{l(t)^2} = l_{rms}^2 \tag{2.31}$$

$$M_0 = R(0) = \int_0^\infty G(\Omega)\,d\Omega \;= \int_0^\infty G(f)\,df \tag{2.32}$$

The moment of order two is equal to Eq. 2.33 and 2.34

$$M_2 = E\left[(\frac{dl}{dt})^2\right] = \lim_{T\to\infty}\frac{1}{2T}\int_{-T}^{+T} l(t)^2\,dt \;= \overline{\dot{l}(t)^2} \tag{2.33}$$

$$M_2 = -\ddot{R}(0) = \int_0^\infty \Omega^2 G(\Omega)\,d\Omega \;= (2\pi)^2\int_0^\infty f^2 G(f)\,df \;= \dot{l}_{rms}^2 \tag{2.34}$$

Moreover, the moment of order four is equal to Eq. 2.35

$$M_4 = R^{(4)}(0) = \int_0^\infty \Omega^4 G(\Omega)\,d\Omega \;= (2\pi)^4\int_0^\infty f^4 G(f)\,df \;= \ddot{l}_{rms}^2 \tag{2.35}$$

More generally, the n^{th} moment can be defined as Eq. 2.36 where M_n are the

moments of the PSD $G(\Omega)$.

$$M_n = \int_0^\infty \Omega^n G(\Omega)\, d\Omega \; = (2\pi)^n \int_0^\infty f^n G(f)\, df \; = \ddot{l}^2_{rms} \tag{2.36}$$

Finally, can be easily derived from the preceding relations that:

$$n_0^+ = \frac{1}{2\pi}\left(\frac{M_2}{M_0}\right)^{\frac{1}{2}} \tag{2.37}$$

$$n_a^+ = n_0^+ e^{-\frac{a^2}{2M_0}} \tag{2.38}$$

However, some authors define $M_n = \int_0^\infty f^n G(f)\, df$ which leads to $n_0^+ = \left(\frac{M_2}{M_0}\right)^{\frac{1}{2}}$

To calculate the fatigue damage, it is extremely useful to know also the vibration's average number of peaks per unit time, occurring between two close levels a and $a + da$, as well as the average total number of peaks per unit time. Considering that the average number of minima per unit time of a Gaussian random signal is equal to the average number the maxima per unit time, the distributions of the minima and maxima being symmetric. A maximum occurs when the velocity (derivative of the signal) cancels out with negative acceleration (second derivative of signal). This remark permits to consider the joint probability density between the processes $l(t), \dot{l}(t), \ddot{l}(t)$ to describe the verage number of peaks per unit time of $l(t)$. The assumption is that $l(t)$ is derivable twice.

S.O. Rice [18] showed that, if $p(a, b, c)$, is the probability density so that $l(t), \dot{l}(t), \ddot{l}(t)$ respectively lie between a and $a + da$, b and $b + db$, c and $c + dc$, the average number the maxima located between levels a and $a + da$ in the time interval t, $t + dt$ is Eq. 2.39:

$$\nu_a = -dtda \int_{-\infty}^0 cp(a, 0, c)\, dc \tag{2.39}$$

where, for a Gaussian signal as well as for its first and second derivatives $p(a, 0, c) = (2\pi)^{-3/2} \mid M \mid^{-1/2} e^{-\frac{\mu_{11}a^2 + \mu_{33}c^2 + 2\mu_{13}ac}{2|M|}}$ and with

$$\parallel M \parallel = \begin{Vmatrix} l^2_{rms} & 0 & -\dot{l}^2_{rms} \\ 0 & \dot{l}^2_{rms} & 0 \\ -\dot{l}^2_{rms} & 0 & \ddot{l}^2_{rms} \end{Vmatrix} \tag{2.40}$$

where $l_{rms}^2 = M_0$, $\dot{l}_{rms}^2 = M_2$ and $\ddot{l}_{rms}^2 = M_4$. The determinant $\mid M \mid$ (alaways positive) is written as Eq, 2.41

$$\mid M \mid = M_0 M_2 M_4 (1 - r^2) \tag{2.41}$$

where r is an important parameter called the irregularity factor and determined by Eq. 2.42

$$r = \frac{\dot{l}_{rms}^2}{l_{rms}\ddot{l}_{rms}} = \frac{M_2}{\sqrt{M_0 M_4}} \tag{2.42}$$

The irregularity factor can vary in the interval $[0, 1]$ according to Cauchy-Schwarz's inequality. It follows that, the average number of maxima per second is defined as $\nu_a = n_p^+ q(a) da dt$ and n_p^+ can be also written:

$$n_p^+ = \frac{1}{2\pi}\sqrt{\frac{M_4}{M_2}} \tag{2.43}$$

The probability density of maxima per unit time of a Gaussian signal whose amplitude lies between a and $a + da$ is thus :

$$q(a) = \frac{\sqrt{1 - r^2}}{l_{rms}\sqrt{2\pi}} e^{-\frac{a^2}{2l_{rms}^2(1-r^2)}} + \frac{ra}{2l_{rms}^2}[1 + erf(\frac{ar}{l_{rms}\sqrt{2(1 - r^2)}})] \tag{2.44}$$

where $erf(\cdot)$ is the error function. The statistical distribution of the minima follows the same law. The probability density $q(a)$ is thus the weighted sum of a Gaussian law and Rayleigh's law, with coefficient functions of parameter r.

The irregularity factor r is defined as the ratio between the average number of zero crossings per unit time with positive slope and the average number of positive and negative maxima per unit time: $r = \frac{M_2}{\sqrt{M_0 M_4}} = \frac{n_0^+}{n_p^+}$ The parameter r helps to measure of the width of the noise. In fact, for a broadband process, the number of maxima is much higher than the number of zeros and in this case $r = 0$. For broadband process, the probability density of the peaks then tends towards to a Gaussian law. When the number of passages through zero is equal to the number of peaks, r is equal to 1 and this is the case of narrow-band signal, for which $q(a)$ tends towards a Rayleigh's law. Thus, the value of the parameter r depends on the PSD through the parameters n_0 and n_p (or the moments M_0 , M_2 and M_4). Fig. 2.9 (from [21]) shows the variations of $q(a)$ for different values of the irregularity factor r, from 0 to 1.

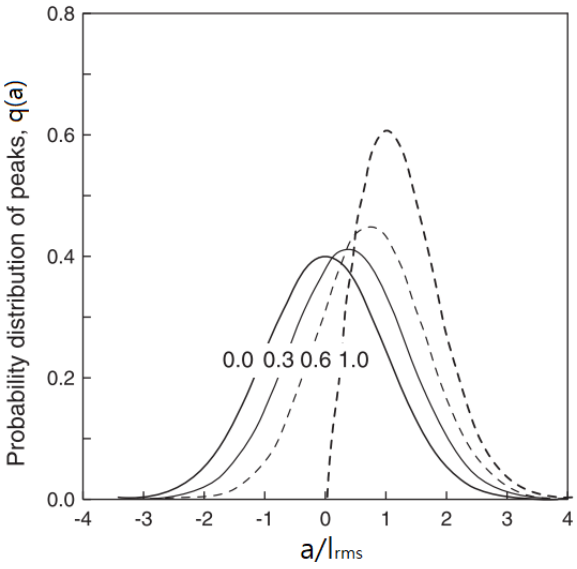

Figure 2.9: Probability distribution of peaks by varying the regularity factor r [21]

In the case of a centered narrow-band normal process ($r \approx 1$), the average of highest peaks, according to A.G. Davenport, is $\overline{u_0} = \int_{-\infty}^{\infty} ue^{-\nu}\, d\nu$ where $u = 2ln(n_0^+ T) - 2ln(\nu)$. For large values of N_p , M.S. Longuet-Higgins showed that an asymptotic expression can be used:

$$\overline{u_0} \approx \sqrt{2ln(n_0^+ T)} + \frac{\epsilon}{\sqrt{2ln(n_0^+ T)}} \tag{2.45}$$

where ϵ is the Euler's constant equal to 0.57721566490. For a wide-band noise ($r \neq 1$), D.E. Cartwright and M.S. Longuet-Higgins showed that the average value of the largest peak in a sample of N_p peaks is equal to

$$\overline{u_0} \approx \sqrt{2ln(rN_p)} + \frac{\epsilon}{\sqrt{2ln(rN_p)}} \tag{2.46}$$

and for large N_p , it is a decreasing function of r. When the spectrum widens, the average value of the highest peak decreases. When $r \to 0$ (Gaussian case), the previous expression can no longer be used and the quantity rN_p becoming small compared to 1.

2.2 Finite Element Model

Random vibrations excite simultaneously all the frequencies of a structure and in contrast to sinusoidal functions, they are made up of a continuous range of frequencies. The amplitude of the signal and its phase vary with respect to time in a random fashion. Thus, the random vibrations are also called noise [19]. In particular, the study concerns random stationary ergodic processes with zero mean and Gaussian distribution. They can be simulated by modal superposition technique with FEMs analysis. Random analysis in Finite Element (FE) software have the modal superposition technique as the basis for the harmonic response analysis. Considering a linear behavior of the component, they are scaled and combined to the input PSDs to get the dynamic response and the stress PSDs. Thus, before the random or harmonic analysis, the modal analysis is essential to understand the dynamic behaviour of the structure. Furthermore, the Steady-State Dynamics (SSD) analysis and the random analysis will be discussed in the following sections. However, the second one can be an useful shortcut in terms of user-friendliness to address the random vibration fatigue analysis, although Abaqus CAE has demonstrated to have some limitation.

Once the FEM model of the component is defined, the structural dynamic analysis has to be performed in order to derive the dynamic stress responses. The idea behind the FEM approach is to use the discrete Multi-Degree-Of-Freedom (MDOF) system to represent such structural components. In the case of dynamic force excitations, the general equilibrium equation of the MDOF system is:

$$M\ddot{u}(t) + C\dot{u}(t) + Ku(t) = F(t) \tag{2.47}$$

where$M$, K, and C are the structural mass, stiffness, and damping matrices, respectively. Moreover, $u(t)$ denotes the absolute displacement vector of the MDOF system and $F(t)$ represents the input force excitation vector. To move to the modal superposition approach, the physical coordinate vector $u(t)$ can be linked with the modal coordinate vector $q(t)$ by the modal decomposition

$$u(t) = \Phi q(t) \tag{2.48}$$

where Φ is the displacement modal shape matrix, which is composed of

the eigenvectors obtained by natural frequency analysis. Using the modal decomposition, Eq. 2.47 can be rewritten as:

$$\Phi^T M \Phi \ddot{q}(t) + \Phi^T C \Phi \dot{q}(t) + \Phi^T K \Phi q(t) = \Phi^T F(t) \tag{2.49}$$

where the symbol T represents the transpose operation. Moving to the frequency domain Eq. 2.49 turns into:

$$(-\omega^2 \Phi^T M \Phi + j\omega \Phi^T C \Phi + \Phi^T K \Phi) q(\omega) = \Phi^T F(\omega) \tag{2.50}$$

where ω is the pulsation. Assuming that the MDOF system has a proportional damping model, Eq.2.50 is decoupled as:

$$(-\omega^2 m_r + j\omega c_r + k_r) q_r(\omega) = f_r(\omega) \tag{2.51}$$

where m_r,k_r,c_r, and f_r denote the r^{th} modal mass, modal stiffness, modal damping, and modal force excitation, respectively. Thus, once the modal responses are computed, the physical responses can be obtained using the modal superposition technique which permit to represent easily all the physical responses of the structure. In particular, the displacement Frequency Response Functions (FRFs) matrix $H_d(\omega)$ of the MDOF system under force excitations is computed as follows:

$$H_d(\omega) = \sum_{r=1}^{N} \frac{\Phi_r \Phi_r^T}{k_r - \omega^2 m_r + j\omega c_r} \tag{2.52}$$

where N denotes the number of degrees of freedom of the MDOF system and Φ_r denotes the r^{th} column vector of the displacement modal shape matrix Φ The dynamic stress responses of the MDOF system, essential for the fatigue analysis, are obtained by:

$$\sigma_s(t) = \Phi^s q(t) = \sum_{r=1}^{N} \Phi_r^s q_r(t) \tag{2.53}$$

where $\sigma_s(t)$ is the stress vector process and Φ^s is the stress modal shape matrix. $q_r(t)$ and Φ_r^s are the r^{th} modal coordinate of the modal coordinate vector $q(t)$ and the r^{th} column vector of the stress modal shape matrix Φ^s ,

respectively. The stress FRF matrix $H_s(\omega)$ of the MDOF system under force excitations can be calculated as:

$$H_s(\omega) = \sum_{r=1}^{N} \frac{\Phi_r^s \Phi_r^T}{k_r - \omega^2 m_r + j\omega c_r} \tag{2.54}$$

However, in the random vibrations environment, the exitation is an acceleration base in form of PSD. Consequently, the stress FRF matrix $H_s(\omega)$ in Eq.2.54 cannot be directly used and the equilibrium equations Eq. 2.47 has to be modified to take into account the case of acceleration base excitations. It can be written as:

$$M\ddot{v}(t) + C\dot{v}(t) + Kv(t) = -MT\ddot{w}(t) \tag{2.55}$$

where $v(t) = u(t) - Tw(t)$ is the relative displacement vector and $\ddot{w}(t)$ denotes the acceleration random base excitation vector, respectively, and T denotes a constant TF matrix. Therefore, in the case of acceleration random base excitations, the stress FRF matrix $H_{as}(\omega)$ turns into:

$$H_{as}(\omega) = -H_s(\omega)MT \tag{2.56}$$

In the FE software, the stress FRF matrix $H_{as}(\omega)$ of the MDOF system is determined trough the frequency response analysis. The relationship between the one-sided response stress PSD matrix, $G_s(f)$, and the one-sided PSD matrix of the random excitation, $G_a(f)$, can be described by the following expression

$$G_s(f) = H_{as}^*(f) G_a(f) H_{as}^T(f) MT \tag{2.57}$$

where $H_{as}(f) = H_{as}(\omega/2\pi)$ and the symbol $*$ represents the complex conjugate operation. For a random stress vector process $\sigma_s(t) = [\sigma_{xx}(t), \sigma_{yy}(t), \sigma_{zz}(t), \sigma_{xy}(t), \sigma_{yz}(t), \sigma_{zx}(t)]^T$, the corresponding one-sided stress PSD matrix, $G_s(f)$, is given as follows

$$G_s(f) = \begin{Vmatrix} G_{11}(f) & \dots & G_{16}(f) \\ \vdots & \ddots & \vdots \\ G_{61}(f) & \dots & G_{66}(f) \end{Vmatrix} \tag{2.58}$$

In order to describe the degree of proportionality between stress components, a stress covariance matrix, C_v, can be introduced as follows:

$$C_v = \begin{Vmatrix} C_{11} & \dots & C_{16} \\ \vdots & \ddots & \vdots \\ C_{61} & \dots & C_{66} \end{Vmatrix} \tag{2.59}$$

where the diagonal term C_{ii} and the non-diagonal term $C_{ij}(i \neq j)$ denote the variance of the stress component and the covariance between the stress components, respectively. More precisely, those diagonal and non-diagonal terms in covariance matrix C_v can be computed as follow

$$C_{ii} = Var(s_i(t)) = \int_0^\infty G_{ii}(f)\, df \tag{2.60}$$

$$C_{ij} = Cov(s_i(t), s_j(t)) = \int_0^\infty Real[G_{ij}(f)]\, df \tag{2.61}$$

Finally, correlation coefficient can be used to quantify the stress component non-proportionality. Such a coefficient $r_{corr,ij}$ can be defined as follow:

$$r_{corr,ij} = \frac{\mid C_{ij} \mid}{\sqrt{C_{ii} C_{jj}}} \tag{2.62}$$

2.2.1 Modal Analysis

Since the vibration fatigue analysis is carried out using a FE model of the structure, it is crucial to create an accurate FE model of the structure. Thus, before studying the response of the structure to random vibration is important to verify the correctness of the model. This can be done by comparing the natural frequencies obtained from experiments and numerical analysis in order to coincide with an acceptable tolerance. Moreover, the mesh quality has to be checked and a mesh convergence analysis must be performed in order to obtain a reliable model for fatigue calculations. Sometimes, some modes are difficult to extract experimentally, due to their low participation factors, especially for high frequencies. A numerical FE modal analysis is performed, using the Lanczos method, to determine the eigenvalues and eigenfrequencies of the structure. Since the dynamic response of a structure can be more easily defined using the mode superposition technique, a classic frequency analysis is thus first performed prior to the vibration fatigue analysis to obtain the natural frequencies and the corresponding mode shapes of the structure. Calculating

the natural frequencies of the structure, it is also possible to understand if the random vibrations are particularly dangerous for the component and hence, it allows to obtain a first insight on the severity of the loading. The closer the load frequencies are to the system resonant frequencies the stronger the dynamic response is. If the highest load frequency is lower than one third of the first system resonant frequency then a pseudo-static solution is acceptable and a random vibration analysis loses sense.

In the modal superposition technique, the problem is projected onto the eigenmodes of the system, which are first extracted from the undamped system, permits to save a lot of calculation time without lose the accuracy. The natural frequencies are obtained from the well known eigensystem $M\ddot{u}(t) + C\dot{u}(t) + Ku(t) = 0$ The natural modes obtained are then linearly combined and used as basis to represent the dynamic steady-state response of the structure to harmonic excitation. This because the eigenmodes represent a orthogonal base across the mass and stiffness matrices. Obviously, the result is more accurate as the number of eigenmodes extracted is increased. The number of eigenfrequencies and eigenmodes necessary to correctly represent the dynamic behavior of the component with a good accuracy should be decided case-by-case. However, analysing the participation factors obtained by the frequency analysis, it is possible to determine the modes with most influence. As general rule, the minimum number of modes to extract should be take as the minimum for which at least 90% of the mass of the structure contributes to all degree of freedom.

Moreover, it is really important to correctly represent the structural damping in the FE model, since the damage is non-linearly related to the difference in damping. A damped vibration system dissipates energy trough friction, heat or sound. In real structures, the damping mechanism can be of different forms and usually more than one form can be present simultaneously. Harmonic modal analysis can be used directly to solve the forced vibration equation of motion Eq. 2.47, however four damping models can be used in modal superposition procedures. A frequently used model to represent the the damping matrix $[C]$ is the proportional damping, also called Rayleigh damping. The damping matrix is written as linear combination of the mass matrix $[M]$ and the stiffness matrix $[K]$, $[C] = \alpha[M] + \beta[K]$, where α and β are constants. A second model is represented as fraction of the critical damping. The damping for each eigenmode can be specified or otherwise, a fraction of the critical damping can be considered for each specified frequency.

Critical damping is defined as $c_{cr} = 2\sqrt{mk}$ where m is the mass of the system and k is the stiffness of the system. A third model is the composite modal damping. A damping factor is defined for each material in the model, as a fraction of critical damping. These factors are then combined into a damping factor for each mode. The last model is the structural damping which assumes that the damping forces are proportional to the forces caused by stressing of the structure and are opposed to the velocity. Therefore, this form of damping can be used only when the displacement and velocity are exactly $90°$ out of phase. Thus, it can be applied only when the excitation is purely sinusoidal, as in SSD analysis. The damping forces are then $F_D = isI$ where F_D are the damping forces, $i = \sqrt{-1}$, s is the user-defined structural damping factor, and I are the forces caused by stressing of the structure. However, structural damping can be defined only for mode-based SSD analysis.

2.2.2 Dynamic Analysis for random vibrations

Once the FE model is constructed and verified with experiments. Usually the input excitation are obtained for example from flight tests or are provided by the regulations. To find the stress response of the system to the input excitation necessary for the fatigue calculation, the system is assumed to behave linearly. The response function can be then found by multiplying the input load with the square of the TF:

$$PSD_{response} = \mid TF \mid^2 PSD_{input} \tag{2.63}$$

In order to obtain the TF by means of FE software, an Harmonic Response Analysis needs to be performed with unit gravity base excitation input. The analysis permits to obtain the stress tensor at each frequency. Since in the most general case, the structures are characterized by a multi-axial stress state, there is a need for a method to combine the stresses. To address this problem several multi-axial stress criteria described in the next section can be adopted. Once theTF is obtained, the stress PSD it is easily obtained by Eq. 2.63. The stress PSD include both the input loading and the system's dynamic behavior. It holds very important statistical parameters for fatigue calculation with spectral methods. A stationary ergodic random load is characterized in the frequency domain by its PSD. This frequency spectrum contains all the statistical information characterizing the random load and it allows to estimate the expected in-service load cycle distribution and fatigue damage. In addition, in many cases, spectral methods are more convenient since sometimes problems are already defined in the frequency-domain [22]

(frequency spectra of wind, sea waves or the roughness of the road) or the frequency spectrum can be found into regulations, as for example test specification, as the MIL-STD 810 standards for the aviation industry. The calculated response frequency spectrum it is used to address the calculation of the fatigue damage through its statistical properties and PDFs. [4] [23]

2.2.2.1 Frequency Response Functions

Following the previous sections, the FT is the basis for the frequency domain analysis where the signal is rewritten as a sum of simple sine and cosine functions and the frequency content is exposed. Following Eq. 2.63, if a component can be modeled as a linear system, its response is represented by the FRF which translates the input $x(f)$ into the output $y(f)$, as represented by figure 2.10

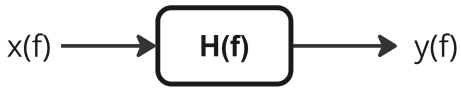

Figure 2.10: Transfer Function

FEM are often employed to determine the FRFs and as described above, for non-deterministic loading (as random vibrations), the best way to represent them is by means of PSDs. The PSD at a discrete frequency can be related to the Fourier coefficients by $G_x(f_k) = 2TX_k^*X_k$ where X^* is the complex conjugate of X and G is the PSD function. Similarly, the CSD functions can also be derived:$G_{yx}(f_k) = 2TY_k^*X_k$ and $G_{xy}(f_k) = 2TX_k^*Y_k$. Hence, the FRFs are complex functions, represented by real and imaginary components or magnitude and phase angle pairs. The Harmonic Response Analysis is used to find the transmissibility plots, *i.e.,* the TF at each node of the structure. To do this, an unit g base excitation input is applied to the structure. The frequency range is the same as the frequency rage of the excitation. It is important to correctly define the damping ratios of each mode, especially if the resonant frequency are exited. The modal superposition harmonic analysis combines the modal results with the modal participation factors to compose the FRFs. The methodology is straightforward, fast and efficient in terms of data storage. The stress PSDs are composed by ASDs which correspond to the diagonal terms (PSD_{ij} with i = j) and the CSDs which correspond to the out of diagonal components (PSD_{ij} with $i \neq j$). ASDs and CSDs components

are complex numbers but ASDs possess only a real part. The CSDs describe the relationship between loading channels *i.e.,* the correlation.
For example, the commercial software Abaqus can be used to carry out the modal analysis and SSD modal analysis. A mesh convergence test and a mesh quality check are performed during the modal analysis since they can affect the results of the subsequent SSD modal analysis and hence the fatigue analysis. However, since Abaqus lack in the fatigue analysis, the results, including the mode shapes and their TFs, are transferred to another software, as Fe-safe. Fe-safe linearly combines the TFs with the input load PSD to obtain the stress PSD, of each element in the FE model, needed to address the fatigue calculation.

2.2.2.2 Random Analysis

Random vibration analyses are performed frequently and in practical cases by means of commercial FE codes. The most common analyses are those wherein the ASDs (and sometimes CSDs) of stationary excitation random processes are specified, and then the response ASDs and CSDs are computed. As described above, the FRFs characterize the structure and they can be derived from an applied harmonic input by means of measurements or FEMs. The SSD analysis is an extension of FRF function where the steady state response of a structure is determined considering an harmonic excitation spectrum *i.e.,* the input excitation can be a complex variable and both the amplitude and the phase angle of the excitation are considered. Random Vibration analysis is similar to the Harmonic Response Analysis, in fact, it adopts the same strategy to obtain the dynamic response of the structure. The only difference is that instead of applying a unit g base excitation input, the complete input PSD of the excitation is applied. Considering that the structrure behaves linearly, the solver takes advantage of the harmonic response analysis and linearly combine the response with the input PSD, in order to obtain the stress PSDs, for each element in the FE model. These stress PSDs are then directly employed for the fatigue calculation.

2.3 Multi-axial Criteria for Fatigue Analysis

Engineering components under in-service conditions often experience complex multi-axial stress with random amplitudes. A wide range of multi-axial criteria in the time-domain are available in literature for fatigue life estimation. However, the amount of methods specifically reformulated in

the frequency-domain remain quite scarce due to the complexity to translate them in statistical parameters based on spectral quantities. Fatigue strength assessment in metallic structures can be carried out with reference to infinite life (fatigue limit) or finite life (fatigue strength as a function of the number of loading cycles, and S-N curves described by either Basquin's equation for HCF).

Traditionally, fatigue can be studied with two different approaches: strain-life approach, typical of Low-Cycle Fatigue (LCF) (below $10^3 - 10^4$ cycles), which considers plastic deformations in region of high stress and stress-life approach, typical of HCF. This second approach is adopted in this study, since considering a linear behaviour of the structure, the random loading is characteristic of HCF, with low stress levels, far below the yield stress, and relatively high number of cycles. How described above, FEM software permits to easily discretize the component studied into elements and calculate the stress response at each node of the structure. The stress-life approach results, hence, the most appropriate for random vibration loading and by using the stress PSD tensor, the fatigue damage of each element can be obtained through fatigue analysis.

Differently from sinusoidal loading or narrow-band loading, in broad-band loading conditions, as random vibrations, the definition of a cycle is not obvious and a criterion must be used to identify the cycles [11]. The most efficient counting method in time domain is the rain-flow method. However, the explicit correlation between the PSD of a random process and the PDF of cycles counted by the rain-flow method is not known analytically and a exact solution exist only for narrow band process. This fact results from the complexity of cycle extraction rules which define the rainflow algorithm, that make the relationship between the rainflow cycle distribution and the PDFs too complicated. However, the approximate solutions found by Dirlik [24] and Tovo-Benasciutti [25], through fitting techniques, are widely used in many sectors and they have demonstrated to achieve better results compared to other methods that employ a correction factor to the narrow-band method. For these reasons, the Bendat narrow-band method [3] and the Dirlik and Tovo-Benasciutti methods will be studied in this thesis. The other type of criteria investigated are the infinite-life criteria. In particular, the Crossland [9] [5], Matsubara [10] and Sines [8] criteria, that do not employ counting methods, will be investigated and compared to the others. These fatigue criteria are based on stress invariant and they were developed in the frequency domain

from the same criteria previously defined in the time domain. A brief review on the critical plane methods will be covered but they will be left as future work on this filed, since the lower computational time of the other methods has determined their preference [26]

2.3.1 Fatigue-limit criteria

Finite-life methods belong to the damage tolerant approach and they are based on the classical Wöhler curve. Most of them are based on the definition of an equivalent uni-axial stress, as the equivalent Von Mises stress. Hence, to deal with realistic fatigue loading, there is a need for multi-axial criteria, reliable cycle counting methods as well as damage accumulations rules. The use of equivalent uni-axial loading to represent complex multi-axial stress states permitted to use spectral methods in frequency-domain for uni-axial variable amplitude fatigue. Three different methods (Equivalent Von Mises, Equivalent Lemaitre and Projection by Projection) are presented and developed into the plug-in tool.

2.3.1.1 Equivalent Von Mieses

It is assumed that the fatigue damage under multi-axial loading can be predicted by calculating an equivalent uni-axial stress on which the classical uni-axial random fatigue theory is applied. Preumont and Piefort (1994) [5] presented a method for determination of the PSD of the equivalent stress using the Huber-Mises-Hencky hypothesis. To present the method, the case of the plane stress state is considered. Under this condition, the equivalent stress takes the form

$$\sigma_{eq}^2 = \sigma_{xx}^2 + \sigma_{yy}^2 - \sigma_{xx}\sigma_{yy} + 3\sigma_{xy}^2 = \sigma^T Q_M \sigma = tr\{Q_M[\sigma\sigma^T]\} \tag{2.64}$$

After defining the vector of stress tensor components $\sigma = [\sigma_{xx}, \sigma_{yy}, \sigma_{xy}]^T$ where

$$Q_M = \begin{Vmatrix} 1 & -0.5 & 0 \\ -0.5 & 1 & 0 \\ 0 & 0 & 3 \end{Vmatrix} \tag{2.65}$$

is the matrix of coefficients for the Huber-Mises-Hencky equivalent stress under the plane stress state and $tr\{\dots\}$ is the trace operator. The quadratic nature of the relationship between Von Mises stress and stress components implies several problems: (i) the Von Mises stress is not Gaussian, nor zero

mean, (ii) it is always positive and does not reduce itself to the applied alternating stress in the simple uni-axial case and (iii) its frequency content is not consistent with that of the stress components. These problems can be overcome moving in the frequency domain and in particular:

$$E[\sigma_{eq}^2] = \sigma^T Q_M \sigma = tr\{Q_M E[\sigma\sigma^T]\} \tag{2.66}$$

Thus, the obtained formula presents the mean-square value of the reduced stress. The mean-square value can be also determined directly from the matrix of PSDs of the stress tensor

$$E[\sigma_{eq}^2] = \int_0^\infty G_{eq}(f)\, df \; = \int_0^\infty tr\{Q_M G_\sigma(f)\, df \tag{2.67}$$

where $G_\sigma(f)$ is the matrix of ASDs and CSDs of the stress vector σ. On the basis of the preceding formulae, Preumont and Piefort [9] postulated a method for determination of PSD of the equivalent stress directly from the matrix of PSD of the stress vector:

$$G_{eq}(f) = tr\{Q_M G_\sigma(f)\} \tag{2.68}$$

This criterion can be related only to materials for which the coefficients of inclination of Wöhler's curves for tension-compression and torsion are equal and the fatigue characteristics of the material satisfy the following equality $\sigma_{aN} = \sqrt{3}\tau_{aN}$, where σ_{aN} and τ_{aN} are amplitudes read out from Wöhler's curves for a constant number of cycles. Determining the reduced PSD using Eq. 2.68, the interactions between the stress components σ_{xx} and σ_{xy} as well as σ_{yy} and σ_{xy} are not taken into account because of the zeros in the coefficient matrix Q_M which is the second downside property of this method.

2.3.1.2 Equivalent Lemaitre

Ge, Sun and Zhou in [6] proposed a novel multi-axial frequency domain method based on stress invariant, considering the effect of hydrostatic stress. It is based on the equivalent Lemaitre stress and multiaxial S–N curve, in order to estimate the fatigue life under multi-axial random loading. A new formula for the stress invariant that includes the effect of hydrostatic stress was proposed. The equivalent stress defined by Lemaitre and Desmorat [27]

in damage mechanics is:

$$\sigma_{eq}^{*} = \sigma_{eq}\left[\frac{2}{3}(1+\nu) + 3(1-2\nu)\left(\frac{\sigma_m}{\sigma_{eq}}\right)^2\right]^{1/2} \tag{2.69}$$

where ν is the Poisson's ratio of the material, σ_{eq} is the Von Mises stress and σ_m is hydrostatic stress. Following the same procedure as the equivalent Von Mises stress, the equivalent Lemaitre stress in frequency domain can be written as:

$$G_{eq}(f) = tr\{Q^{*}G_{\sigma}(f)\} \tag{2.70}$$

where Q^{*} is defined as Eq. 2.71 where, if the Poisson's ratio is 0.5, the equivalent stress becomes equivalent to the equivalent Von Mises.

$$Q^{*} = \begin{Vmatrix} 1 & -\nu & -\nu & 0 & 0 & 0 \\ -\nu & 1 & -\nu & 0 & 0 & 0 \\ -\nu & -\nu & 1 & 0 & 0 & 0 \\ 0 & 0 & 0 & 2(1+\nu) & 0 & 0 \\ 0 & 0 & 0 & 0 & 2(1+\nu) & 0 \\ 0 & 0 & 0 & 0 & 0 & 2(1+\nu) \end{Vmatrix} \tag{2.71}$$

Moreover, to predict the fatigue life in the multi-axial case, a reference S–N curve is used. In particular, the materials' fatigue life under multi-axial cyclic loading can be represented by a new S–N curve which keeps a linear relation in the logarithmic graph between the equivalent Lemaitre stress amplitude σ_{eq} and the number of cycles to failure N, as shown described in the section 2.5.1. The reference S–N curve can be obtained from the fully-reversed axial and torsional loading by linear interpolation using a parameter ρ. A statistical expression of ρ in frequency domain is:

$$\rho = \frac{3\hat{\sigma}_m}{\hat{\sigma}_{eq}} = \frac{3\sqrt{M_{0,m}}}{M_{0,eq}} \tag{2.72}$$

where σ_m and σ_{eq} can be calculated from the 0^{th} spectral moment of PSD in frequency domain as showed by Eq. 2.72. The reference S–N curve is then obtained following the method proposed by Susmel and Lazzarin [15] and described in 2.5.1.

2.3.2 Infinite-life criteria

The second type of criteria are called infinite-life criteria and they belong to the safe-life approach. They are used to understand the risk of fatigue problem and hence if the stress levels are critical or not. Endurance limit has its common accepted definition is the stress level leading to the initiation of macroscopic crack, which is usually observed after about $N_e = 10^7$ cycles. The extension of this concept to multiaxial stress states implies a separation of the stress space into two parts, the unsafe one and the safe one. The safe part contains the origin and is bounded by a closed surface defined by the fatigue criterion. The stress tensor $\sigma_{ij}(t)$ at a location in the structure is a periodic function of time and a fatigue criterion can be defined as a function g such that: $g(\sigma_{ij}(t)) < 1$ for $t \in [0, T]$. If the inequality is satisfied at every point of the structure, no fatigue cracks will initiate before N_e. Many fatigue criteria have been developed over the past decades. Some of these criteria are based on global approach using stress invariants such as the hydro-static pressure and the Von Mises stress.
Most of the existing multi-axial fatigue limit criteria are formalized as a linear combination of a generalized shear stress amplitude C_a and a normal stress N:

$$C_a + kN \leq \lambda \tag{2.73}$$

where k e λ are material constants. The main difference among all the different criteria is how the shear and normal stress terms are defined. In critical plane criteria (*e.g.,* Findley, Matake, Carpinteri-Spagnoli) C_a and N represent the shear and the normal stresses calculated on the critical plane, while in stress-invariant based criteria (*e.g.,* Sines, Crossland, Matsubara) C_a is the amplitude of the square root of the second invariant of the stress deviator, while N is the hydro-static stress. The combination of shear an normal stresses defines a loading path Ψ. It can be closed (*e.g.,* for periodic loading) or entangled (*e.g.,* for random loading). Thus, as shown by Fig. 2.11, if the loading path Ψ remains under the line defined by the infinite-life criteria, it means that no fatigue cracks will occur and the loading path is in the safe region (A). Otherwise, if the loading path cross the line, it switch into the unsafe region (B) and hence, a fatigue crack might initiate and grow.

2.3.3 Sterss-invariant criteria

This type of multi-axial criteria is based on the second invariant of the deviator stress tensor. Crossland's criterion is one of the most known and it has been first reformulated in frequency-domain by Preumont [9], by adopting the

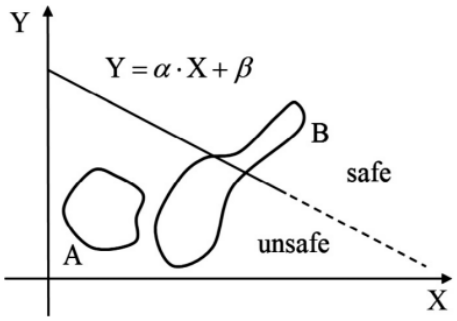

Figure 2.11: Representation of the safe and unsafe regions for the safe-life criteria

same statistical definition of Minimum Circumscribed Circle (MCC) method used for Matake's criterion. Lately, another stress invariants multi-axial criterion has been proposed and it is called "Projection-by-Projection", since the damage of the stress path $d(\psi)$ is computed by summing-up the damage values of stress projections ψ_i in a "principal reference frame" of maximum variance. Differently from Crossland's criterion, this method belongs to the finite-life approach and it provides a closed form analytical expression to compute the fatigue damage of multi-axial stress, which depends on the uni-axial spectral method used to estimate damage $d(\psi)$ for each projection. There are common parameters used among the different stress invariants criteria. These are: the stress deviator related to the second stress tensor invariant and the hydrostatic pressure related to the first stress tensor invariant. The stress deviator can be calculated by means of the Equivalent Von Mises stress method proposed by Preumont and Piefort [5] Eq. 2.68. The PSD of equivalent stress is computed using full spatial PSD matrix and the Von Mises coefficient matrix of the form:

$$Q_M = \begin{Vmatrix} 1 & -0.5 & -0.5 & 0 & 0 & 0 \\ -0.5 & 1 & -0.5 & 0 & 0 & 0 \\ -0.5 & -0.5 & 1 & 0 & 0 & 0 \\ 0 & 0 & 0 & 3 & 0 & 0 \\ 0 & 0 & 0 & 0 & 3 & 0 \\ 0 & 0 & 0 & 0 & 0 & 3 \end{Vmatrix} \tag{2.74}$$

The PSD of the stress deviator can be obtained from the PSD of Von Mises stress $G_{sd}(f) = \frac{G_{eqMH}(f)}{\sqrt{3}}$. Similarly, the Hydrostatic pressure can be computed using the same methodology for Equivalent Von Mises stress, Eq.

2.68, following the formula:

$$G_{eqH}(f) = tr\{Q_h G_\sigma(f)\} \tag{2.75}$$

where

$$Q_h = \frac{1}{9}\begin{Vmatrix} 1 & 1 & 1 & 0 & 0 & 0 \\ 1 & 1 & 1 & 0 & 0 & 0 \\ 1 & -1 & 1 & 0 & 0 & 0 \\ 0 & 0 & 0 & 0 & 0 & 0 \\ 0 & 0 & 0 & 0 & 0 & 0 \\ 0 & 0 & 0 & 0 & 0 & 0 \end{Vmatrix} \tag{2.76}$$

The first stress tensor invariant is directly related to the hydrostatic pressure $G_I(f) = 9G_{eqh}(f)$

2.3.3.1 Projection by Projection

In 2008 Cristofori proposed a method to determine the damage based on the second invariant of the stress-tensor deviator and in 2011 it was reformulated for the frequency domain. The stress invariant $S_{inv} = [S_1, S_2, S_3, S_4, S_5]^T$ is defined in the E_5 Euclidean space (the deviatoric five-dimensional space of Ilyushin) according to $S_1 = \frac{\sqrt{3}}{2}\sigma_{xx}$, $S_2 = \frac{1}{2}(\sigma_{yy} - \sigma_{zz})$, $S_3 = \sigma_{xy}$, $S_4 = \sigma_{xz}$, $S_5 = \sigma_{yz}$ where $\sigma = [\sigma_{xx}, \sigma_{yy}, \sigma_{zz}, \sigma_{xy}, \sigma_{xz}, \sigma_{yz}]^T$ are the components of the stress-deviator tensor, defined together with the hydrostatic stress s_h: $s = \sigma + Is_h$ where I is the identity matrix. The essence of the method is the transformation of the CSD matrix $S_{inv} = s_{inv}s_{inv}^T$ into the sub-space of eigenvectors of the stress invariant covariance matrix C'. For this purpose, the eigenvectors U of C' are obtained, which can be used to transform C' into a diagonal matrix C_0'

$$C = \begin{Vmatrix} \sigma^2_{xx,xx} & \cdots & \sigma^2_{xx,yz} \\ \vdots & \ddots & \vdots \\ \sigma^2_{yz,xx} & \cdots & \sigma^2_{yz,yz} \end{Vmatrix} \tag{2.77}$$

and $C_0' = U^T C U$ and are applied to the frequency-domain, stress-state definition $G_{inv}(\omega)$, yielding the transformed matrix of $G_u(\omega)$: $G_u(\omega) = U^T G_{inv}(\omega) U$ A group of five uncorrelated uni-axial processes $\Psi_i(\omega)$ is thus defined. Each process is treated separately and the damages $d(\Psi_i)$, calculated using a chosen spectral moment method are then summed according to a

quadratic damage-accumulation rule:

$$d(\Psi) = [\sum_{i=1}^{5} (d(\Psi_i))^{\frac{2}{k_{ref}}}]^{\frac{k_{ref}}{2}} \tag{2.78}$$

where k_{ref} defines the slope of the reference S-N curve, derived from the axial ($J_{A,axi}$,k_{axi}) and torsion ($J_{A,tor}$, k_{tor}) S-N curves via the following linear interpolation derived from the Susmel modified S-N curve (defined in section 2.5.1), where the reference stress ratio is determined from the load characteristics using:

$$\rho_{ref} = \sqrt{3} \frac{\sqrt{2M_{0,h}}}{\sqrt{2\sum_{i=1}^{5} M_{0,i}}} \tag{2.79}$$

As shown by Fig. 2.12, the method, by means of a rotation of the reference system, fundamentally projects the loading into multiple completely uncorrelated loading where the damage can be calculated for each projection using the spectral methods for uni-axial loading. Finally, to determine the damage of the whole loading, the quadratic combination is used considering the modified S-N curve. The method has shown to provide highly accurate

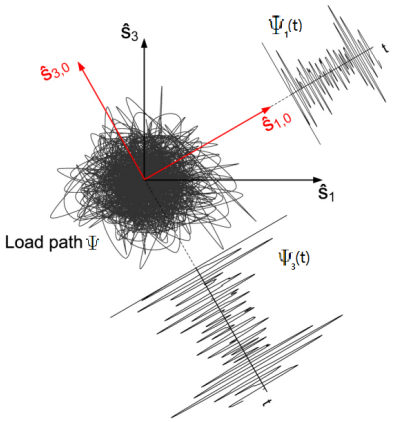

Figure 2.12: Example of random loading path Ψ in two-dimensional deviatoric space and its projections Ψ_1 and Ψ_2 [7]

estimates for constant amplitude multi-axial loadings regardless of the degree of proportionality, and it is also equally applicable to variable amplitude multi-axial loadings. The Projection by Projection (PbP) method then gives a simple interpretation to the problem of cycle identification in variable amplitude

multiaxial loadings, with a strong simplification in overall fatigue damage evaluation. The theoretical framework behind the PbP method easily allowed the formulation in frequency-domain. The frequency-domain PbP criteria considers a 5-dimension Euclidean space of the path Ψ is mapped by the tip of stress vector $s(t)$. The loading path Ψ is first projected along the axes of a principal reference frame S_0 in the deviatoric space, which is located by the eigenvectors U of covariance matrix C' of the deviator stress vector $s(t)$: $C_0 = U^T C' U$. The projection of multi-dimensional path Ψ along fixed directions results in a set of distinct uni-axial loading $\Psi_{p,i}(t)$. The damage due to each projection is then evaluated considering the uni-axial spectral method as for the equivalent uni-axial PSD. A unique reference curve in a modified Wöhler diagram, according to the Susmel method reported in the section 2.5.1, is considered and the Palmgren–Miner linear accumulation rule ia adopted to determine the damage intensity $d(\Psi_{p,i})$ for i^{th} projected loading is calculated. Finally, a quadratic accumulation rule applied to the damages $d(\Psi_{p,i})$ is used to obtain the damage for the complete loading path Ψ. This above accumulation rule was recognized to be appropriate by many authors, since it accounts for the load non-proportionality, as well as it employs a non linear combination rule to handle damaging events occurring at the same time instant on different projected loading.

2.3.3.2 Crossland

One of the more widely used criteria for infinite-life fatigue calculation has been proposed by Crossland. Comparison studies report that Crossland's criterion can be in error from -30% to +15% with respect to experiments. The Crossland's criterion in the time domain is written as

$$\frac{\sqrt{J_{2,a}} + \alpha Max[p(t)]}{\beta} \leq 1 \tag{2.80}$$

where $\sqrt{J_{2,a}}$ is the maximum amplitude of the second invariant of the stress deviator defined following the MCC and $p(t)$ is the hydrostatic pressure. $Max[\cdot]$ stands for maximum value over the period $[0, T]$. The following figure, Fig. 2.13, shows an example of MCC and Minimum Circumscribed Ellipse (MCE) definition for a random loading path. Both, the deterministic defimition in the time domain and the statistical definition are represented. In the frequency domain the contribution of the stress deviator can be obtained from the Equivalent Von Mises stress process $\sqrt{J_{2,a}} \simeq \nu_c \sigma_c / \sqrt{3}$ where $\sigma_{eq} = \{E[s_{eq}^2]\}^{1/2}$ is the standard deviation and ν_c is the peak factor over

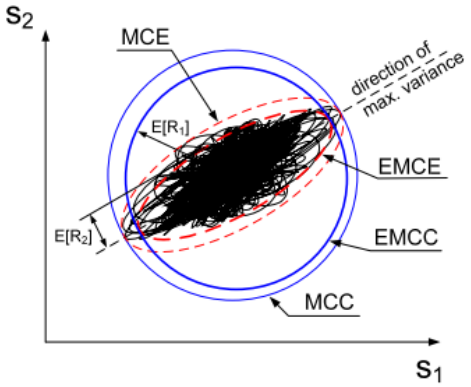

Figure 2.13: Example of Minimum Circumscribed Circle (MCC) and Minimum Circumscribed Ellipse (MCE) definitions for a random loading path. The Expected Minimum Circumscribed Circle (EMCC) and Expected Minimum Circumscribed Ellipse (EMCE) refer to the statistical definition in the frequency domain [28]

the observation period and defined as the extreme value of the process normalized with respect to the standard deviation. In the bidimensional case the hydrostatic pressure $p = (s_x + s_y)/3$ and hence $Max[p(t)] \simeq \nu_p \sigma_m$ where ν_p is the peak factor of the hydrostatic pressure and σ_m is its standard deviation. So, Pitoiset et al. [9] redefined the criterion proposed by Crossland as follows:

$$\frac{\sigma_{eq} F(2N_1)/\sqrt{3} + \alpha \sigma_m F(N_2)}{\beta} \leq 1 \tag{2.81}$$

where: σ_{eq} and $2N_1$ are the standard deviation and expected number of half-cycles of the Equivalent Von Mises stress and N_2 is the number of cycles of the hydrostatic pressure; $F(\cdot)$is the function for amplitude extremes according Davenport, see Eq. 2.46;

$$\alpha = \frac{t_1 - f_1/\sqrt{3}}{f_1/3} \tag{2.82}$$

$$\beta = t_1 \tag{2.83}$$

α and β are Crossland's multi-axial fatigue criterion coefficients, respectively.

2.3.3.3 Matsubara

An other stress-invariant criterion similar to Crossland and that belongs to the infinite-life approach is the Matsubara's criterion for multi-axial fatigue

damage, developed by Mastubara. The criterion is represented in Eq. 2.84 where α and β are constants related to material. f_1 defines the fully reversed axial fatigue limit and f_m is the true fracture strength which is defined as the fracture load divided by the actual final cross-sectional area. Matsubara assumes that f_m can be substituted by 1.84 times the tensile strength R_m (f_m = 1.84 R_m). So, the Matsubara's criterion is:

$$\frac{\sqrt{J_{2,a}} + \alpha S_{max}}{\beta} \leq 1 \tag{2.84}$$

$$\alpha = \frac{f_1}{\sqrt{3}} \frac{1}{f_m - f_1} \tag{2.85}$$

$$\beta = \frac{f_1}{\sqrt{3}} \frac{f_m}{f_m - f_1} \tag{2.86}$$

Matsubara's criterion consists of two parameters that governs crack initiation: $\sqrt{J_{2,a}}$ and initial crack growth S_{max} . The crack initiation parameter, $\sqrt{J_{2,a}}$, is the equivalent shear stress amplitude follows that in Li criterion which is the same as that proposed by Crossland following the MCC criteria but with different definition of $\sqrt{J_{2,a}}$. In fact, the crack initiation parameter in Matsubara's criterion is dominated solely by the shear stress amplitude. S_{max} is the parameter proposed by Matsubara which defines the crack growth. It is considered to be controlled by the maximum of the stress intensity factor range.The crack in stage II grows perpendicularly to the maximum principal stress direction. Hence, S_{max} is defined as follows: among the cyclic normal stresses on all the planes at a evaluate area, the cyclic normal stress with the maximum stress range is selected.
Considering a structure with linear behaviour and subject to stationary ergodic Gaussian loads. The Matsubara's criterion can then be defined in the ferquency domain by:

$$\frac{E[\sqrt{J_{2,a}}] + \alpha E\_S_{max}}{\beta} \leq 1 \tag{2.87}$$

For zero mean stress value, E_S_{max} can be determined as follow: for each normal stress, the mean value of the extreme of the Gaussian process over the observation period T is calculated. The maximum of these mean values are then estimated by applying the peak factor theory and it defines E_S_{max}. In fact, since $s(t)$ is a zero mean stationary Gaussian, random process, E_S_{max}

can be obtained, according to Davenport, as:

$$E[max(s_{ii})] \simeq \sigma_{sii}\sqrt{2ln(N_p(s_{ii})} + \frac{0.5772}{\sqrt{2ln(N_p(s_{ii}))}}\ i = x, y, z \tag{2.88}$$

Then, E_S_{max} obtained by applying

$$E\_S_{max} = max_i(E[max(s_{ii})]);\ i = x, y, z \tag{2.89}$$

2.3.3.4 Sines

The main purpose of multi-axial fatigue criteria is to determine the location of the critical point in a structure. As seen for the others stress-invariant criteria, it can be assumed that the crack initiation is governed by the second invariant of the deviator stress tensor. The same assumption is considered also in the Sines criterion where $J_{2,a}$ is the second invariant of the deviator stress tensor. The Sines criterion in the time domain is written as:

$$\frac{\sqrt{J_{2,a}} + \alpha E[p(t)]}{\beta} \leq 1 \tag{2.90}$$

Where $p(t)$ is hydrostatic pressure which is determined by the normal stresses components S_{xx}, S_{yy} and S_{zz} of the stress tensor S_{ij} and α and β are constants related with the material. For the Sines criterion, they are defined by the endurance limit in alternating traction f_1, the endurance limit in alternating torsion t_1 and the breaking strength R_m

$$p(t) = \frac{1}{3}(S_{xx} + S_{yy} + S_{zz}) \tag{2.91}$$

$$\alpha = \frac{3t_1(R_m + f_1)}{f_1 R_m} - \sqrt{6} \tag{2.92}$$

$$\beta = t_1 \tag{2.93}$$

As can be noted, the Crossland's criterion need the calculation of maximum of the hydrostatic pressure while the Sines criterion uses it's mean, reducing the calculation time. Moreover, the crack will not initiate before N_e repetitions of the periodic random load of duration T if the average of the damage should not exceed the fatigue limit. Thus, the Sines criterion is defined then by Eq.

2.94 in the frequency domain:

$$\frac{E[\sqrt{J_{2,a}}] + \alpha E[p(t)]}{\beta} \leq 1 \tag{2.94}$$

To determine of the average of the shear stress amplitude $E[\sqrt{J_{2,a}}]$, Lambert proposes a strategy of calculation of $E[\sqrt{J_{2,a}}]$. This strategy is based on two steps: the first one is to replace the number of up-crossings of level zero N_0 by the number of maxima N_p. This allow to considerate the width of the band. For a proportional loading, $\sqrt{J_{2,a}}$ can be defined by:

$$\sqrt{J_{2,a}} = \sqrt{\frac{1}{6}[(S_{xx,a} - S_{yy,a})^2 + (S_{yy,a} - S_{zz,a})^2 + (S_{zz,a} - S_{xx,a})^2 + 6(S_{xy,a} - S_{yz,a} - S_{xz,a})^2]} \tag{2.95}$$

To facilitate the calculation of $J_{2,a}$, the trasformation in the Euclidean space (similar to the Projection by Projection approach in 2.3.3.1) is commonly used:

$$\sqrt{J_{2,a}} = \sqrt{D_{1,a}^2 + D_{2,a}^2 + D_{3,a}^2 + D_{4,a}^2 + D_{5,a}^2} \tag{2.96}$$

$D_{1,a} = \frac{\sqrt{3}}{2}(\frac{2}{3}S_{xx} - \frac{1}{3}S_{yy} - \frac{1}{3}S_{zz})$, $S_2 = \frac{1}{2}(S_{yy} - S_{zz}), S_3 = S_{xy}, S_4 = S_{xz}, S_5 = S_{yz}$. For a non-proportional load, the expression is not available. For this reason, many approaches have been proposed in order to determinate $\sqrt{J_{2,a}}$. The same method used in the Matsubara's criterion, proposed by Bin li. With reference to Fig. 2.13, it considers the smallest ellipse of the semi-axes R_1 and R_2 circumscribing the path of $\sqrt{J_{2,a}}$ to realize the non-proportional loading. Thus, $\sqrt{J_{2,a}}$ is approached by $\sqrt{J_{2,a}} = \sqrt{R_1^2 + R_2^2}$. To determine the equivalent shear stress amplitude, the semi-axes R_1, R_2,R_3,R_4 and R_5 of the five-dimension ellipsoid circumscribed to the loading path of $\sqrt{J_{2,a}}$ are considered and oriented in its principal directions. $\sqrt{J_{2,a}}$can then be written as well $\sqrt{J_{2,a}} = \sqrt{R_1^2 + R_2^20 + R_3^2 + R_4^2 + R_5^2}$. So, for a random load, the estimation of $J_{2,a}$ consists in the estimation of the semi-axes R_i. Thus, similar to the Projection by Projection approach, this can be done by the analysis of the principal components of the covariance matrix C' of the stress invariant PSD in the Euclidean space S_{inv}. C' can also be defined from the covariance

matrix of the stress C_v as follow: $C' = PC_vP^T$ with

$$P = \begin{Vmatrix} \frac{\sqrt{3}}{3} & -\frac{\sqrt{3}}{6} & -\frac{\sqrt{3}}{6} & 0 & 0 & 0 \\ 0 & \frac{1}{2} & -\frac{1}{2} & 0 & 0 & 0 \\ 0 & 0 & 0 & 1 & 0 & 0 \\ 0 & 0 & 0 & 0 & 1 & 0 \\ 0 & 0 & 0 & 0 & 0 & 1 \end{Vmatrix} \tag{2.97}$$

C' is an even symmetric matrix. The diagonal terms of C' presents the variance of each component. However, the terms out of diagonal presents the variance between each component and in general, those terms are different of zero. However, C' is not diagonal and as done in the Projection by Projection approach, there is an orthonormal basis of eigenvectors U such that $C'_0 = UC'U^T = diag(\sigma_1^2, \sigma_2^2, \sigma_3^2, \sigma_4^2, \sigma_5^2,)$ and the projected PSD are $\hat{S_{inv}} = US_{inv}$ so, according to Davenport

$$E[R_i] \simeq \sigma_i(\sqrt{2ln(N_p(\hat{S_{inv}}))} + \frac{0.5772}{\sqrt{2ln(N_p(\hat{S_{inv}}))}}) \tag{2.98}$$

For a random loading, it can be assumed that

$$E[\sqrt{J_{2,a}}] \approx \sqrt{E[R_1]^2 + E[R_2]^2 + E[R_3]^2 + E[R_4]^2 + E[R_5]^2} \tag{2.99}$$

Thus, to evaluate the stresses covariance matrix, the covariance matrix C' has to be determined as first step and then, the covariance matrix C'_0 and the PSD S_{inv} are obtained by the orthogonal transformation of the U matrix. Then, the number of maxima N_p calculated for each PSD of $\hat{S_{inv}}$ are needed to determine the average of the shear stress amplitude $E[\sqrt{J_{2,a}}]$. Finally, the fatigue damage is determined at each point of the structure using the Sines criterion in Eq. 2.94.

2.3.4 Critical plane criteria

The Critical plane criteria determine the equivalent stress $S_{eq}(\omega)$ from the combination of stress components on the critical plane. Three different criteria exists for the critical plane approach, i.e., the maximum normal stress, the maximum shear stress and the criterion of maximum normal-and-shear stress. The equivalent stress $S_{eq}(\omega)$ can be interpreted as the single output derived by linear combination of six inputs corresponding to the components of the stress matrix $S_s(\omega)$. Hence $S_{eq}(\omega) = aS_s(\omega)a^T$ where a is a vector of the

coefficients a suiting the respective multi-axial criterion [28]. These criteria look at the plane where crack nucleation and propagation is likely to occur, which depends on the specific definition of the critical plane criteria. The shear stress on the critical plane is a vector $\tau(t)$ that describes a stress path Ψ. As defined previously for the other methods, the definition of the amplitude τ_a of the curve Ψ is non trivial and usually, the MCC or MCE criteria are implemented. Hence, τ_a is defined by the radius or semi-axis of circumscribed circle/ellipse. As seen for the stress-invariant criteria, statistical definition of the MCC and MCE methods are a useful toll when random stresses are analyzed in the frequency domain. For example, an expected radius $E[R]$ based on the "maximum variance" concept is an intuitive measure of the expected amplitude $E[\tau_a] = E[R]$ also on the critical plane. Then, the critical plane can be defined as the plane with the maximum expected radius $E[C_a] = E[R]$. The MCE concept can be used in order to take into account for non-proportional stress paths. The estimations by the spectral definitions of MCC and MCE only depend on the statistical properties of the multi-axial random stress. Once the critical plane is defined, the resolved stress PSDs on the critical plane are linearly combined to determine an equivalent uni-axial stress PSD. These PSDs are combined by means of a function of direction cosines a_i defined by the critical plane. This approach is similar to the multi-axial spectral methods based on the equivalent uni-axial PSD and subsequently, the uni-axial spectral method can be applied to determine the damage for each element of the model. An example of this type of methods is the Carpinteri-Spagnoli method, presented in the following section. However, Preumont [9] extended the Matake's criterion, considering the spectral definition of the MCC and defining also a critichal plane method within the infinite-life approaches. The main difference between the stress-invariant methods and the critical plane criteria, regardless the computational time, is that the stress-invariant approach produce a result for element, (without considering the orientation of the critical plane) while critical-plane methods produce different results for different plane's orientation. Experimentally has been found that the critical-plane approach is better suited to proportional loads, when principal axes are fixed, while the stress-invariant-based methods are better suited to non-proportional loads where the principal axes rotate with time [9]

2.3.4.1 Matake

The spectral definition of MCC has been used by Preumont and Pitoiset et al. [9] to reformulate in frequency-domain the critical plane criterion of Matake,

which can be written as follow:

$$\frac{\sigma_1^* F(N_1^*)/\sqrt{3} + \alpha\sigma_n^* F(N_2^*)}{\beta} \leq 1 \tag{2.100}$$

where: σ_1^* and N_1^* are are standard deviation and number of cycles of the shear stress on the critical plane; σ_n^* and N_2^* are standard deviation and number of cycles of normal stress on the critical plane; $\alpha = (2t_1/f_1) - 1$ and $\beta = t_1$ are Matake's multi-axial fatigue criterion coefficients, respectively. The definition of the Matake criterion in the frequency domain following the definition of the MCC is based on the concept of largest variance of the shear stress to define the orientation of the critical plane. In other word, in the presence of random loading, the plane experiencing the maximum shear amplitude is replaced by the plane of largest variance of the shear stress. Thus, the stress PSD is rotated by means of two angles since two angles are needed for determining the normal to a material plane. A third angle is needed to determine the orientation such that a diagonalized covariance matrix is obtained. This direction permits to define the maximum of the variance of the shear stress in the critical pane by using the expected value of extreme of a Gaussian process through the Davenport's formula Eq. 2.46. Once the critical plane orientation is determined, the formulation of the Matake criterion yields to Eq. 2.100.

2.3.4.2 Carpinteri-Spagnoli

Carpinteri et al. [12] [29] proposed a reformulation of the criterion in the frequency domain:

$$G_{eq} = G_{w,w} + \left(\frac{f_1}{t_1}\right) G_{vw,vw} \tag{2.101}$$

where $G_{w,w}$ is the PSD function of the normal stress σ_w, and $G_{vw,vw}$ is the PSD function of the shear stress τ_{vw}, both related to the critical plane. This critical plane criteria is a multi-axial fatigue criterion which is an extension of the criterion proposed by Susmel [15] [30] to the range of variable-amplitude loading. Using the stress ratio $\rho_{ref} = \frac{\sqrt{3}\sigma_m}{\sqrt{\sum_i \sqrt{J_{2,aij}}^2}}$ defined in terms of hydrostatic mean stress σ_m and the amplitude of the second invariants of the stress deviator $\sqrt{J_{2,aij}}$, the following equation Eq. 2.102 were proposed for an equivalent value of the second stress invariant:

$$\sqrt{J_{2a\rho_{ref}}} = (\sqrt{J_{2a\rho=-1}} - \sqrt{J_{2a\rho=0}})\rho_{ref} + \sqrt{J_{2a\rho=0}} \tag{2.102}$$

where $\sqrt{J_{2a\rho=-1}}$ and $\sqrt{J_{2a\rho=0}}$ are the fatigue limits expressed in terms of the amplitude of the square root of the second invariant of the stress deviator under fully-reversed uniaxial and torsional loading, respectively. The critical plane is linked to averaged principal stress directions and for random loading, these directions are obtained as follows.

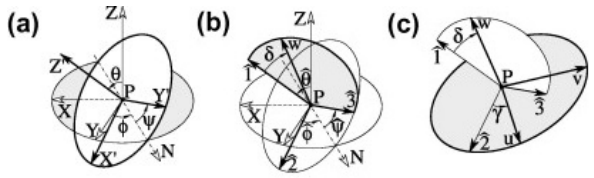

Figure 2.14: Critical plane definition for the Carpinteri-Spagnoli criterion [29]

With reference to Fig. 2.14, for given values of the angles ϕ, θ, the PSD function $G_{z'z'} = G_{3'3'}$ of the normal stress $\sigma_{z'}$ related to the general direction z' can be computed by means of n_0^+, which is the expected rate of zero up-crossings of $\sigma_{z'}$ and which is determined according to Eq. 2.37. Therefore, the total number of loading cycles over the observation period T is $N_1 = n_0^+ T$, and using the Davenport formula Eq. 2.46, the maximum value of the peaks for $\sigma_{z'}$ can be determined. By varying the angles ϕ, θ ($0 \leq \phi \leq 2\pi$, $0 \leq \theta \leq \pi$), the direction z' experiencing the maximum normal stress can be found and the direction is regarded as the averaged principal direction $\hat{1}$, defined by the angles $\hat{\Phi}$ and $\hat{\Theta}$. Then, the angle Ψ (rotation about axis $\hat{1}$) is made to vary with the aim of determining the direction where the corresponding shear stress component attains the maximum variance. This can be obtained by maximizing the variance of the stress $\tau_{y'z'} = S_{6'6'}$ that corresponds to maximize the spectral moments of order 0 of the PSD function $G_{6'6'}$. Thus, the obtained direction y' is regarded as the averaged principal direction $\hat{3}$. Once the angles $\hat{\Phi}$, $\hat{\Theta}$ and $\hat{\Psi}$, describing the plane $\hat{1}\hat{3}$ of averaged maximum shear, are defined, also the averaged principal direction $\hat{2}$ is defined (Fig. 2.14 (b)). Finally, the normal to the critical plane is defined by an off-angle δ (clockwise rotation) about the axis $\hat{2}$ [29]. Once the critical plane is determied, to reduce the PSDs matrix to an equivalent un-axial PSD five successive rotations have to be performed, considering directions u and v belonging to the critical plane and w normal to the critical plane. (i) the angles $\hat{\Phi}$, $\hat{\Theta}$ and $\hat{\Psi}$; (ii) the angle δ ; (iii) the angle γ, which represents a counterclockwise rotation about the w axis, so that the u axis defines the direction that maximizes the variance of $G_{6'6'}$. After these five rotations, the PSDs $G_{3'3'} = G_{w,w}$ and $G_{6'6'} = G_{vw,vw}$, are determined and hence the equivalent PSD is computed following the linear

combination:

$$G_{eq} = G_{w,w} + \left(\frac{f_1}{t_1}\right) G_{vw,vw} \tag{2.103}$$

2.4 Rain-flow counting and Probability Density Function

The first straightforward method to study random vibration fatigue is the classical time domain approach which is usually based on cycle counting schemes, as the rain-flow counting algorithm, and damage accumulation models, as the linear damage rule. In the time domain analysis, the fatigue damage of a random time history $s(t)$ is determined in two steps. First of all, a counting method, as the commonly used rain-flow counting method, is applied to the process in order to identifying the fatigue cycles. Due to the randomness of the process, the counted cycles have different amplitudes values and thus they contribute to the damage in different proportion. Therefore, the damage accumulation rule, as the linear Palmgren–Miner linear law, is applied in the second step to account the damage of every counted cycle.

$$D = \sum_{i}^{N(T)} \frac{n_i}{N_i} \tag{2.104}$$

This summation extends over the total number of cycles $N(T)$ counted in $s(t)$ to consider the whole process, where n_i is the number the cycles with amplitude s_i, which would cause a failure after N_i repetitions in a constant amplitude test. Often, the relationship between stress amplitude s_i and cycles to failure N_i is expressed by a straight line in a log–log diagram, through the S-N curve represented by the Basquin's law $Ns^b = K$ which is fitted to experimental data by regression analysis. In the Palmgren–Miner rule, fatigue failure is predicted to occur when damage D reaches a critical value of 1, even though lower values are recommended in some design codes and regulations. The summation in Eq. 2.104 assumes that the cycles counted in $s(t)$ are grouped into bins of n_i cycles, all having the same amplitude s_i. Since $s(t)$ is a random variable, it follows that n_i and s_i are both random variables. Thus, due to the randomness of the loading, many stress time histories (simulated or measured on real prototypes) are needed in order to obtain consistent and reliable distributions of rain-flow cycles. Moreover, due to practical implication, these cycles have to be extrapolated from short time recording

and extended to the overall in-service life, by using adequate statistical investigations. Moreover, it is also computationally costly to evaluate stresses and the fatigue damage from time series data of long duration, especially for complex models with large number of elements. Consequently, the most common way to represent the dynamic response of the random loading input is by spectral methods in the frequency domain using the PSD of the load [2]. Therefore, in the frequency domain the summation in Eq. 2.104 needs to be reformulated in a probabilistic way.

$$D = n_{rfc} \int_0^{+\infty} \frac{1}{N(s)} p(s)\, ds \tag{2.105}$$

This equation is nothing more than the Palmgren–Miner rule in Eq. 2.104 extended to continuously distributed amplitudes. $p(s)$ is the probability distribution of the amplitudes of rain-flow cycles, n_{rfc} is the number of rain-flow cycles counted in T, and $N(s)$ is the number of cycles to failure at constant amplitude s. Eq. 2.105 can be solved in closed form if the analytical expressions of $p(s)$ is known but this occurs only when $s(t)$ is a narrow-band process. However, $p(s)$ can be related to the properties of the underlying spectrum. In particular, the stress range PDFs are based on linear combination of Weibull distributions (one corresponding mainly to small stress ranges and the other to large stress ranges) and a Rayleigh distribution. These distributions are modified through parameters that are based on the requirements that the shape of the PDF should agree with the shape of the histogram obtained by the time-domain simulation and the rain-flow counting procedure. However, the accuracy of the multi-axial spectral method does not depend only on the equivalent stress adopted but it also depends on the accuracy of the uni-axial spectral method used to estimate the PDF distribution. Even if many spectral methods are available in literature, different studies have confirmed that Dirlik and Tovo-Benasciutti uni-axial spectral methods are exceptionally superior to others for wide-band spectrum [4].

2.4.1 Rainflow counting method

A random loading process produces a large number of stress reversals and these in turn cause fatigue damage. The magnitude of the stress ranges and the corresponding number of cycles are of critical importance in determining the fatigue damage. In the time domain, the number of cycles and corresponding stress ranges are determined, in a deterministic way, using the rain-flow

counting method. The details of the rain-flow algorithm have been described by Wirsching and Shehata [31]. In brief, for each local peak u in a sample time history $l(t)$, the rain-flow algorithm will find a local trough v to form a hysteresis loop, so that the stress range is $S = u - v$ and it corresponds to one cycle. In the frequency domain, the cycle courting is performed in a statistical sense by means of the PDF derived by simulation. So, it assumes that the number of cycles are equal to the number of peaks. Thus, under stationary random loading, the expected number of cycles in time t is given by $E[N(t)] = \nu_p\, t$ where $N(t)$ is the total number of cycles in time t and ν_p is the peak rate given by $\nu_p = \sqrt{M_4/M_2}$. The stress ranges are hence defined by the specific PDF deployed. The following figures (Fig. 2.15, 2.16 2.17) represent the number of cycles and the corresponding stress ranges obtained applying the rain-flow counting method to the signal represented in Fig. 2.5, 2.7 and 2.8c. In particular, Fig. 2.15 has only one bin since the sine signal 2.5 has constant amplitude.

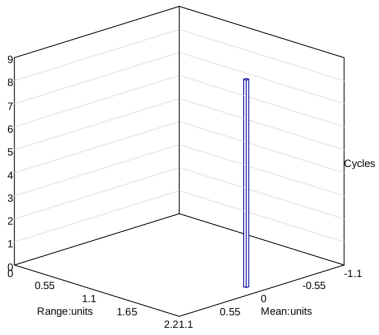

Figure 2.15: Examples of rain-flow counting applied to the signal in Fig. 2.5

Fig. 2.16, which represent the rain-flow counting applied to the random signal 2.7, has multiple bins with different amplitudes.

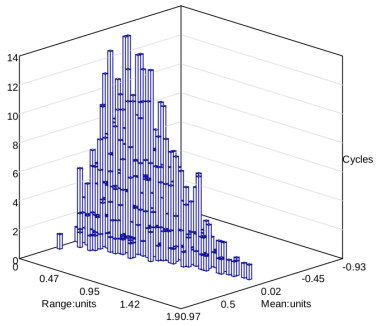

Figure 2.16: Examples of rain-flow counting applied to the signal in Fig. 2.7

Fig. 2.17 also has different amplitudes but all the bins have same zero mean since it is obtained from the PSD of the random signal 2.7 with the assumption of stationary and ergodicity.

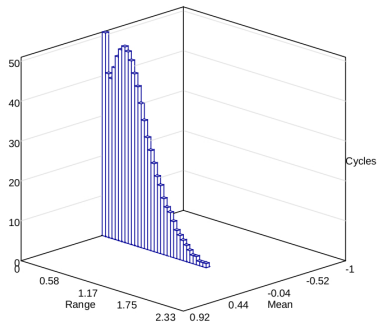

Figure 2.17: Examples of rain-flow counting applied to the PSD in Fig. 2.8c

2.4.2 Narrow-band method

In case of narrow-band process, peaks and valleys are placed symmetrically, and each cycle is formed by pairing each peak to the adjacent valley which corresponds also to the peak counting method. Consequently, each cycle has zero mean and amplitude coincident with the peak value, following a Rayleigh distribution. In a narrow-band process, the number of cycles counted is also known, it being equal to the number of crossings of the mean value, $n_{rfc} = n_0^+ T$ which yields to the expression of the "narrow band" damage in time interval T.

$$D_{NB} = \frac{n_0^+ T}{K} (\sqrt{2M_0})^b \Gamma(1 + \frac{b}{2}) \tag{2.106}$$

in which $\Gamma(\cdot)$ is the gamma function. The expression is credited to Miles and Bendat and it is restricted to a straight S-N line described by two parameters of the Basquin's law. In case of the S-N curve is not straight, Eq. 2.106 can be solved numerically, considering different Basquin's constants. Even if this result is an exact solution for narrow-band processes, the narrow-band definition of the damage represents the upper limit for the wide-band processes. Hence, applying it also to wide-band processes, it results to be a conservative way to determine the damage of a wide-band processes.

2.4.3 Wide-band methods

When the random process is no longer narrow-band, the previous formula becomes too conservative. In a wide-band process, fatigue cycles cannot be obtained by joining a peak with a symmetric valley, as done with the peak counting method, because it would yield cycles with amplitudes larger than those identified by the rain-flow counting method. However, the algorithm of the rain-flow counting is too complex to determine, in closed form, the expression of the PDF of amplitudes related to the bandwidth parameters of the wide-band process. For this reason, in the literature, initially, the approach followed was to introduce a correction factor less than unity, by which to reduce the narrow-band damage. However, the only feasible way to calibrate the damage correction factor was based on simulation results. Moreover, a lot of methods have been developed since there is not a specific bandwidth parameter that can be used to set this correction factor. The first spectral method was proposed by Wirsching and Light,in 1980 [32], in which the correction factor depends solely on the spectral parameter M_2. After that, other methods following the same idea were proposed and the correction factors were refined by introducing the dependency on other bandwidth parameters. However, the use of a correction factor for estimating the damage of a wide-band process, has the drawback of not providing the PDF $p(s)$ of amplitudes of the cycles causing that damage. In fact, knowing $p(s)$ it permits to makes it possible to compute the fatigue damage not only for a straight S-N line, but also for any smooth curve with continuous change of slope, with or without endurance limit. Consequently, the PDF permits to determine the cumulative spectra of rain-flow cycles and for these reasons, the most widely used methods for wide-band processes are the Dirlik and the Tovo-Benasciutti methods. They correlate the spectral properties of the stress PSD to an amplitude PDF determined by simulations. They belong to the category of approaches that provide an estimate of the amplitude PDF of rain-flow cycles and they are illustrated in the following paragraphs.

2.4.3.1 Dirlik method

This method, developed due to the complexity to derive in a closed form the distribution of rain-flow cycles from the PSD, is known to be a milestone among spectral methods. A Monte Carlo approach was employed to generate a sample stress history $l(t)$ from the PSD $G(f)$ using inverse FFT methods. Subsequently, the rain-flow algorithm was applied on $l(t)$ to extract the cycles and the PDF of rain-flow counted ranges. This permitted to calculate

the fatigue damage for any given material constants in an S-N curve. The idea of the Monte Carlo approach is based on concept that the sample average converges in probability towards the expected value if the sample size increases. For this reason, it was important that the sample stress histories used for the numerical simulations were sufficiently long in order to catch also the rare events. In particular, the method was developed considering 70 PSDs of various shapes. The PSD were normalized so that all had the same RMS value and the same expected rate of peaks ν_p (hence, the same number of rain-flow cycles counted in a time interval). These two parameters were kept fixed and the irregularity factor γ was made to vary by adjusting the parameters defining the power spectrum shape. It corresponds to varying the spectral moments of order zero, two, and four (M_0, M_2, M_4). The rectangular bimodal spectrum was used extensively because of its simplicity to assume a wide range of values of the irregularity factor γ, having the same RMS value and rate of peaks ν_p. In preliminary simulations trials, it was observed that the mean frequency ω_1 of the spectrum, *i.e.,* its first order moment M_1, also has a role in changing the fatigue damage of a simulated time history. Thus,, 42 out of 70 PSDs were shaped so as to have the same RMS value , rate of peaks ν_p, irregularity factor γ but different M_1. Moreover, a normalized mean frequency $x_m = \omega_1/\nu_p$ was introduced, where $x_m = \frac{M_1}{M_0}\sqrt{\frac{M_2}{M_4}}$. Due to the low disk capacity of computers available at that time, a single generated stress time history had only 1024 points and hence the simulation procedure was repeated 20 times in order to obtain a sufficiently long record of stress time history. Consequently, the fatigue cycles of this long record were extracted by means of the rain-flow counting method in time domain. The probability distribution of rain-flow ranges were finally calculated. This permitted to approximate the PDF of rain-flow ranges as a mixture of three distributions: an exponential function, a Rayleigh function with variable parameter and a standard Rayleigh function. The full expression in terms of a normalized variable $Z = \frac{r}{2\sqrt{M_0}}$ where r is the rain-flow range is:

$$p_{DK}(Z) = \frac{1}{2\sqrt{m_0}}[\frac{D_1}{Q}e^{-\frac{Z}{Q}} + \frac{D_2 Z}{R^2}e^{-\frac{Z^2}{2R^2}} + D_3 Z e^{-\frac{Z^2}{2}}] \tag{2.107}$$

The coefficients D_1, D_2, D_3 , R and Q are defined as $D_1 = \frac{2(x_m-\alpha_2^2)}{1+\alpha^2}$, $D_2 = \frac{1-\alpha_2-D_1+D_1^2}{1-R}$, $D_3 = 1 - D_1 - D_2$, $R = \frac{\alpha_2-x_m-D_1^2}{1-\alpha_2-D_1+D_1^2}$, $Q = 1.25\frac{(\alpha_2-D_3-D_2R)}{D_1}$

The quantities D_1, D_2, D_3 and R are the "best fit" parameters that turned out after minimizing the difference between the approximate PDF and the

range distribution obtained in the time-domain. The probability distribution in Eq. 2.107 represents the link between the rain-flow counted ranges and the PSD and it determines the PDF of rain-flow ranges needed for the life estimations with any form of S-N data using the Miner's rule. In the case of single slope S-N line, $Ns^b = K$, the substitution of $p_{DK}(Z)$ into Equation Miner 2.105 returns a closed-form expression for the damage in time interval T.

2.4.3.2 Tovo-Benasciutti method

The theory of this method was presented in 2005 [25]. For a stationary Gaussian process, considering the the linear damage rule, the rain-flow damage is always bounded between two damage values, *i.e.*, $D_{RC} \leq D_{RFC} \leq D^+ \leq D_{NB}$ where D_{RC} is the damage given by the range-mean counting and D_{NB} is the damage provided by the Narrow-band method. Thus, the Tovo-Benasciutti PDF is based on the fact that the amplitude PDF of rain-flow cycles lies between these two limit distributions and it can be estimated by their linear combination:

$$p_{TB}(s,m) = w_{TB}p_{LCC}(s,m) + (1-w_{TB})p_{RC}(s,m) \tag{2.108}$$

w_{TB} is a weight factor that defines the actual shape of rain-flow cycle distribution. Unlike Dirlik, the Tovo-Benasciutti methods provides the joint distribution of amplitudes and mean values of rain-flow cycles. The two functions $p_{LCC}(s,m)$ and $p_RC(s,m)$ represent the amplitude–mean distributions of the Level-Crossing Counting (LCC) and of the Range Counting (RC) where the latter is only approximated. The same weighted sum holds also for the probability distributions $p_{TB}(s), p_{LCC}(s), p_{RC}(s)$. Thus, the damage become:

$$D_{TB} = w_{TB}D_{LCC} + (1-w_{TB})D_{RC} \cong [w_{TB} + (1-w_{TB})\alpha_2^{b-1}]D_{NB} \tag{2.109}$$

The latter inequality takes advantage of the fact that $D_{LCC} = D_{NB}$ and that the simple range counting damage is approximated as $D_{RC} \cong \alpha_2^{b-1} D_{NB}$. Hence, the quantity $[w_{TB} + (1-w_{TB})\alpha_2^{b-1}]$ can be interpreted as a correction factor of the narrow-band damage. However, it has been demonstrated that the Tovo-Benasciutti method has a theoretical basis. After the definition of the weighted sum that links PDFs and damage values through w_{TB}, a proper expression for w_{TB} has to be found to completely define the Tovo-Benasciutti method. Theoretically, the parameter w_{TB} is a function of the whole set of spectral and

bandwidth parameters of the PSD of the random process. In the narrow-band case, for example, the rain-flow distribution must converge to the Rayleigh distribution (i.e., LCC function), which in turn requires that $w_{TB} \simeq 1$ for a narrow-band process, in which α_1 and α_2 both approach unity. Moreover, many numerical simulations, following the approach described for the Dirlik method, *i.e.,* generating stress time histories from PSD of different shapes, have been performed and the expression of w_{TB} used today has finally been developed:

$$w = \frac{(\alpha_1 - \alpha_2)[1.112(1 + \alpha_1\alpha_2 - (\alpha_1 + \alpha_2))e^{2.11\alpha_2} + (\alpha_1 - \alpha_2)]}{(1 - \alpha_2)^2} \quad (2.110)$$

Where $\alpha_1 = \frac{M_1}{\sqrt{M_0 M_2}}$ and $\alpha_2 = \frac{M_2}{\sqrt{M_0 M_4}}$ This expression is a result of a best fitting on simulation results from PSD of various shapes. Moreover, as for the Dirlik method, this formula assumes that the rain-flow probability distribution is linked to four spectral moments, M_0, M_1, M_2, and M_4 which provide good accuracy between frequency domain estimations and time domain simulation results.

2.5 Material Properties and S-N curve

The multi-axial criteria and the spectral method are not enough to address the random vibration fatigue calculation. The material properties of the component is another fundamental characteristic needed to correctly estimate the damage accumulation. Over the years, many models of the material properties have been evolved, in particular related to the fatigue problem for HCF. However, the properties of a metallic material are usually represented by the S-N curve, also called Wöhler curve. The S-N curve is a graph representing the relation between of the alternating stress versus the number of cycles to failure for a given material, as represented by Fig. 2.18. Typically, the stress ranges and the number of cycles are represented in a logarithmic scales. Moreover, these curves are obtained by testing a metal specimen into the testing machine where the specimen is subjected to a cyclic stress time history until the failure is reached. Testing several specimens at different stress levels and reporting the number of cycle to failure permits to develop the S-N curve of the material. As can be seen in Fig. 2.18, the curve usually contain several different areas: a plastic region (between A and B), an elastic region (between

B and C) and an infinite life region (between C and D) typical of materials like steel. In the graph, the ultimate strength stress is defined as the value that causes a failure for one cycle. Moreover, the yield strength stress is the stress level that divides the plastic and elastic region., corresponding to the stress level at the point B.

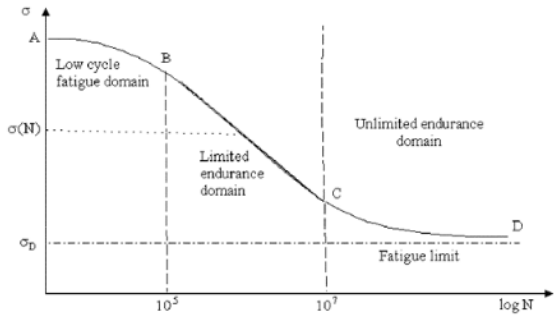

Figure 2.18: Regions of S-N curve [11]

In the infinite life region, if the stress levels are below a certain level called fatigue limit, an infinite number of cycles can be applied without causing failure. Many non-ferrous metals, such as aluminum, do not exhibit well-defined endurance limits, however sometimes a fatigue limit is defined also for these material as the stress level for which the failure happen at a number of cycles grater than $10^7 \div 10^8$ cycles. In the elastic region, the relationship between stress and strain remains linear and when a cycle is applied and removed, the material returns to its original shape, without any plastic deformation. This region is also called the HCF region, due to the high number of stress cycles, at low amplitude. The slope of the S-N curve in elastic region in the log-log chart can be represented by a line which is determined by linear regression from the test's results. In particular this line can be defined by the Basquin's equation

$$C = S^b N \tag{2.111}$$

where: "b factor" governs the relationship between the stress level and the number of cycles to failure and is the slope of the line, C is the Basquin's constant, S is the stress level and N is the corresponding number of cycles. However, the tests needed to determine the S-N curve of a material are usually performed in simplified experimental conditions, involving uni-axial stress derived from pure torsion or pure axial loading. For example, it stands out the approximation of the Equivalent Von Mises criterion, pointed out in [25], which considers only the S-N line for normal stress in the fatigue

damage calculation, neglecting the torsion fatigue properties. A simple way to overcome this limitation is to use a "reference S-N line" that is calibrated on the S-N lines for both normal and shear stress in a so-called Modified Wöhler Diagram, as presented by Susmel and Lazzarin [15]. This method permits to take into account the multi-axial loading also into the material parameters.

2.5.1 Modified S-N curve

Susmel and Lazzarin in [15] proposed a method to take into account the multi-axial stress state into the material properties and in particular considering the Basquin's parameters representing the elastic region of HCF. The method defines a new reference curve for an arbitrary multi-axial loading located by a reference stress ratio (as Eq. 2.113) which quantifies the proportionality degree of multi-axial stress. It is evaluated in terms of the mean value of the maximum hydrostatic pressure and the mean amplitude of all cycles counted in i^{th} projected process $\Psi_{p,i}(t)$. As showed by Fig. 2.19, a value $\rho = 1$ locates the curve under pure axial loading so the curve will correspond to the S-N curve for pure axial loading. Instead, for $\rho = 0$, it indicates pure torsion loading and the reference curve will match with that. All other stress states are taken into account considering the parameter ρ and by means of a linear combination of the curves for pure axial loading and pure torsion loading.

In particular, J_A is used to indicate a reference fatigue strength evaluated

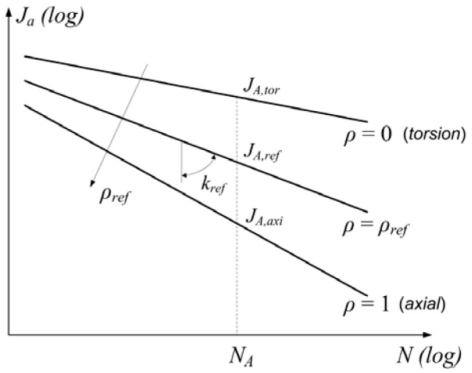

Figure 2.19: Reference S-N lines determined as modified S-N curves [7]

at N_A cycles in the modified Wöhler diagram, expressed in terms of the amplitude of the square root of the second invariant of the stress deviator. J_{Aaxi} and J_{Ator} denote, respectively, the fatigue strength values under fully-reversed axial and torsion loading. Denoting with σ_a and τ_a the reference fatigue strength amplitudes at N_A cycles for fully-reversed axial and torsion

loading, respectively, it is straightforward to verify that $J_{Aaxi} = \sigma_a/\sqrt{3}$ and $J_{Ator} = \tau_a$. Instead, symbols k_{axi} and k_{tor} indicate the corresponding inverse slopes of S-N curves. The calculated reference value ρ allows estimating the fatigue strength $J_{A,ref}$ and the inverse slope k_{ref} of the reference S-N curve by a linear interpolation as following:

$$J_{A,ref} = J_{A,tor} + \rho_{ref}(J_{A,axi} - J_{A,tor}) \tag{2.112}$$

$$k_{ref} = k_{tor} + \rho_{ref}(k_{axi} - k_{tor}) \tag{2.113}$$

Many non-ferrous metals do not exhibit well-defined endurance limits or otherwise stress levels below the fatigue limit can contribute to the crack propagation also in materials like steel, in case of multi-axial loading with variable amplitudes. For these reasons, the recommendation of [14] is to extend the reference line also above elastic region, after the knee point, considering a different slope. In particular, in this new region, the damage sum is determined by modifying the Wöhler-line according to Haibach, which assumes the slope b of the line representing the elastic region after the knee point as $b' = 2b - i$, with $i = 1$ for wrought and $i = 2$for cast, welded or sintered materials.

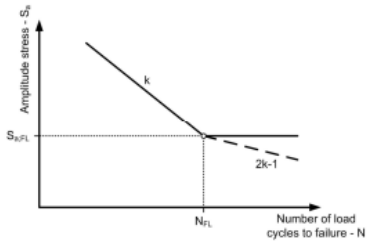

Figure 2.20: Bi-linear S-N fatigue-life curve with the Haibach assumptions [13]

Fig. 2.20 represent a schematic of the modified S-N curve with the extended region according to the Haibach assumptions. As can bee seen, the S-N curve in this case becomes a curve with two slopes and the total damage can be computed numerically taking into account the two different regions. Furthermore, the damage sum D_{th} that leads to failure is theoretically equal to 1.0, however, in most applications, a different allowable value is considered in order to take into account the uncertainties of the loading definition, the material properties and the FE model. So a safe margin is assumed and the damage that leads to failure is usually recommended as $D_{al} = 0.5$ for non welded components and $D_{al} = 0.3$ for welded components.

Chapter 3

Method

The purpose of this chapter is to provide an overview of the research method used in this thesis to address the random vibration fatigue calculation in Abaqus CAE. In particular, an overview on important features of the data handling of Abaqus CAE are presented in 3.1. Section 3.2 describes how the estimation of the fatigue life can be determined without a plug-in tool in Abaqus CAE. For this purpose, the post-processing of the results obtained in Abaqus is carried out by Simulia Fe-Safe, since the support of other commercial software is needed. This method was then used to validate the results obtained by the plug-in developed. Section 3.3 details the method used to determine the fatigue damage with the help of the plug-in tool. Hence, the following section 3.3.1 describes the Abaqus CAE RSG module used to developed the GUI application of the plug-in tool. Finally, section 3.3.2 deeps into the Random Vibration Fatigue plug-in tool developed, describing its properties and functionalities, with reference to the methods and assumptions described in the previous chapter 1.1.

3.1 Abaqus CAE

Abaqus is a commercial software package for FE analysis, released in 1978. One of the main product is Abaqus CAE (Complete Abaqus Environment) which permits both pre-pocessisng and post-processing operations. In particular, it carries the modeling and analysis of mechanical components as well as the visualization of the FE analysis result. One of the main advantage of Abaqus is that it uses the open-source scripting language Python for scripting and customization, making possible to easily create custom plug-in tools.

Even if the general concept of FE analysis used in Abaqus is equivalent to other CAE software, there are some specific definitions that are typical of Abaqus and they have to be clarified in order to correctly understand the plug-in function. In Abaqus CAE, 'Step' refers to a specific phase of the simulation and hence a specific analysis. This means that a 'Step' is characterized by its specific loads and boundary conditions as well as type of analysis. The results of each 'Step' are saved into different 'Frames' corresponding to different time periods of the analysis or in the case of the frequency domain analysis, they refers to different frequencies. The results obtained from the Abaqus solver, in terms of 'Filed output results' or 'History output results', are written into an Output DataBase (ODB) file. The ODB file is a repository of data, including all the variables defining the simulation and all the output variables defined by the user. In particular, for each 'Frame' corresponding to a specific 'Step', the ODB file saves the results calculated. For examples in case of stress output, it writes the values obtained at each integration point, node or centroid of each element. In Abaqus CAE the user can then extracts the desired results and obtain graphs and plots from the data saved into the ODB file.

3.2 Analysis with Fe-Safe

To determine the fatigue damage accumulated in a component subjected to random vibrations by means of Abaqus CAE, an external software is needed since the calculation cannot be executed entirely in Abaqus CAE. For this purpose, Simulia Fe-Safe is widely used by the industries. It handles fatigue analysis of FE models and it directly suits with all major FE program as Abaqus, ANSYS or Nastran. As shown in Fig. 3.1, the random vibration analysis is performed in Abaqus CAE and the fatigue analysis, instead, is carried out by Fe-Safe.

In addition, the figure highlights the sub-steps needed to correctly perform the random vibration analysis in Anaqus CAE and to obtain the results needed for the following fatigue analysis in Fe-Safe. Once the model is completely defined and the modal analysis is performed to extract all the necessary eigenfrequqncies, the TF at each node of the component has to be determined. For this reason a SSD analysis with modal superposition technique in performed. It permits, by applying a unit acceleration loading, to determine the TF for each frequency, in terms of amplitude and phase. Then Fe-Safe takes these TF in terms of generalized displacement (the amplitude of the response in the corresponding mode) for all the modes extracted by the modal analysis. Moreover, Fe-Safe requires an external file which defines

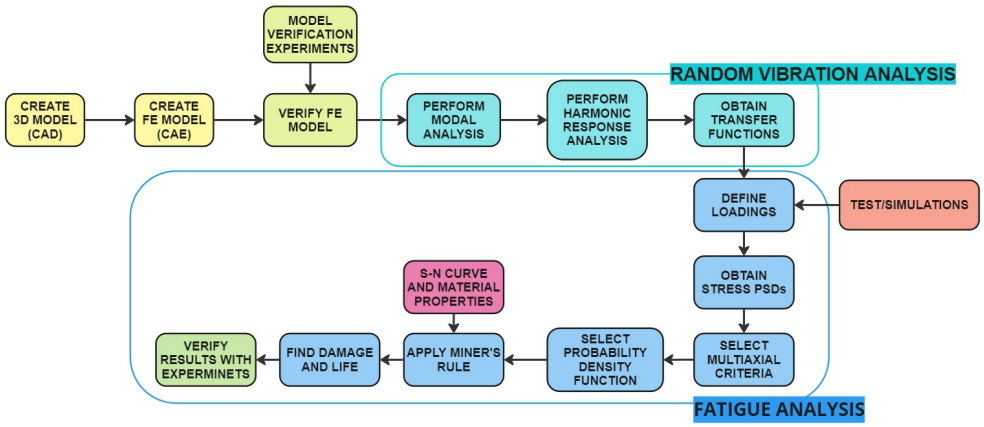

Figure 3.1: Random Vibration Fatigue analysis by Fe-Safe

the PSD matrix of the loading (in terms of ASD and CSD defined by real and imaginary part). Considering a linear behavior of the component, Fe-Safe linearly combine the results from Abaqus with the input PSD, in order to define the stress PSD matrix. The stress PSD is then used to perform the fatigue analysis, following the stress analysis approach available in Fe-Safe to address random vibration fatigue calculations. In case of multi-axial stresses, Fe-Safe permits two type of multi-axial criteria. The first one is the equivalent PSD defined by the Equivalent Von Mises method, as described in section 2.3.1.1. The second type of multi-axial criteria are the different definitions of the critical plane criteria. However, these are presented but not investigated since the critical plane criteria were not developed in the Abaqus' plug-in tool. In addition, Fe-Safe uses both Dirlik and the Tovo-Benasciutti spectral methods to compute the PDF. The linear damage rule is adopted to determine the whole damage for each element of the component. Finally, a contour plot of the component representing the damage for each element can be saved on a output file and then displayed in Abaqus CAE.

3.3 Analysis with Abaqus CAE Plug-in tool

Random Vibration Fatigue analysis by means of the Abaqus CAE Plug-in tool takes advantage of the properties of the random analysis in Abaqus CAE. In fact, the analysis step in this case are a bit different compared to the previous approach, as shown by Fig. 3.2, in order to have a more user friendly tool and minimize the steps' definition. In fact, the random vibration analysis performed in Abaqus is based on the SSD analysis but it permits to directly

define the PSD of the loading and ehence to obtain the stress PSDs as output. This means that it carries the linear combination between the response of the structure and the loading PSD. However, the drawback of this analysis is that Abaqus CAE calculates only the stress ASD (diagnoal terms of the PSD matrix) and the stress CSD (out-of-diagnoal terms of the PSD matrix) are missed. Missing the CSD means that the phase information are completely lost and this can be significant in case of out-of-phase stresses. For this reason, the tool try to fill this lack by approximating the CSD with the product of the square routs of the corresponding ASD.

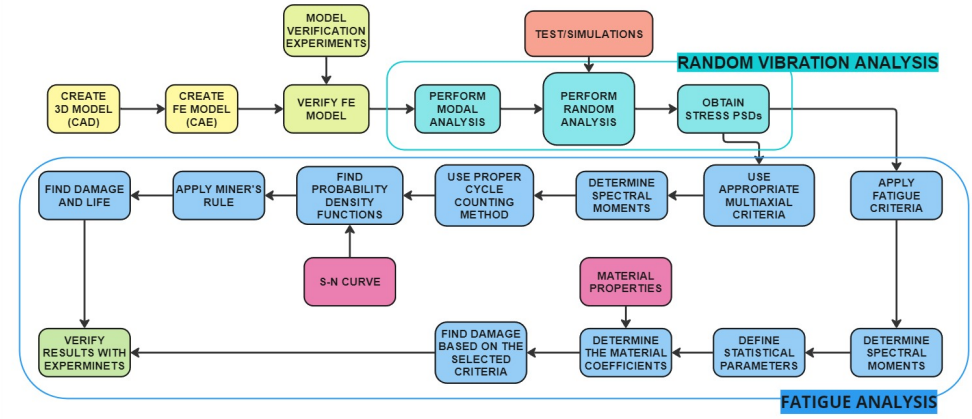

Figure 3.2: Random Vibration Fatigue analysis by plug-in tool in Abaqus CAE

Once the stress PSDs are defined, the plug-in tool, described in section 3.3.2, extract them from the Odb file of results generated by Abaqus CAE. The tool, differently from Fe-Safe, permits both types of fatigue analysis approaches. Following the finite-life approach, as Fe-Safe, the different multi-axial criteria described in 2.3 can be applied. Moreover, the PDF has to be selected as described in 2.4 and finally the material properties in terms of Basquin's constants of the S-N line have to be indicated. As reported in 2.5, based on the case of analysis, the modified S-N curve can be used to take into account of the multi-axial stress state into the material properties and the damage sum can be extended below the fatigue limit following the Haibach criteria. However, the tool handles also infinite-life criteria, as described in 2.3.2. For these criteria, the spectral parameters are defined from the spectral moments derived from the stress PSDs and the damage is calculated based on the material properties and the selected criteria. Finally, for both approaches, the tool permits to determine the whole damage for each element of the component according to the selections done. It is saved in the same

Odb file with the random vibrations results but into a new step. This permits to open the Odb result's file in Abaqus and visualize a contour plot of the damage for the entire component. Moreover, the contour plot allows to easily find the hot-spot of the structure and also have an insight on the estimated life of the component due to the applied random vibrations.

3.3.1 Abaqus CAE RSG

The Abaqus plug-ins are used to customize Abaqus CAE in order to efficiently address repetitive tasks of pre-processing or post-processing. In particular, concerning the post-processing of results data, Abaqus plug-in tools are used to implement specific feature not directly available in the software. There are two types of plug-ins: (i) Kernel Plug-ins (ii) GUI Plug-ins. While a kernel plug-in consists of functions written using the Abaqus Scripting Interface,an extension of the Python programming language, a GUI plug-in is written using the Abaqus GUI Toolkit. The GUI plug-in permits to easily create these plug-in tools without expensive scripting effort by means of the RSG Dialog Builder. The RSG Dialog Builder consists of two parts, the effective GUI builder and the executing script in the kernel of Abaqus CAE (the script to be executed). The RSG Dialog Builder contains commands that create an interface (the GUI of the custom plug-in) which in turn send commands to the kernel. The Abaqus GUI Toolkit, instead, is an extension of the FOX GUI Toolkit. Thus, the RSG dialog builder is an alternative to using the Abaqus GUI Toolkit commands and a text editor to create dialog boxes. In fact, the RSG Dialog Builder plug-in enables to create dialog boxes and connect them to kernel commands without writing any code. In the RSG Dialog Builder it is possible to select items from a toolbox to add them to an empty dialog box, editing their properties and creating a simple GUI for the specific task. The RSG dialog builder provides access to a subset of the commands in the Abaqus GUI Toolkit, but it requires no programming experience to produce a working dialog box. The dialog boxes created, they become the new plug-ins to Abaqus-CAE. However, this dialog boxes send a list of variables defied in them based on the user selections to the kernel program. The Kernel is the main part of the plug-in tool. It is a python program that contains all the tasks that have to be performed and when it is executed, it produces the results of the plug-in tool. This program is usually developed separately from the GUI and then is integrated into the RSG dialog builder. For this reason, values name and names of the variables have to match between the GUI and the kernel program. Moreover, as explained in section 3.3.2, the kernel program usually

contains multiple function definitions, so special attention should be paid in the definition of the main function which is firstly executed.

3.3.2 Fatigue plug-in tool

Using the Abaqus plugin RSG Dialog Builder the GUI of the random vibration fatigue plug-in tool was created. The GUI is represented in the following Fig. 3.3

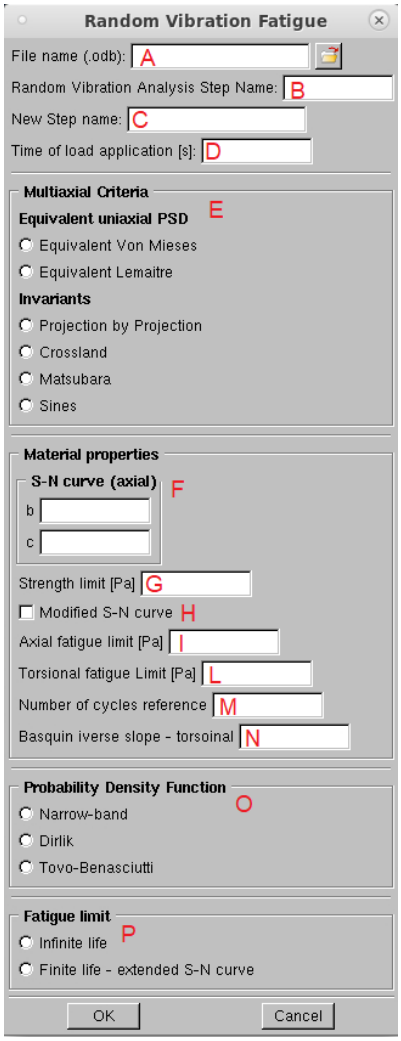

Figure 3.3: GUI of Random Vibration Fatigue plug-in tool in Abaqus CAE

To address the calculation without errors the following advice need to be fulfilled.

A An .Odb file has to be selected

B The correct name of the Random Analysis Step, saved into the .Odb file, has to be typed

C A new name for the Random Vibration Fatigue Calculation has to be entered

D The duration of the vibration corresponding to the PSD used in the Random Analysis has to be digit

E A multiaxial criteria has to be selected. Equivalent Von Mises, Equivalent Lemaitre and Projection by Projection belong to the fatigue-limit criteria corresponding to the damage tolerant approach. Crossland, Matsubara and Sines are infinite-life criteria that belong to the safe-life approach.

F If a fatigue-limit criteria is selected, the Basquin's constants (b and C), related to the axial S-N curve of the component's material, have to be typed

G For any criteria, enter the strength limit of the material in Pa

H Selecting the Modified S-N curve the modified curve based on the Susmel's model is adopted

I If a infinite-life criteria is selected the axial fatigue limit of the material has to be entered in Pa

J If a infinite-life criteria is selected the torsional fatigue limit of the material has to be entered in Pa

K If a the Modified S-N curve option is selected, the reference number of cycles (same for axial and torsional) has to be typed for the linear interpolation

L If a the Modified S-N curve option is selected, the Basquin's inverse slope b corresponding to the torsional S-N curve has to be entered

M If a fatigue-limit criteria is selected, the PDF model has to be selected between Narrow-band, Dirlik and Tovo-Benasciutti

N If a fatigue-limit criteria is selected, the infinite life button has to be selected to limit the calculation above the knee point. In orther to consider also the stresses under the fatigue limit, the finite-life button has to be selected and the double slope S-N curve with the Haibach's assumtions is considered.

The python code for the 'Random Vibration Fatigue Tool' is explained in the following pseudo-codes. As described above, the GUI is connected to the "main function" which handles the variables defined in the GUI and checks the correctness of the user-defined parameters. Moreover, the 'main function' checks that all the required data were provided based on the multi-axial criteria selected by the user, otherwise an error message is printed in the Abaqus Message area. If all the values and settings of the 'Random Vibration Fatigue GUI' are filled in a correct manner, the "main function" runs the specific multi-axial criteria and spectral method with the gathered parameters. Thus, the "main function" and all the subsequent functions are described in the following by means of pseudo-codes. The pseudo-codes presents the algorithms with an high-level description and without strictly following the rules of python scripting, in order to present the code in a simple and understandable way. These pseudo-codes permit to display the logic and the structure of the algorithm, allowing to easily provide its functionality.

Thus, the first function executed by the fatigue tool is the following "main function" and its pseudo-code can be seen below in 3.1.

Once that one of the multi-axial criteria is selected, the corresponding function is executed. The following listings 3.2, 3.3, 3.4, 3.5, 3.6 and 3.7 report the pseudo-codes corresponding to all the multiaxial criteria.

The methods are based on the spectral moments derived from the stress PSD and hence a separate function, described in 3.8, is used to determine them.

Moreover, the fatigue-limit approches require the calculation of the PDFs and hence the some statistical parameter are needed to define them. These parameters are determied by the following code 3.9.

Once all the parameters are determine, the PDFs can be determined. The following pseudo-codes 3.10, 3.11, 3.12 represent the function needed to define the Narrow-band PDF, the Dirlik PDF and the Tovo-Benasciutti PDF.

Consequently, for the fatigue -limit approaches, the damage accumulation rule is applied to calculate the total damage for each element. In particular the linear Miner's rule is adopted in the following code 3.13.

Finally, once the damage for each element is determined, the map of the total damage is saved in a new step within the same Odb file where the results of the random analysis are saved. This function is executed for all the methods, fatigue-limit and infinite-life approaches, and it is described in the following list 3.14.

Algorithm 1: Main Function
Main feature: checks the user-defined parameters, extract the data from the Odb file and select the fatigue function based on the user input **Inputs:** odbName , RandomStep , FatigueStep, Time, MC, b, c, SL, ModifiedSN, AFL, TFL, NCA, NCT, PDF, INF
1. Open the Odb file. 2. Check if the new steps name are correct and if the values provided are suitable with the options selected. If not, print an error message end stop the program. 3. Check if the torsional fatigue limit is provided but the modified S-N curve is not selected. If yes, print a warning message end the torsional fatigue limit is ignored. 4. Extract the frames (frequencies) and the Poisson's ratio of the material from the ODB file. 5. Save the Basquin's parameters, b and C from the user-input. 6. Extracts the stress PSDs data of each element from the Random Vibration Analysis, considering the integration point with the higher stress. The CSD are approximated. If the model is made of shell elements, a 3x3 PSD matrix is considered. If the model is made of solid elements, a 6x6 PSD matrix is considered. 7. The equivalent PSDs of the Equivalent Von Mises and Equivalent Lemaitre methods are computed. 8. Submission of the data to the appropriate function based on the user selection. Equivalent Von Mises Equivalent Lemaitre Projection by Projection Crossland Matsubara Sines 9. Submit the data to the *ContourPlot* function to create the new step with the damage results

Table 3.1: Random Vibration Fatigue Tool - Main Function

Algorithm 2: Equivalent Von Mieses Function
Main feature: compute the damage according to the PDF selected and the feature of the S-N curve **Inputs:** Time,AFL,SL,b,c, PDF, INF,$g_m ises$,fr,numElements,NCA
1. Calculate the spectral moments from the Equivalent PSDs using the function *SpectralMoments* 2. Determine the statistical parameters from the spectral moments using the function *Parameters* 3. Define the PDF by means of the corresponding function (*Narrow-band, Dirlik or Tovo-Benasciutti*) based on the user-selection 4. Return the damage calculated by the function called *Damage* to the *Main Function*

Table 3.2: Random Vibration Fatigue Tool - Equivalent Von Mises Function

Algorithm 3: Equivalent Lemaitre Function
Main feature: compute the damage according to the PDF selected and the feature of the S-N curve **Inputs:** Time, AFL,SL,TFL,NCT,b,c, ModifiedSN,PDF, INF,$g_{lemaitre}$, g_m ,fr,numElements,numFrames,deltaf,nu,NCA
1. Calculate the spectral moments from the Equivalent PSDs using the function *SpectralMoments* 2. Determine the statistical parameters from the spectral moments using the function *Parameters* 3. Define the PDF by means of the corresponding function (*Narrow-band, Dirlik or Tovo-Benasciutti*) based on the user-selection 4. In the modified S-N curve is selected, it determines the new Basquin's constants ($k_{ref} and J_{A,ref}$) based on the parameter ρ according to the Susmel model 5. Return the damage calculated by the function called *Damage* to the *Main Function*

Table 3.3: Random Vibration Fatigue Tool - Equivalent Lemaitre Function

Algorithm 4: Projection by Projection Function
Main feature: compute the damage according to the PDF selected and the feature of the S-N curve **Inputs:** Time,AFL,SL,TFL,NCA,NCT,b,c, ModifiedSN, PDF, INF,sPSD,fr,numElements,numFrames,deltaf,shell,solid
1. According to the type of element, it determines the covariance matrix 2. Project the covariance matrix in the Euclidean space 3. Determine the eigenvalue and eigenvector of the projected covariance matrix 4. Project the PSDs using the eigenvectors basis and it determines the spectral moments 5. Determine the statistical parameters from the spectral moments using the function *Parameters* 6. Define the PDF by means of the corresponding function (*Narrow-band, Dirlik or Tovo-Benasciutti*) based on the user-selection 7. In the modified S-N curve is selected, it determines the new Basquin's constants ($k_{ref} and J_{A,ref}$) based on the parameter ρ according to the Susmel model 8. Calculate the damage of each PDF of the projected stress considering or not the extended S-N curve 9. Return the total damage, determined with the non-linear accumulation rule, to the *Main Function*

Table 3.4: Random Vibration Fatigue Tool - Projection bu Projection Function

Algorithm 5: Crossland Function
Main feature: compute the damage according to the Crossland criterion **Inputs:**Time,AFL,SL,sPSD,fr,numElements,numFrames,deltaf,shell,solid
1. Determine the material's paramaters α and β according to the Crossland definition 2. Determine the spectral moments from the Equivalent Von Mises PSD and the hydrostatic PSD 3. Calculate the average number of picks n_p 4. Using the Davenport formula, it calculates the expected amplitude extremes 5. Determine the maximum amplitude of the second invariant $\sqrt{J_{2,a}}$, following the MCC and the maximum expected value of hydrostatic pressure $Max[p(t)]$ 6. Return the damage to the *Main Function* determined with the Crossland's criterion

Table 3.5: Random Vibration Fatigue Tool - Crossland Function

Algorithm 6: Matsubara Function
Main feature: compute the damage according to the Matsubara criterion **Inputs:**Time, AFL,TFL,g_{mises},g_m,fr,numElements,numFrames,deltaf
1. Determine the material's paramaters α and β according to the Matsubara definition 2. According to the type of element, it determines the covariance matrix 3. Project the covariance matrix in the Euclidean space 4. Determine the eigenvalue and eigenvector of the projected covariance matrix 5. Project the PSDs using the eigenvectors basis and it determines the spectral moments 6. Calculate the average number of picks n_p amd using the Davenport formula, it calculates the expected amplitude extremes 7. Determine the maximum amplitude of the second invariant $\sqrt{J_{2,a}}$, following the MCE 8. Determine the spectral moments from the PSDs corresponding to the normal stresses 9. Calculate the average number of picks n_p and using the Davenport formula, it calculates the expected amplitude extremes 10. Determine the expected maximum of normal stress E_S_{max} 11. Return the damage to the *Main Function* determined with the Matsubara's criterion

Table 3.6: Random Vibration Fatigue Tool - Matsubara Function

Algorithm 7: Sines Function
Main feature: compute the damage according to the Sines criterion **Inputs:**Time, AFL,TFL,SL,sPSD,fr,numElements,numFrames,deltaf,shell,solid
1. Determine the material's paramaters α and β according to the Sines definition 2. According to the type of element, it determines the covariance matrix 3. Project the covariance matrix in the Euclidean space 4. Determine the eigenvalue and eigenvector of the projected covariance matrix 5. Project the PSDs using the eigenvectors basis and it determines the spectral moments 6. Calculate the average number of picks n_p amd using the Davenport formula, it calculates the expected amplitude extremes 7. Determine the maximum amplitude of the second invariant $\sqrt{J_{2,a}}$, following the MCE 8. Determine the spectral moments from the PSDs corresponding to the hydrostatic PSD 9. Calculate the average number of picks n_p and using the Davenport formula, it calculates the expected amplitude extremes 10. Determine the expected mean values $E[p(t)]$ 11. Return the damage to the *Main Function* determined with the Sines' criterion

Table 3.7: Random Vibration Fatigue Tool - Sines Function

Algorithm 8: SpectralMoments Function
Main feature: compute the spectral moments of order $0, 1, 2$ and 4 of the PSD **Inputs:** PSD,fr,numElements
1. calculates the spectral momets of each orders by integration over the frequency range

Table 3.8: Random Vibration Fatigue Tool - SpectralMoments Function

Algorithm 9: Parameters Function
Main feature: compute the statistical parametrs from the spectral moments of order $0, 1, 2$ and 4
Inputs: m0,m1,m2,m4, numElements
1. Calculate number of upword zero crossing per second n_0^+
2. Calculate the number of peaks per second n_p
3. Determine the irregularity factor γ
4. Determine the root mean square rms
5. Calculate the mean frequency x_m

Table 3.9: Random Vibration Fatigue Tool - Parameters Function

Algorithm 10: Narrow-band Function
Main feature: Compute the PDF for Narrow-band process
Inputs: m0,s,numElements
1. Determine the PDF of narrow-band process based on the Bendat's definition

Table 3.10: Random Vibration Fatigue Tool - Narrow-band Function

Algorithm 10: Dirlik Function
Main feature: Compute the Dirlik PDF for wide-band process
Inputs: Gamma, xm, m0, s,numElements
1. Compute the parameters D_1, R, D_2, D_3, Q and Z
2. Determine the PDF of wide-band process based on the Dirlik's definition

Table 3.11: Random Vibration Fatigue Tool - Dirlik Function

Algorithm 11: Tovo-Benasciutti Function
Main feature: Compute the Tovo-Benasciuti PDF for wide-band process
Inputs: m0,m1,m2,Gamma,s,numElements
1. Compute the parameter α_1 and the factor w
2. Determine the PDF of wide-band process based on the Tovo-Benasciuti 's definition

Table 3.12: Random Vibration Fatigue Tool - Tovo-Benasciuti Function

Algorithm 12: Damage Function
Main feature: Compute the total damage for each element **Inputs:** e_P,c,b,numElements,s,ds,pdf, Time, INF, AFL, NCA
1. If the extended S-N curve is not selected, it linearly sums (Miner's rule) the damage defined accordingly with the PDF and the material parameters until the fatigue limit 2. Otherwise, it linearly sums the damages (Miner's rule), accordingly with the PDF and the material parameters, until the fatigue limit and the Haibach model is used under the knee point

Table 3.13: Random Vibration Fatigue Tool - Damage Function

Algorithm 13: ContourPlot Function
Main feature: Define a new step in the Odb file with the damage of each element saved as filed output **Inputs:** FatigueStep,damage,numElements,MC, PDF,myInstance,Odb
1. Define the new step 2. Define the new frame within the new step 3. Save the field output of Damage for each element in the new frame 4. Save and close the Odb file

Table 3.14: Random Vibration Fatigue Tool - Contourplot Function

Chapter 4

Application

The validation of the Abaqus plug-in tool developed has been carried out comparing the results obtained in two different case studies. Firstly, the L-plate subjected to random vibrations studied by Preumont in [9] was used. This case study was widely investigated by many authors with different approaches. This made possible to compare the results in terms of hotspost definition and the magnitude of the damage accumulated. Moreover, the same sample has been also studied by using the commercial software Fe-Safe in other to take into account different mesh of the structure. After that the PbP and the Crossland approaches have been selected and the real component has been tested. Hence the second case study compares the results of the plug-in tool with the results obtained by Fe-Safe for a real application. In the following subsections, the case study iis described in 4.1 and the case study iiconcerning the real component is presented in 4.2.

4.1 Case study I: L-plate

The first case study is a simple geometry defined by Pitoiset and Preumont in [9] and then adopted by many authors in literature to compare and validate their results. The plate is represented in Fig. 4.1 where the dimensions are in millimeters and its thickness is $e = 0.8$ mm. The plate is made of steel and the material properties considered for the FE model are reported in table 4.1

Elastic Modulus	Density	Poisson's Ratio
$210GPa$	$7000Kg/m^3$	0.33

Table 4.1: Material properties of L-plate

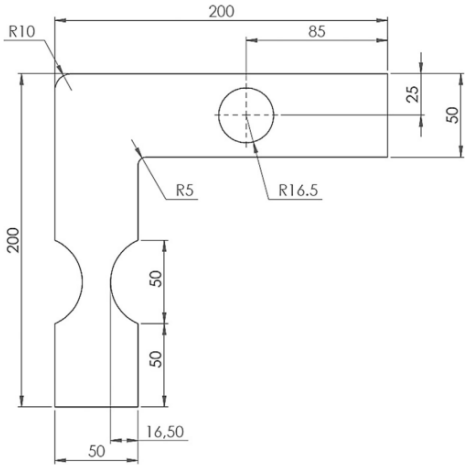

Figure 4.1: L-Plate Geometry [33]

As highlighted by Fig. 4.2, both ends of the plate are clamped and subjected to a band-limited white noise acceleration in the z direction, perpendicular to the plane of the plate. This white noise acceleration is characterized by a PSD with constant amplitude of $25\frac{(m/s^2)^2}{Hz}$ over the frequency specrtum between 0 Hz and 400 Hz. Moreover, the two supports are subjected to random vibrations completely uncorrelated.

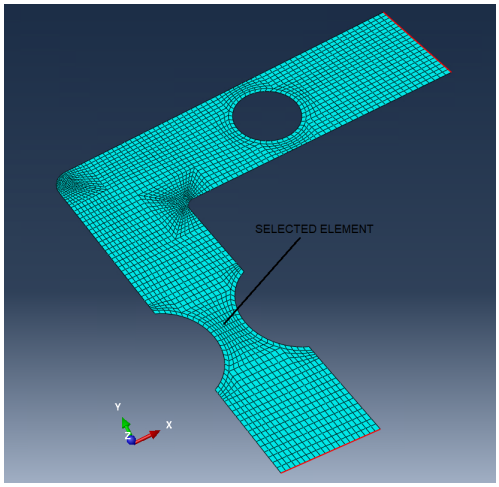

Figure 4.2: L-Plate - Case study I

The plate was discretized into a total number of 2694 linear quadrilateral shell elements of type S4R. These elements have four nodes with six degrees of freedom at each node. Before of the Harmonic analysis or the Random analysis, the Modal analysis has been performed to extract the modal basis.

The first ten eigenfrequencies and eigenmodes were determined corresponding to: $f_1 = 27.64$ Hz, $f_2 = 108.22$ Hz, $f_3 = 128.19$ Hz, $f_4 = 291.37$ Hz, $f_5 = 296.39$ Hz, $f_6 = 407.33$ Hz, $f_7 = 489.94$ Hz, $f_8 = 597.83$ Hz, $f_9 = 668.82$ Hz, $f_{10} = 739.27$ Hz. The first 5 modes are represented in the following figure 4.3

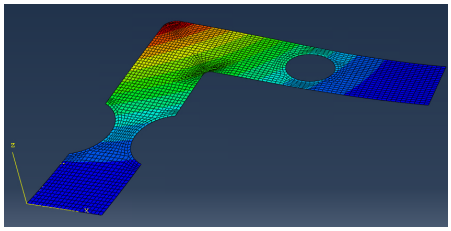

(a) First Mode

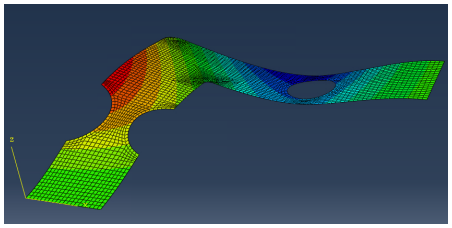

(b) Second Mode

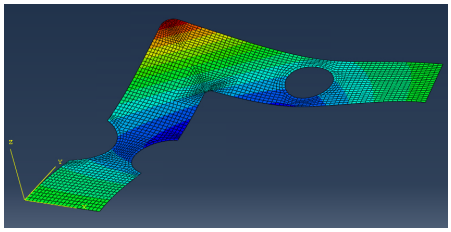

(c) Third Mode

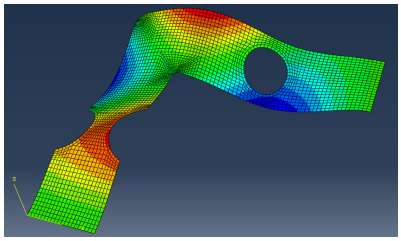

(d) Fourth Mode

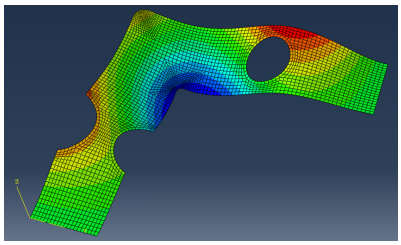

(e) Fifth Mode

Figure 4.3: Normal modes

Then, the Random analysis was performed considering a modal damping of 3.5% equal for each mode. Fig. 4.4 shows the stress PSDs obtained from the Random Analysis, for the element in the center of the notched area, as highlighted by Fig. 4.2. The unit for the stress PSD is $\frac{Pa^2}{Hz}$ and the unit for the frequencies is Hz.

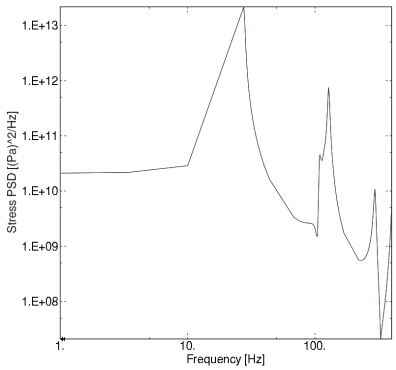

(a) PSD $G_{xx,xx}$

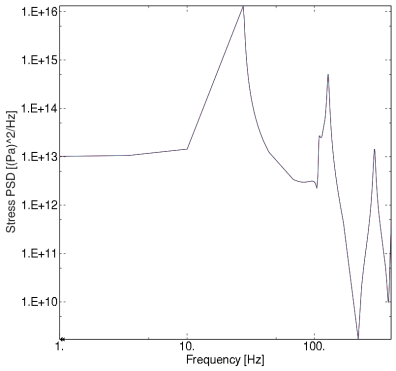

(b) PSD $G_{yy,yy}$

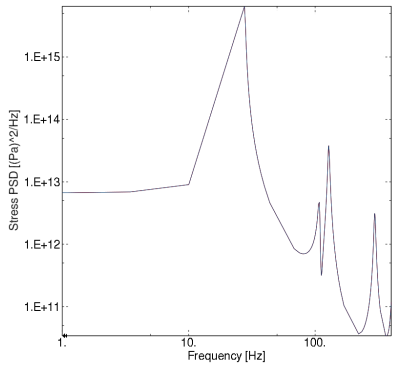

(c) PSD $G_{xy,xy}$

Figure 4.4: Stress PSDs of the element in the middle of the notched area

4.2 Case study II: Bracket

In order to apply and validate the tool against a real component, a bracket with aerospace application is studied. The geometry of the bracket is represented in Fig. 4.5. It is obtained from an aluminium sheet with $t = 1.0$ mm thickness and the material properties considered for the FE model are reported in table 4.2. The bracket finds application in the helicopters field and it is used to fix three cable connectors to the structure. For this reason it is subjected to a random vibration background which can cause a fatigue failure.

Elastic Modulus	Density	Poisson's Ratio
$70GPa$	$2700Kg/m^3$	0.33

Table 4.2: Material properties of bracket

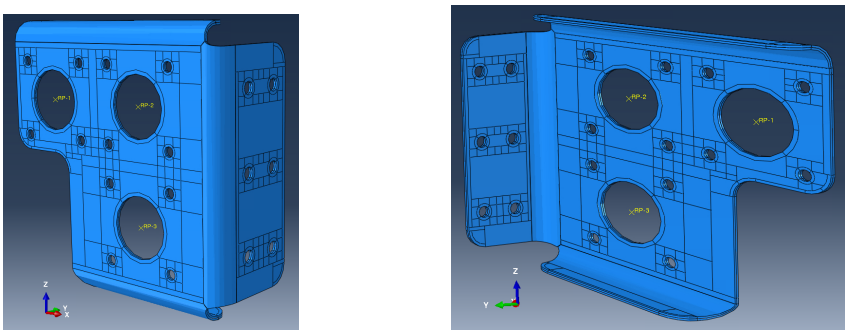

Figure 4.5: Bracket Geometry

The vibration spectrum in a helicopter is characterized by the combination of two effects: a continuous wide-band low-level background and strong narrow-band peaks superimposed. The narrow-band picks correspond to the main and tail rotors rotation frequency (f_1) and their harmonics (f_n). However, the vibration environment is defined also by a low-level random component due to aerodynamic flow. Thus, the tool is applied to study the fatigue damage caused by these random vibrations on the bracket. In particular, the standard MIL-STD-810F [16] is considered to define the PSD of the random vibrations and in particular, Fig. 4.6 represent the PSD of the acceleration applied to all three orthogonal axis of the Cartesian system of reference. As highlighted by Fig. 4.7a, the bracket is considered to be fixed to the main structure of the helicopter through the six holes to the right. With reference to Fig. 4.6, the random acceleration PSD is characterized by a constant amplitude of $W_1 = 0.02\ \frac{g^2}{Hz}$ between 100 and 300 Hz, starting from $W_0 = 0.002\ \frac{g^2}{Hz}$ at 10 Hz and ending at the same value at 2000 Hz. Moreover, the random vibrations transmitted by the six holes are considered completely uncorrelated.

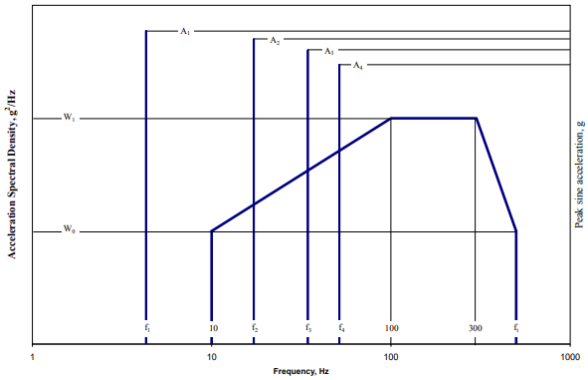

Figure 4.6: Acceleration PSD representing the helicopter vibration environment [16]

In order to represent the mass of the cable connectors which are fixed to the three bigger holes of the bracket, a concentrated mass of $0.3Kg$ is positioned in the center of each hole and it is rigidly connected to all the nodes on the perimeter of the hole. These concentrated masses, represented by the green squares in Fig. 4.7b, permit to simplify the study of the component dynamic behavior since the complete model of the connector it is not more needed.

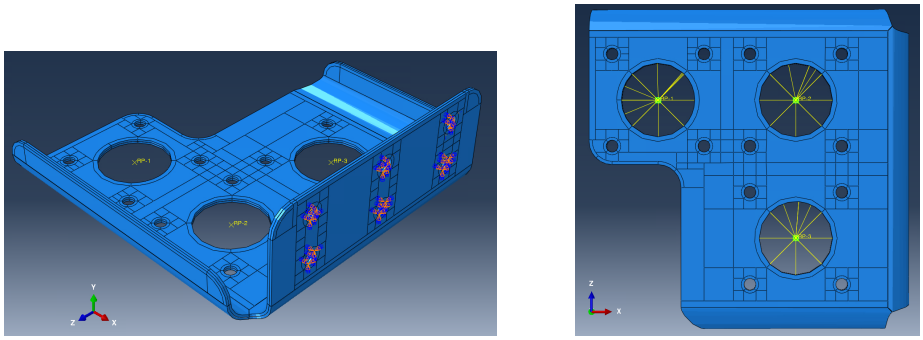

(a) Bracket boundary conditions (b) Mass elements

Figure 4.7: Bracket's model

The component has been discretized into a total number of 6356 linear quadrilateral shell elements of type S4R which have four nodes with six degrees of freedom at each node. As done for the L-plate, a Modal analysis has been performed to extract the modal basis. The first ten eigenmodes were determined and the cooresponding eigenfrequencies are reported on the table 4.3. The first 8 modes, which are within the helicopter frequency spectrum, are represented in the following figure 4.8 and their contour plots refer to the magnitude of the displacements.

Mode	Frequency [Hz]
1	20.65
2	90.43
3	128.3
4	234.9
5	308.5
6	1121.5
7	1542.5
8	1966.9
9	2720.3
10	3156.8

Table 4.3: First ten natural frequencies of the bracket

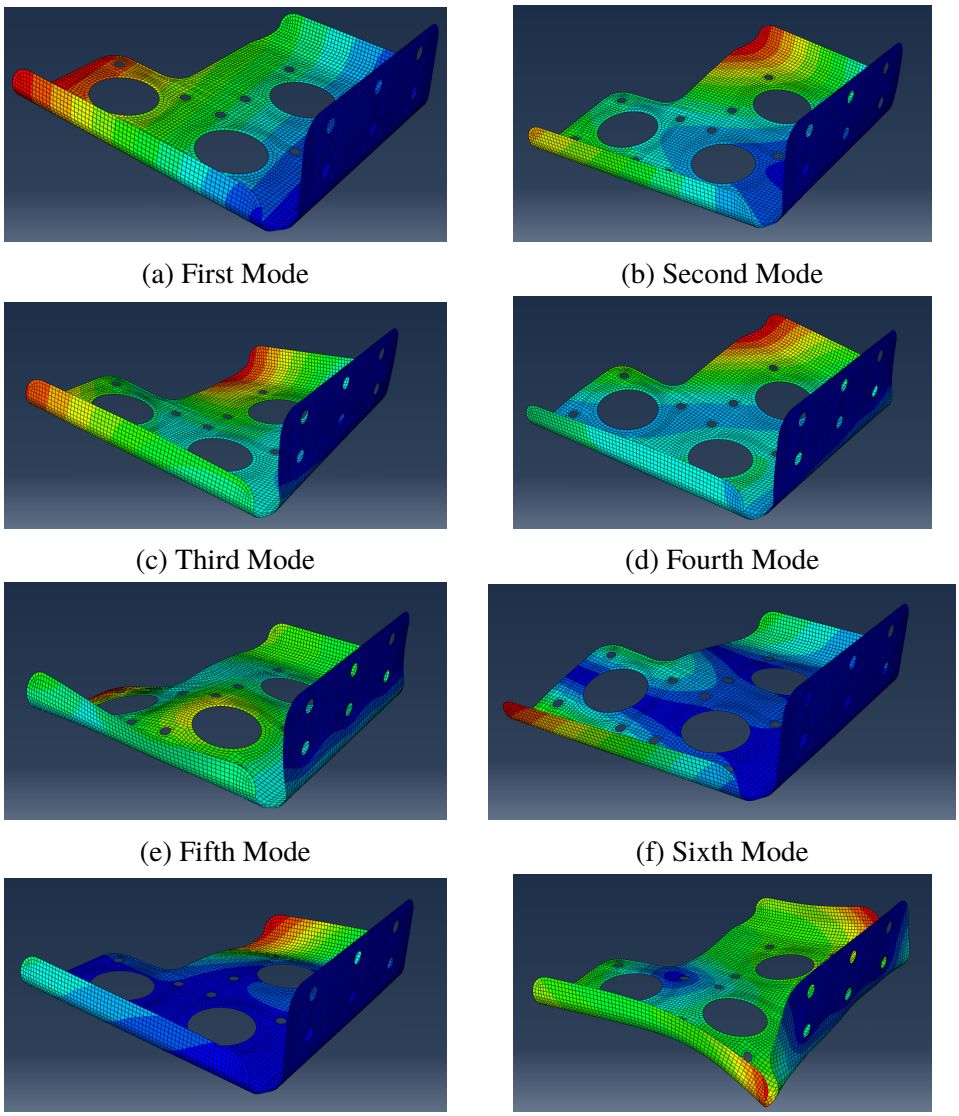

(a) First Mode (b) Second Mode

(c) Third Mode (d) Fourth Mode

(e) Fifth Mode (f) Sixth Mode

(g) Seventh Mode (h) Eighth Mode

Figure 4.8: Normal modes

Then, in order to generate the stress PSDs needed for the fatigue analysis, the Random analysis was performed considering a modal damping of 2.5% for each mode and considering the acceleration PSD defined by the standard MIL-STD-810F [16] from 10 Hz to 2000 Hz.

Chapter 5

Results

This chapter presents, the results obtained, for both case studies, with the random vibration fatigue tool developed and the Fe-Safe software. In particular, the fatigue hotspot identification and the value of the maximum damage accumulated are compared considering the results obtained with the fatigue tool and the commercial software Fe-Safe. All different methods are analysed for the fist case study and then only the Projection by Projection method and the Crossland method are applied to the second case study.

5.1 Comparison between the Fatigue Tool and Fe-Safe

5.1.1 L-Plate

Once the Modal analysis and the Random analysis with modal superposition were performed, the Random Vibration Fatigue tool developed has been applied to estimate the damage accumulated on the L-plate by these random vibrations. The first purpose of this study was to validate the tool against the results found in literature. Moreover, this case study permitted to compare all the six multi-axial approaches with focus on the ability to determine the right hotspot and an acceptable total damage. The following table 5.1 contains the material properties used for the analysis. As mentioned before, these properties are derived from the elastic region of the axial and torsional S-N curves of the material. Moreover, the previous defined PSD is considered to represent the a random vibration loading of 12 seconds.

Axial Inverse Slope b	9.82
Axial Constant C [Pa]	$4.0641 \cdot 10^{88}$
Strength limit [Pa]	$340 \cdot 10^{6}$
Axial Fatigue Limit [PA]	$252 \cdot 10^{6}$
Torsional Fatigue Limit [Pa]	$180 \cdot 10^{6}$
Reference Number of Cycles	$1.28 \cdot 10^{6}$
Torsional Inverse Slope b_t	9.0

Table 5.1: Fatigue Material Properties - Case Study I

The first approach investigated was the Equivalent Von Mises, considering the Dirlik PDF and the fatigue limit, so the stresses under the knee point were not considered damaging. The contour plot of the damage obtained for this analysis is shown by the following figure 5.1 where the maximum damage obtained is $5.31 \cdot 10^{-4}$.

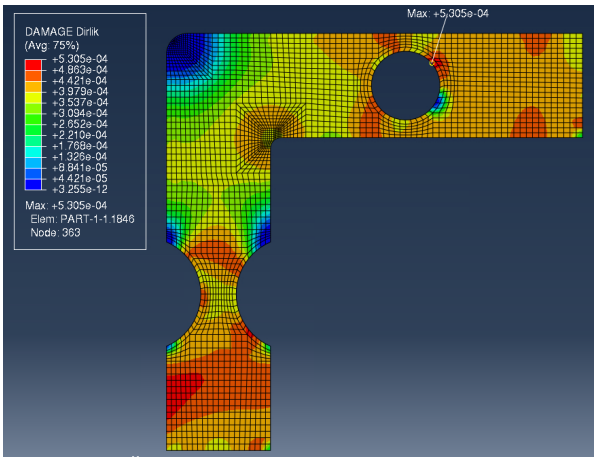

Figure 5.1: Equivalent Von Mises - Case study I

The same considerations about the Dirlik PDF and the fatigue limit were made, then, for the Equivalent Lemaitre method. Without considering the modified S-N curve, it differs to the Equivalent Von Mises only for the Poisson's ratio. Hence, for this reason, Fig. 5.2 shows the same map as the case of Equivalent Von Mises and the results are almost the same, leading to the maximum damage of $5.23 \cdot 10^{-4}$.

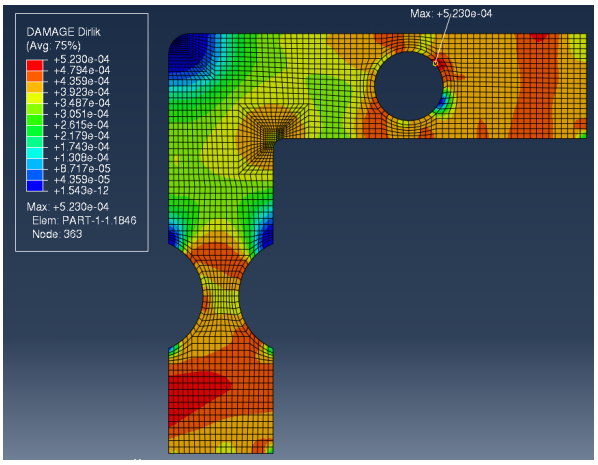

Figure 5.2: Equivalent Lemaitre - Case study I

The last fatigue-limit approach implemented is the Projection by Projection method which presents a different map compared to the previous spectral methods. With the same assumptions as before, Fig. 5.3 shows that the maximum damage of $2.93 \cdot 10^{-4}$ moves from the top right side of the hole to the middle of the left side of the notch, even if the modified S-N curve is not considered in this contour plot.

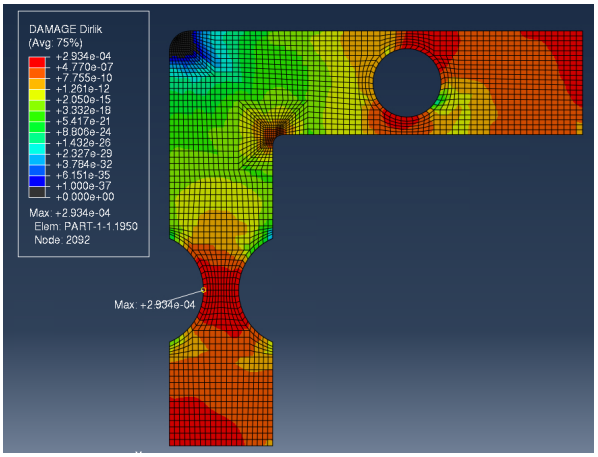

Figure 5.3: Projection by Projection - Case study I

Moving to the infinite-life approaches, the Crossland criterion was applied to the L-Plate and Fig. 5.4 shows the contour plot obtained. The map is similar to the Projection by Projection method but there is an effect of the Boudary conditions. The maximum damage of 2.76, excluding the elements near the

supports of the plate, moves to the middle of the left side of the notch where it is 2.65. Moreover the maximum damage exceed the maximum value of 1 so this means that the stresses obtained from the random vibrations exceed the fatigue limit and hence are damaging. It turns out that the previous analysis were correct since only the stresses above the knee point were considered.

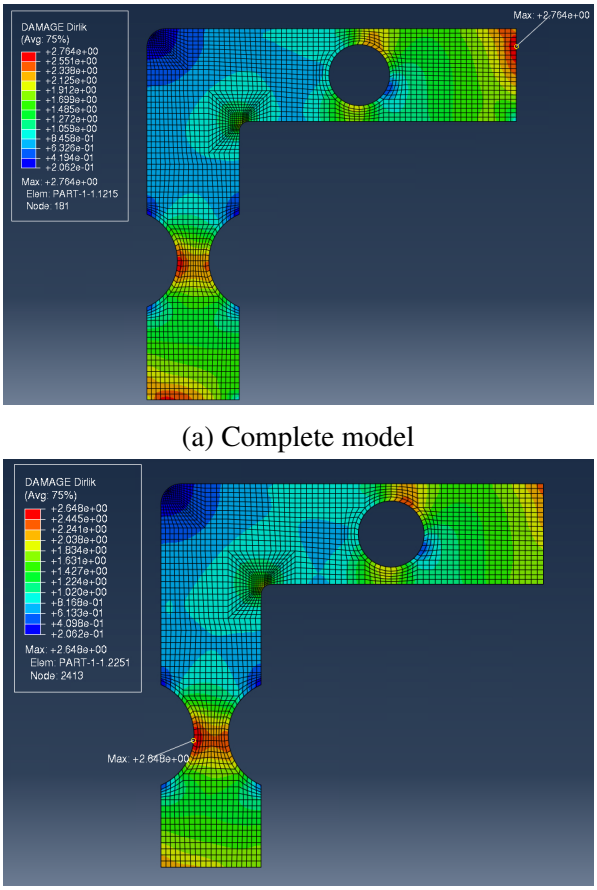

(a) Complete model

(b) Without Boundary Conditions effects

Figure 5.4: Crossland - Case study I

Following the same approach, also the Matsubara criteria was applied. As for the Crossland criterion, Fig. 5.5 shows that there is an influence of the boundary conditions. In fact, as for Crossland, the maximum damage of 5.36 moves to the left side of the notch with a value of 4.67. However, the map obtained is the same as the Crossland criterion and the Matsubara method predicts even more damaging random vibrations.

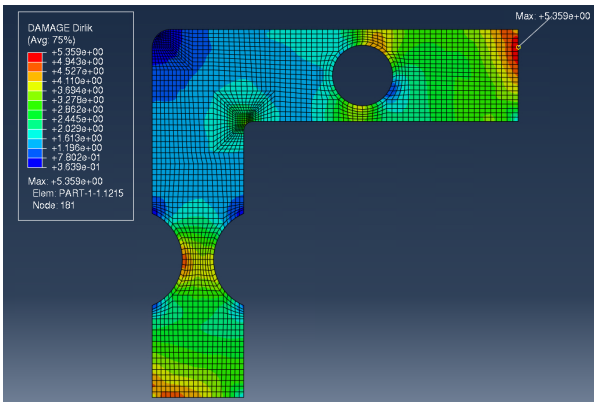

(a) Complete model

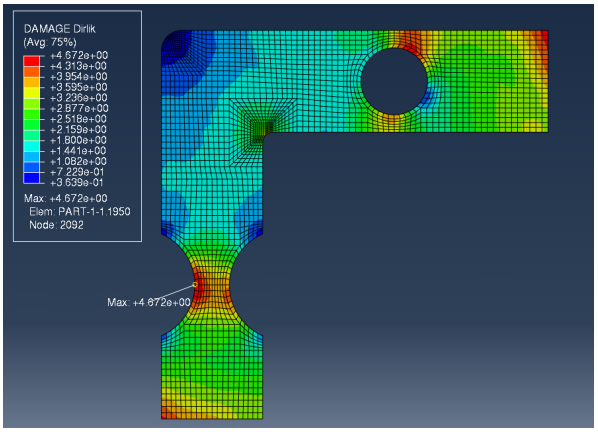

(b) Without Boundary Conditions effects

Figure 5.5: Matsubara - Case study I

The last method implemented is the Sines criteria, very similar to the Crossland criterion. In fact, this feature is reflected on the map of damage, as shown by Fig. 5.6 where the boundary effects were excluded and leading to a maximum damage of 2.97.

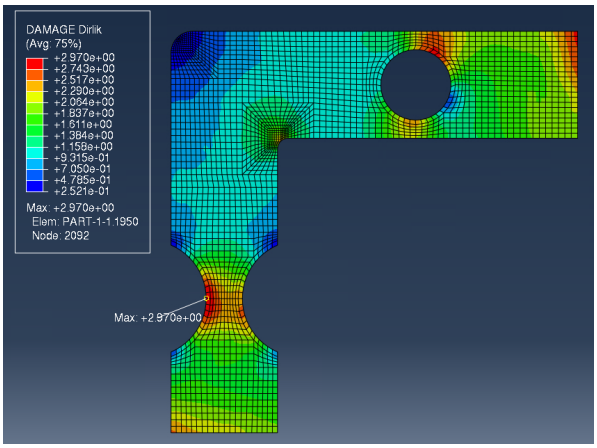

Figure 5.6: Sines - Case study I

Using the Tovo-Benasciutti's PDF the results are very similat to the Dirlik's PDF. In particular, Fig. 5.7 shows that the map obtained with the Projection by Projection method is the very similar to the previous one. Also the maximum total damage estimated is affected by a very small variation and in this case is $2.93 \cdot 10^{-4}$.

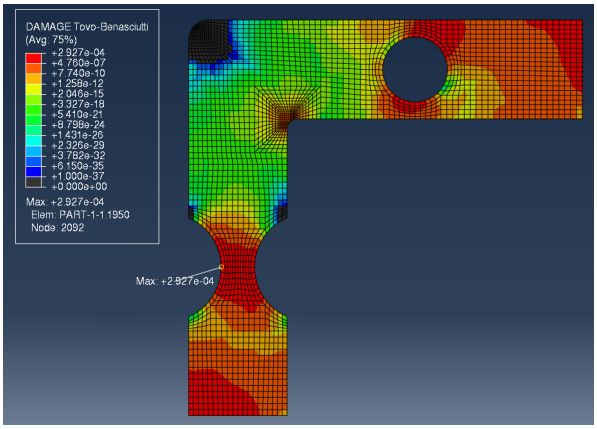

Figure 5.7: Projection by Projection with Tovo-Benasciutti's PDF - Case study I

Using the Narrow-band PDF instead, the map determined is completely different compared to the previous but also the total damage determined become very conservative. Fig. 5.8 shows that the maximum total damage of $1.78 \cdot 10^{-1}$ is three orders of magnitude higher than with the Dirlik's and Tovo-Bneasciutti's PDFs. However, excluding the boundary effect it become

$6.44 \cdot 10^{-2}$ and hence two orders of magnitude higher compared to the others methods.

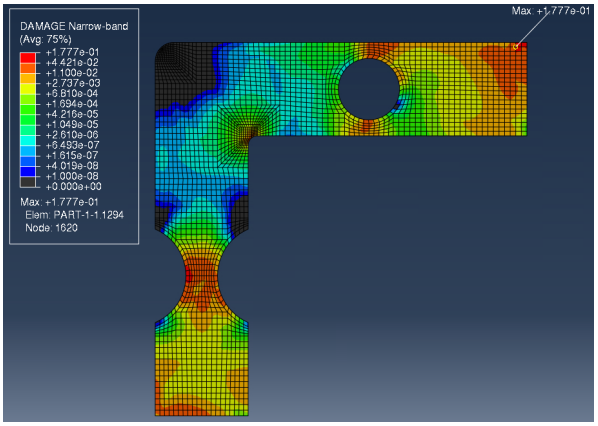

(a) Complete model

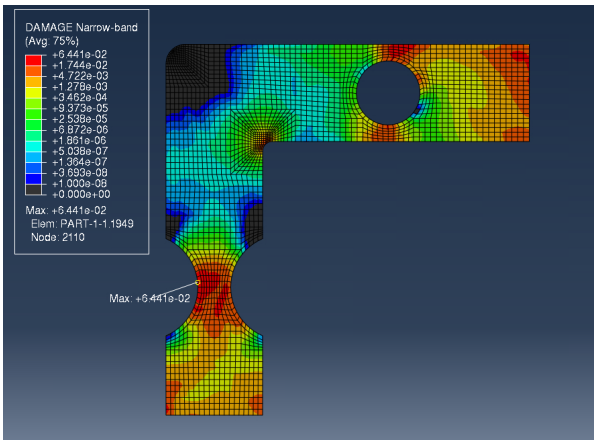

(b) Without Boundary Conditions effects

Figure 5.8: Projection by Projection with Narrow-band PDF - Case study I

The extended S-N curve with the Haibach assumptions was applied to all three multi-axial criteria with the Dirlik method. As can be seen in Fig. 5.9, the maximum total damage determined increases in all three cases and it becomes $5.47 \cdot 10^{-4}$ for the Equivalent Von Mises method, $5.39 \cdot 10^{-4}$ for the Equivalent Lemaitre method and $3.73 \cdot 10^{-4}$ for the Projection by Projection method. However, they does not change significantly since the stresses below the fatigue limit turn out to be not particularly damaging.

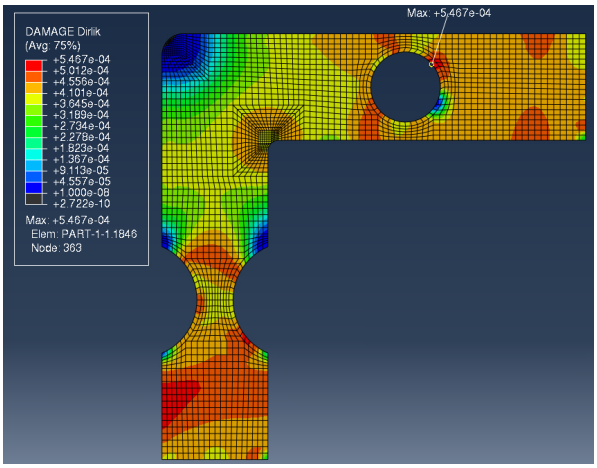

(a) Equivalent Von Mises

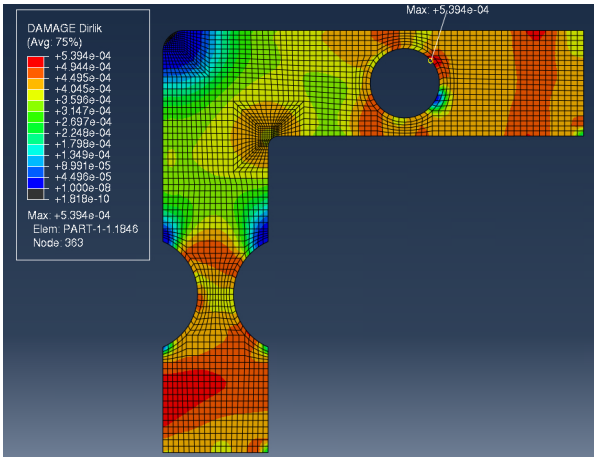

(b) Equivalent Lemaitre

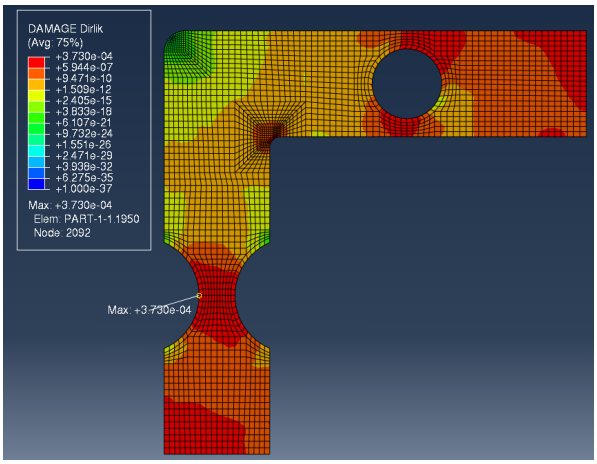

(c) Projection by Projection

Figure 5.9: Multi-axial criteria with extended S-N curve

Lastly, the modified S-N curve with the Susmel's assumptions was considered. It takes into account also the torsional S-N curve of the material as well as the axial S-N curve. In particular, the Equivalent Lemaitre e the Projection by Projection approaches were analyzed and the results are reported in the following figure 5.10. The maximum damages obtained in this case are $2.37 \cdot 10^{-4}$ for the Equivalent Lemaitre method and $4.86 \cdot 10^{-2}$ for the Projection by Projection method.

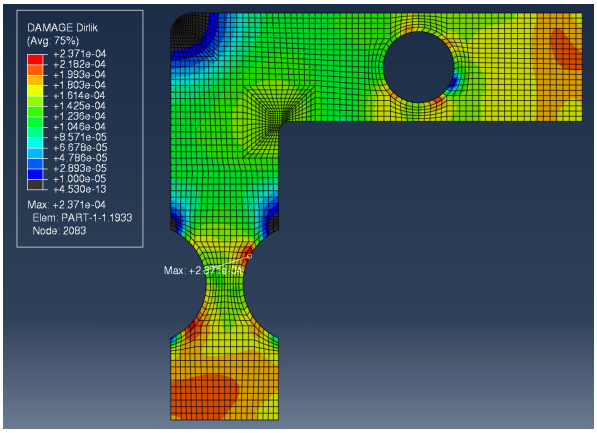

(a) Equivalent Lemaitre

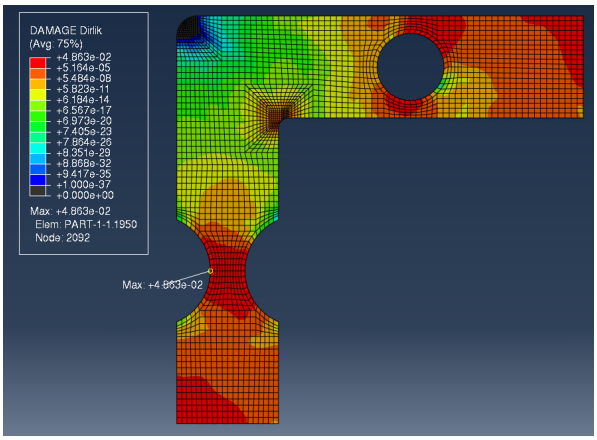

(b) Projection by Projection

Figure 5.10: Multi-axial criteria with modified S-N curve

To validate and compare the results obtained, the commercial software Fe-Safe was used. In particular, the following Fig. 5.11 shows the map of total damage accumulated by the component in the same conditions of loading as the previous analysis performed with the plug-in tool in Abaqus. This

contour plot has been obtained considering the Equivalent Von Mises multiaxial criteria and the Dirlik's PDF. The maximum damage obtained with Fe-Safe is $4.73 \cdot 10^{-4}$ and hence it is the same order of magnitude of the damages determied by the methods implemented into the fatigue tool.

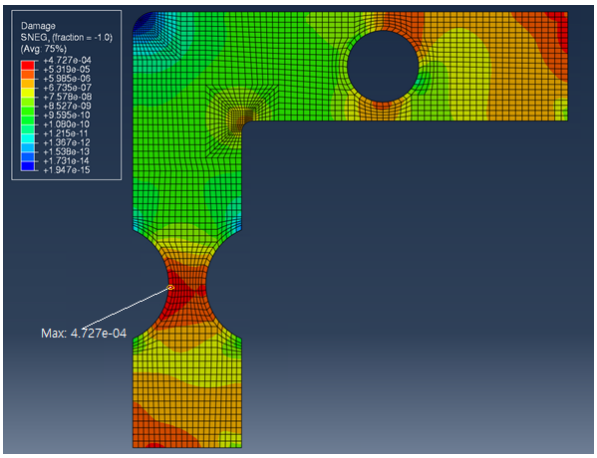

Figure 5.11: Fe-Safe result with Equivalent Von Mises multiaxial criteria and Dirlik's PDF - Case study I

As expected, the same map of damage is obtained with the Tovo-Benasciutti's PDF, as shown by Fig. 5.12. The maximum total damage determined of $4.72 \cdot 10^{-4}$ is equal to the maximum obtained with the Dirlik's PDF and the same hotspot is determined.

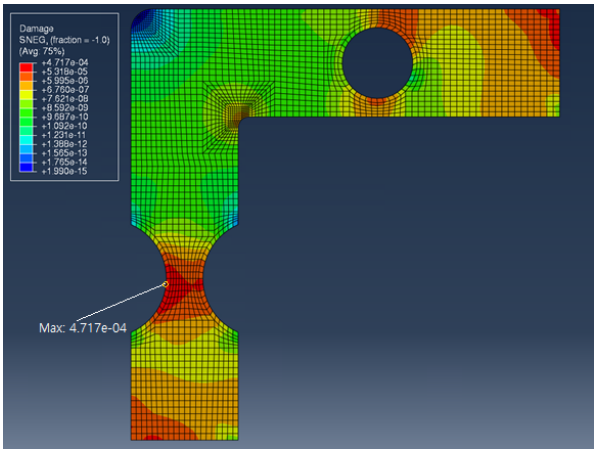

Figure 5.12: Fe-Safe result with Equivalent Von Mises multiaxial criteria and Tovo-Benasciutti's PDF - Case study I

The results obtained with Fe-Safe show that the lack of the phase information in the plug-in tool mean that the hotspot determined with the Equivalent Von Mises and the Equivalent Lemaitre in the pug-in tool could be not exactly correct. However, the Fe-Safe's results confirm the good estimation of the hotspot and the maximum total damage obtained with the Projection by Projection multi-axial criteria. Also in the safe-life approaches the map obtained is consistent with the results showed by Fe-Safe. However, Fe-Safe does not implement this type of approach and hence a direct comparison is not possible. However, in literature other authors have studied this L-plate by using safe-life approaches. The results obtained for the Crossland criterion are reported in [9] [34] and are shown in Fig. 5.13 where the maximum damage corresponds to about 2.5.

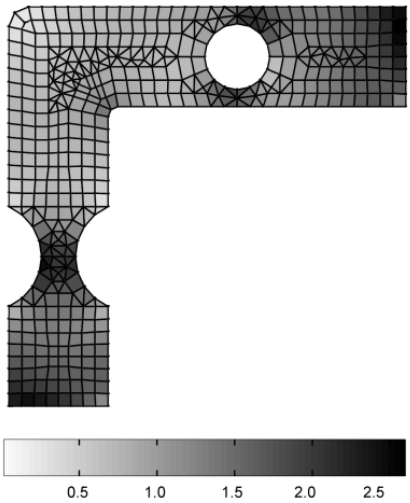

Figure 5.13: Damage map obtained with the Crossland criterion [34] - Case study I

Anyway, Fe-Safe allows to use critical plane criteria to define the equivalent uniaxial PSD. In particular, the three different definition of critical plane lead to different results in the total damage accumulated. However, as shown by Fig. 5.14, excluding the boundary conditions effects, all three criteria define the same hotspot. The critical plane defined by the maximum normal stress leads to a maximum damage of $6.54 \cdot 10^{-5}$. The critical plane defined by the maximum shear stress, instead, leads to a maximum damage of $1.47 \cdot 10^{-3}$. Finally, combining the two definitions with a factor $k = 0.25$ on the shear stress, the maximum damage becomes $5.96 \cdot 10^{-4}$.

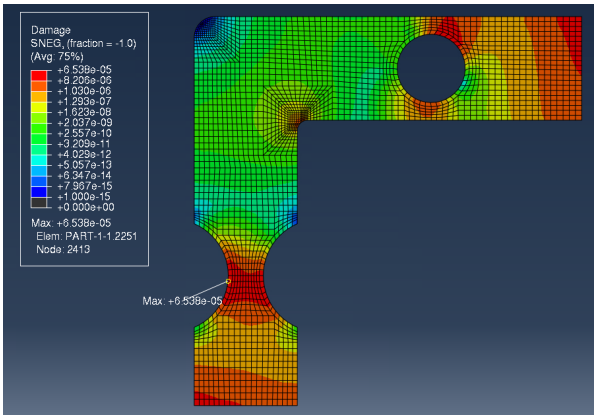

(a) Maximum Normal Stress

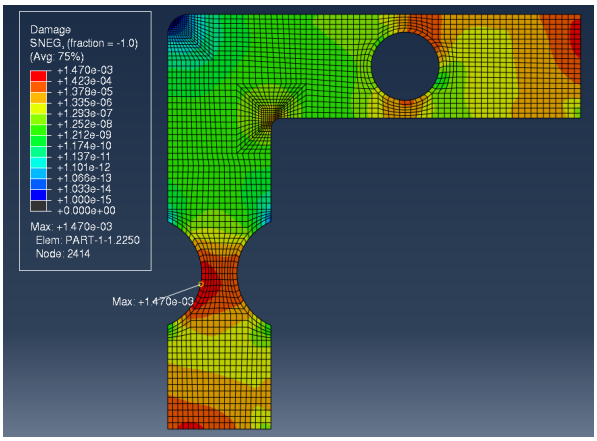

(b) Maximum Shear stress

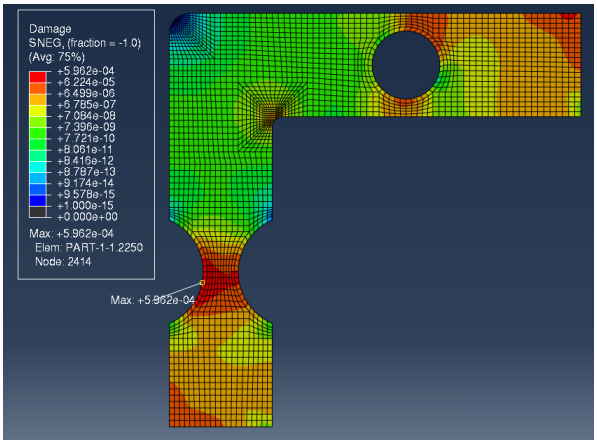

(c) Combination of Normal and Shear stress with factor k=0.25

Figure 5.14: Fe-Safe's results with Critical Plane criteria

5.1.2 Bracket

As done for the L-plate, once the modal analysis and the random analysis are performed, the Random Vibration Fatigue tool developed can be applied to estimate the total damage accumulated on the component. In fact, the aims of the study are to determine the hot-spot where the fatigue failure can happen first and to calculate the total damage accumulated in order to address the life of the component. In particular, in order to limit the study to one fatigue-limit criteria and one infinite-life criteria, the Projection by Projection and the Crossland criteria were applied to study the bracket since these two have demonstrated better results when applied to the first case study. The following table 5.2 contains the material properties used for the analysis and the previous defined PSD is considered to represent the a random vibration loading of 10 seconds.

Axial Inverse Slope b	8.55
Axial Constant C [Pa]	$1.62 \cdot 10^{82}$
Strength limit [Pa]	$360 \cdot 10^{6}$
Axial Fatigue Limit [PA]	$120 \cdot 10^{6}$
Torsional Fatigue Limit [Pa]	$80 \cdot 10^{6}$
Reference Number of Cycles	$2.0 \cdot 10^{6}$

Table 5.2: Fatigue Material Properties - Case Study II

The following Fig. 5.15 represents the contour plot of the total damage obtained with the fatigue-limit approach. In particular, the damage is obtained considering the Projection by Projection method in combination with the Tovo-Benasciutti PDF and excluding the stresses below the knee point. As highlighted by the figure, the maximum damage is obtained on the top left hole used to fix the bracket to the structure and hence the value of the total damage could suffer of the boundary condition effect. However, the maximum damage determined by the tool is $1.85 \cdot 10^{-6}$ which corresponds to a total life of around 2800 hours before the a crack might occur.

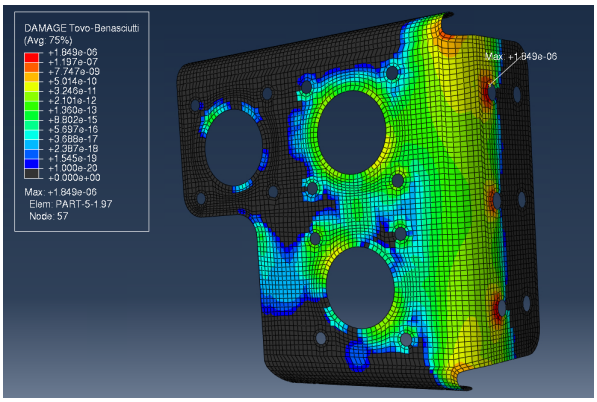

Figure 5.15: Projection by Projection - Case study II

Considering the infinite-life approach instead, Fig. 5.16 shows the damage contour plot obtained considering the Crossland criterion. The map is limited to the elements that exceed the damage value of 1, hence the elements for which a fatigue failure can occur. Also in this second case, the maximum value of 12.5 is obtained on the top left hole and thus it could be effected by the Boudary conditions. However, the maximum damage largely exceed the maximum value of 1 and hence this means that the stresses obtained from the random vibrations could lead to a fatigue crack starting from the hole. This analysis confirms the correctness of the previous one, since only the stresses above the knee point were considered.

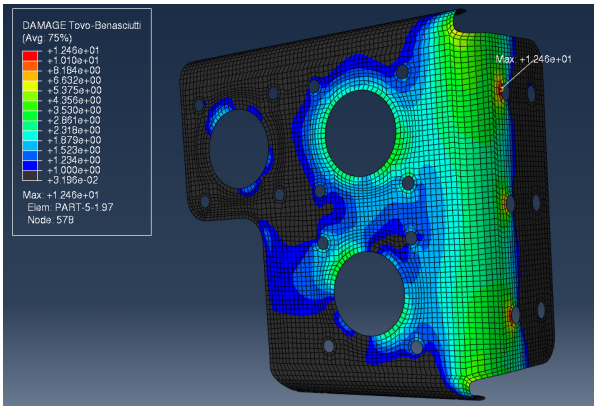

Figure 5.16: Crossland - Case study II

As done for the L-plate, also for this second case study, the results obtained with the tool are validated and compared to the damage map obtained using the commercial software Fe-Safe. Considering the same loading conditions

applied to the analysis with the the plug-in tool in Abaqus, the following Fig. 5.17 shows the map of total damage accumulated by the component determined with Fe-Safe. In particular the contour plot has been obtained considering the Equivalent Von Mises multi-axial criteria, the Dirlik's PDF and the same material properties as used into the tool. The maximum damage determined by the commercial software is $9.20 \cdot 10^{-7}$.

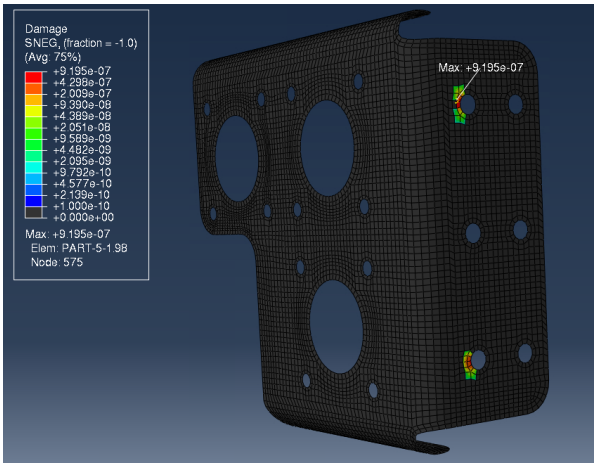

Figure 5.17: Fe-Safe result with Equivalent Von Mises multiaxial criteria and Dirlik's PDF - Case study II

As showed, the Fe-Safe's results confirm the good estimation of the hotspot and the maximum total damage obtained with both criteria. Moreover, the order of magnitude of the maximum total damage obtained with Fe-Safe is the same as for the fatigue-limit approach with the plug-in tool, even if for both there could be boundary effects that affect the real life of the component. However, also the damage map obtained for the safe-life approaches with the Crossland criteria is consistent with the results showed by Fe-Safe.

Chapter 6

Discussions

This last chapter aims to present the main findings derived from the work done. In particular, the purpose of this chapter is to highlight the main characteristics of the results obtained and define the future employment of the tool in the study of random vibration fatigue. Moreover, a final section is dedicated to future works on this field that can extend and improve the fatigue tool in Abaqus.

6.1 Conclusions

The two case studies used to validate the fatigue tool permitted to derive some clear result on the application of the plug-in tool in Abaqus for random vibration fatigue calculation.

Firstly, the employment of spectral methods permits to determine the hotspot of the component, where the fatigue crack can more likely appear, more quickly compared to time domain approaches. This means that the analysis of also detailed components characterized by thousands of elements can be performed in a few tens of minutes. However, these methods, as described, are limited to zero mean random vibrations with Gaussian distribution, which could be not always the case.

Moreover, the tool permits to simplifies the procedure requested to the user since it takes advantage of the Abaqus random analysis, where the PSDs of the acceleration can be directly defined. To address the same calculation with a commercial software as Fe-Safe, it requires the definition of an additional file which contains the acceleration PSDs. However, this has demonstrated

an important drawback of the random analysis in Abaqus. In fact, it does not determine the stress CSD and hence the phase information of the stress are lost. This can be very significant especially for out-of-phase stress components. The Equivalent Von Mises and the Equivalent Lemaitre methods make use of the real part of the stress CSD, which was approximated. This assumption can lead to error on the equivalent PSD, generating a different damage map as obtained in the first case study for the L-Plate. Moreover, as demonstrated by [35], the Equivalent Von Mises stress PSD formula is better suited for in-phase since it neglects phase differences between the bi-axial stresses leading to errors in case of out-of-phase stress components.

In addition, the Equivalent Von Mises approach can be applied only to a very small class of materials and for this reason the modified S-N curve was implemented. It demonstrated that quite significant different damages can be obtained if also the torsional fatigue curve is considered. The extension of the S-N curve under the knee point could lead or not to important differences in the damage map which depends on the specific case of the material properties and the intensity of the loading.

The first case study has also highlighted that the results obtained with the Dirlik's PDF and the Tovo-Benasciutti's are equivalent and it confirmed that the Narrow-band method define a conservative determination of the damage when it is applied to broad-band spectra.

Among the finite-life approaches, the Projection by Projection approach has demonstrated to achieve good results compared to Fe-Safe and hence it was adopted to study the bracket in the second case study. As evidenced, it permitted to correctly define the fatigue hotspot and obtain similar results in terms of maximum total damage accumulated on the component.

For what concerns the infinite-life approaches, the Crossland, Sines and Matsubara methods showed to obtain very similar results and hence the preference of one method depends only on the specific case. Since this type of methods are not implemented on commercial software as Fe-Safe, a direct validation could not be done but however the results obtained for the L-plate are consistent with the finite-life approach results and the literature.

However, all the methods developed refers to HCF and hence to the stress state. For this reason, caution has to be made when the random vibration

loading is particularly intense and high level of stress are reached in the component. In this case, the assumption could not be valid and it could lead to significant errors.

Moreover, also the modal damping used in the random analysis has to be defined correctly, especially when the natural frequency are exited. A smaller or higher damping could lead to significant difference in the stress PSD and hence leading to significant variations in the total damage accumulated.

Finally, the methods developed are defined in a statistchal sense and the random nature of the processes analysed are such that only appropriate test campaigns can correctly evaluate the damage accumulation on the component, especially for non-proportional loading.

6.2 Future works

Some assumptions were made to develop the fatigue tool and hence they define all potential future works to extend the tool to more general cases.

In particular, the effects of temperature or corrosion, as the surface roughness or the stress concentrations were not considered and are some possible feature that might be included into the tool.

However, the main restriction of the study is that it is limited to random stationary ergodic processes with zero mean and Gaussian distribution, which is a strong simplification needed to address the problem with the existing methods.

However, some method as the Tovo-Benasciutti were developed also for non Gaussian [36] or for non stationary switching random loads [22] cases even if they are limited to the uni-axial case. Thus, future works on this field might extend the tool to non Gaussian or non stationary random processes in more general cases.

In addition, the study does not take into account the mid stress correction and only zero mean stress processes are considered. Thus, a further development of the fatigue tool concerns the mean stress.

For this purpose, in vibration fatigue analysis, it is common to determine the static stress level (*i.e.,* the mean stress levels) and then shift the S–N curve by applying mean stress correction theories (Goodman, Soderberg).

However, as suggested by Aykan in [37], a better and faster solution is to calculate the damage, considering the mid stress correction, of the most critical point only after calculating the damage with the oscillating stresses for

the entire component.

An additional improvement to the work concerns the inclusion of the exact stress CSDs, which are not directly available in the random analysis with Abaqus CAE.

This upgrade can extend, in a more accurate way, the tool to the study of also out-of-phase stresses.

Finally, in the helicopter field but also in other engineering sectors, the environmental excitation is not strictly random but it is composed of sinusoidal contributions superimposed to random vibrations.

Thus, a further study could involve the implementation of spectral methods to directly study Sine-on-Random excitation, as proposed in [38] without the need of an harmonic removal technique to separate the deterministic and the random components.

References

[1] G. Teixeira, R. Hazime, J. Draper, and D. Jones, "Random vibration fatigue: Frequency domain critical plane approaches," vol. 9, 11 2013. doi: 10.1115/IMECE2013-62607 [Pages ix and 3.]

[2] L. Y. Quigley J. and W. L., "Review and assessment of frequency-based fatigue damage models," vol. 9(3):565-577, 05 2016. doi: 10.4271/2016-01-0369. p. 13. [Pages ix, 5, and 54.]

[3] J. S. Bendat, "Probability functions for random responses: prediction of peaks, fatigue damage, and catastrophic failures," 1964. [Pages 5 and 36.]

[4] T. Dirlik and D. Benasciutti, "Dirlik and tovo-benasciutti spectral methods in vibration fatigue: A review with a historical perspective," *Metals*, vol. 11, no. 9, 2021. doi: 10.3390/met11091333. [Online]. Available: https://www.mdpi.com/2075-4701/11/9/1333 [Pages 5, 34, and 54.]

[5] P. X. and P. A., "Spectral methods for multiaxial random fatigue analysis of metallic structures," *International journal of fatigue*, vol. 22, no. 7, pp. 541–550, 2000. [Pages 6, 36, 37, and 41.]

[6] J. Ge, Y. Sun, and S. Zhou, "Fatigue life estimation under multiaxial random loading by means of the equivalent lemaitre stress and multiaxial s–n curve methods," *International Journal of Fatigue*, vol. 79, pp. 65–74, 2015. doi: https://doi.org/10.1016/j.ijfatigue.2015.04.022. [Online]. Available: https://www.sciencedirect.com/science/article/pii/S0142112315001383 [Pages 6 and 38.]

[7] C. Alessandro and B. Denis, ""projection-by-projection" approach: A spectral method for multiaxial random fatigue," vol. 1, 04 2014. doi: 10.4271/2014-01-0924 p. 13. [Pages ix, x, 6, 43, and 62.]

[8] A. Yaich, G. Kharmanda, A. El Hami, L. Walha, and M. Haddar, "Reliability based design optimization for multiaxial fatigue damage analysis using robust hybrid method," *Journal of mechanics*, vol. 34, no. 5, pp. 551–566, 2018. [Pages 6 and 36.]

[9] R. I. Pitoiset X. and P. A., "Spectral methods to estimate local multiaxial fatigue failure for structures undergoing random vibrations," *Fatigue fracture of engineering materials structures*, vol. 24, no. 11, pp. 715–727, 2001. [Pages 6, 36, 38, 40, 45, 50, 81, and 99.]

[10] A. Yaich and A. El Hami, "Multiaxial fatigue damage estimation of structures under random vibrations using matsubara's criterion," *International Journal of Fatigue*, vol. 124, pp. 253–264, 2019. doi: https://doi.org/10.1016/j.ijfatigue.2019.03.003. [Online]. Available: https://www.sciencedirect.com/science/article/pii/S0142112319300696 [Pages 6 and 36.]

[11] C. Lalanne, *Fatigue damage*, third edition. ed., ser. Mechanical Vibration and Shock Analysis ; Volume 4. London, England ;: ISTE Ltd, 2014 - 2014. ISBN 1-5231-1094-5 [Pages x, 6, 36, and 61.]

[12] C. A. Marques Julian Marcel Enzveiler, Benasciutti Denis and S. Andrea, "An algorithm for fast critical plane search in computer-aided engineering durability analysis under multiaxial random loadings: Application to the carpinteri–spagnoli–vantadori spectral method," *Fatigue fracture of engineering materials structures*, vol. 43, no. 9, pp. 1978–1993, 2020. [Pages 6 and 51.]

[13] J. Klemenc and B. Podgornik, "An improved model for predicting the scattered s-n curves," *Journal of Mechanical Engineering*, pp. 265–275, 05 2019. doi: 10.5545/sv-jme.2018.5918 [Pages x, 7, and 63.]

[14] A. F. Hobbacher, *Recommendations for Fatigue Design of Welded Joints and Components*. Springer Cham, 01 2016, vol. IIW Collection. ISBN 978-3-319-79530-0 [Pages 7 and 63.]

[15] L. Susmel and P. Lazzarin, "A bi-parametric wöhler curve for high cycle multiaxial fatigue assessment," *Fatigue & Fracture of Engineering Materials & Structures*, vol. 25, no. 1, pp. 63–78, 2002. doi: https://doi.org/10.1046/j.1460-2695.2002.00462.x. [Online]. Available: https://onlinelibrary.wiley.com/doi/abs/10.1046/j.1460-2695.2002.00462.x [Pages 7, 39, 51, and 62.]

[16] D. O. DEFENSE, *Military Specification MIL-STD-810F*. TEST METHOD STANDARD ENVIRONMENTAL ENGINEERING CONSIDERATIONS AND LABORATORY TESTS, revision F, January 2000. [Pages x, 7, 85, and 88.]

[17] A. Einstein, "On the movement of small particles suspended in stationary liquids required by the molecular-kinetic theory of heat," *Annalen der Physik*, pp. 549–560, 1905. [Page 11.]

[18] S. O. Rice, "Mathematical analysis of random noise," *The Bell System Technical Journal*, vol. 24, no. 1, pp. 46–156, 1945. doi: 10.1002/j.1538-7305.1945.tb00453.x [Pages 11, 22, and 25.]

[19] C. Lalanne, *Random vibration*, third edition. ed., ser. Mechanical Vibration and Shock Analysis ; Volume 3. London, England ;: ISTE Ltd, 2014 - 2014. ISBN 1-5231-1093-7 [Pages ix, 12, 13, 14, 15, and 28.]

[20] J. W. Cooley and J. W. Tukey, "An algorithm for the machine calculation of complex fourier series," *Mathematics of Computation*, vol. 19, no. 90, pp. pp. 297–301, 1965. [Online]. Available: http://www.jstor.org/stable/2003354 [Page 22.]

[21] A. Carpinteri, A. Spagnoli, and S. Vantadori, "Reformulation in the frequency domain of a critical plane-based multiaxial fatigue criterion," *International Journal of Fatigue*, vol. 67, pp. 55–61, 2014. doi: https://doi.org/10.1016/j.ijfatigue.2014.01.008 Multiaxial Fatigue 2013. [Online]. Available: https://www.sciencedirect.com/science/article/pii/S0142112314000097 [Pages ix, 26, and 27.]

[22] D. BENASCIUTTI and R. TOVO, "Frequency-based fatigue analysis of non-stationary switching random loads," *Fatigue & Fracture of Engineering Materials & Structures*, vol. 30, no. 11, pp. 1016–1029, 2007. doi: https://doi.org/10.1111/j.1460-2695.2007.01171.x. [Online]. Available: https://onlinelibrary.wiley.com/doi/abs/10.1111/j.1460-2695.2007.01171.x [Pages 33 and 107.]

[23] D. Benasciutti and R. Tovo, "Frequency-based analysis of random fatigue loads: Models, hypotheses, reality," *Materialwissenschaft und Werkstofftechnik*, vol. 49, no. 3, pp. 345–367, 2018. [Page 34.]

[24] T. Dirlik, "Application of computers in fatigue analysis," Ph.D. dissertation, University of Warwick, 1985. [Page 36.]

[25] D. Benasciutti and R. Tovo, "Spectral methods for lifetime prediction under wide-band stationary random processes," *International journal of fatigue*, vol. 27, no. 8, pp. 867–877, 2005. [Pages 36, 59, and 61.]

[26] A. Niesłony, "Comparison of some selected multiaxial fatigue failure criteria dedicated for spectral method," *Journal of Theoretical and Applied Mechanics*, vol. 48, pp. 233–254, 01 2010. [Page 37.]

[27] J. Lemaitre and R. Desmorat, *Engineering Damage Mechanics. Ductile, Creep, Fatigue and Brittle Failure*, 01 2005. [Page 38.]

[28] D. Benasciutti, F. Sherratt, and A. Cristofori, "Recent developments in frequency domain multi-axial fatigue analysis," *International Journal of Fatigue*, vol. 91, pp. 397–413, 2016. doi: https://doi.org/10.1016/j.ijfatigue.2016.04.012 Variable Amplitude Loading. [Online]. Available: https://www.sciencedirect.com/science/article/pii/S0142112316300603 [Pages ix, 45, and 50.]

[29] A. Carpinteri, A. Spagnoli, and S. Vantadori, "Reformulation in the frequency domain of a critical plane-based multiaxial fatigue criterion," *International Journal of Fatigue*, vol. 67, pp. 55–61, 2014. doi: https://doi.org/10.1016/j.ijfatigue.2014.01.008 Multiaxial Fatigue 2013. [Online]. Available: https://www.sciencedirect.com/science/article/pii/S0142112314000097 [Pages x, 51, and 52.]

[30] L. SUSMEL, R. TOVO, and D. BENASCIUTTI, "A novel engineering method based on the critical plane concept to estimate the lifetime of weldments subjected to variable amplitude multiaxial fatigue loading," *Fatigue & Fracture of Engineering Materials & Structures*, vol. 32, no. 5, pp. 441–459, 2009. doi: https://doi.org/10.1111/j.1460-2695.2009.01349.x. [Online]. Available: https://onlinelibrary.wiley.com/doi/abs/10.1111/j.1460-2695.2009.01349.x [Page 51.]

[31] P. H. Wirsching and A. M. Shehata, "Fatigue Under Wide Band Random Stresses Using the Rain-Flow Method," *Journal of Engineering Materials and Technology*, vol. 99, no. 3, pp. 205–211, 07 1977. doi: 10.1115/1.3443520. [Online]. Available: https://doi.org/10.1115/1.3443520 [Page 55.]

[32] P. H. Wirsching and M. C. Light, "Fatigue under wide band random stresses," *Journal of the Structural Division*, vol. 106, no. 7, pp.

1593–1607, 1980. doi: 10.1061/JSDEAG.0005477. [Online]. Available: https://ascelibrary.org/doi/abs/10.1061/JSDEAG.0005477 [Page 57.]

[33] A. Yaich, A. El Hami, L. Walha, and M. Haddar, "Local multiaxial fatigue damage estimation for structures under random vibrations," *Finite Elements in Analysis and Design*, vol. 132, pp. 1–7, 2017. doi: https://doi.org/10.1016/j.finel.2017.04.003. [Online]. Available: https://www.sciencedirect.com/science/article/pii/S0168874X16302840 [Pages x and 82.]

[34] X. Pitoiset, "M´ethodes spectrales pour une analyse en fatigue des structures m´etalliques sous chargements al´eatoires multiaxiaux," Master's thesis, Universite´ Libre de Bruxelles, Faculte´ des Siences Applique´es, March 2001. [Pages xi and 99.]

[35] M. Bonte, A. de Boer, and R. Liebregts, "Determining the von mises stress power spectral density for frequency domain fatigue analysis including out-of-phase stress components," *Journal of Sound and Vibration*, vol. 302, no. 1, pp. 379–386, 2007. doi: https://doi.org/10.1016/j.jsv.2006.11.025. [Online]. Available: https://www.sciencedirect.com/science/article/pii/S0022460X06008753 [Page 106.]

[36] D. Benasciutti and R. Tovo, "Cycle distribution and fatigue damage assessment in broad-band non-gaussian random processes," *Probabilistic Engineering Mechanics*, vol. 20, no. 2, pp. 115–127, 2005. doi: https://doi.org/10.1016/j.probengmech.2004.11.001. [Online]. Available: https://www.sciencedirect.com/science/article/pii/S0266892004000712 [Page 107.]

[37] M. Aykan and M. Çelik, "Vibration fatigue analysis and multiaxial effect in testing of aerospace structures," *Mechanical Systems and Signal Processing*, vol. 23, no. 3, pp. 897–907, 2009. doi: https://doi.org/10.1016/j.ymssp.2008.08.006. [Online]. Available: https://www.sciencedirect.com/science/article/pii/S0888327008002069 [Page 107.]

[38] A. Angeli, B. Cornelis, and M. Troncossi, "Fatigue damage spectrum calculation in a mission synthesis procedure for sine-on-random excitations," *Journal of physics. Conference series*, vol. 744, no. 1, pp. 12 089–, 2016. [Page 108.]

Appendix A

Supporting material

A.1 Gaussian and Rayleigh distribution

The instantaneous values of a Gaussian random process $l(t)$ follows the PDF in Eq. A.1, where m is the mean value (generally zero in the case of vibratory phenomena) and s is the standard deviation.

$$p(l) = \frac{1}{s\sqrt{2\pi}} exp\left(-\frac{[l(t)-m]^2}{2s^2}\right) \tag{A.1}$$

The Rayleigh distribution, instead has the PDF in Eq. A.2

$$p(l) = \frac{l}{s^2} e^{-\frac{l(t)^2}{2s^2}} \tag{A.2}$$

A.2 Auto-correlation and Cross-correlation functions

The auto-correlation function for a random process $l(t)^i$ is defined by the Eq. A.3

$$R(t_1, t_1+\tau) = \lim_{\Delta l \to \infty} \frac{1}{N} \sum_i l(t_1)^i l(t_1+\tau)^i = E[l(t_1) l(t_1+\tau)] \tag{A.3}$$

Where N is the number of recordings of a random phenomenon varying with time from 0 to T [$i \in [1, N]$] and $E[\cdot]$ is the mathematical expectation. For a continuous process the auto-correlation function is Eq. A.4

$$R(\tau) = \int_{-\infty}^{\infty} l(t_1) l(t_1 + \tau) p[l(t_1)]\, dl(t_1) \tag{A.4}$$

Given the two processes $l(t)$ and $u(t)$ (for example, the excitation and the response of a mechanical system), the cross-correlation function is the function defined by the Eq. A.5

$$R(t_1, t_1 + \tau)_{lu} = \lim_{\Delta l \to \infty} \frac{1}{N} \sum_i l(t_1)^i u(t_1 + \tau)^i = E[l(t_1) u(t_1 + \tau)] \tag{A.5}$$

If all Δt_i tend towards zero and if $N \to \infty$, the quadratic mean is defined by Eq. A.6 where the RMS value takes into account the totality of the frequencies of the signal.

$$\overline{l^2(t)} = \frac{1}{T} \int_0^T l^2(t)\, dt \tag{A.6}$$

Thus, in the time domain, the auto-correlation function $R_l(\tau)$ of the calculated signal, for a given τ delay, of the product $l(t)l(t + \tau)$ is defined by Eq. A.7

$$R_l(\tau) = E[l(t) l(t + \tau)] = \lim_{T \to \infty} \frac{1}{2T} \int_{-T}^{T} l(t) l(t + \tau)\, dt \tag{A.7}$$

The function $R_l(\tau)$ indicates the influence of the value of l at time t on the value of the function l at time $t + \tau$. If $R_l(\tau)$ tends towards zero quickly when τ becomes large, the random signal probably fluctuates quickly and contains high frequency components.

At the same way it is possible to define the the cross-correlation function between two random functions $l(t)$ and $u(t)$. It is defined by Eq. A.8

$$R_{lu}(\tau) = E[l(t)u(t+\tau)] = \lim_{T\to\infty} \frac{1}{2T} \int_{-T}^{T} l(t)u(t+\tau)\, dt \tag{A.8}$$

The cross-correlation function makes it possible to establish the degree of resemblance between two functions of the same variable (time in general).

A.3 Power spectral density

In vibration mechanics the mean power of an excitation is defined by Eq. A.9. Considering the signal $l(t)$ between $-T/2$ and $+T/2$ by Eq. A.9 where $l_T(t) = l(t)$ for $|t| \leq T/2$ and $l_T(t) = 0$ for $|t| > T/2$

$$P_m = \lim_{T\to\infty} \frac{1}{T} \int_{-T/2}^{+T/2} |l_T(t)|^2\, dt \tag{A.9}$$

the function $l_T(t)$ has as a Fourier transform $L_T(f)$ and according to Parseval's equality

$$\int_{-\infty}^{+\infty} |l_T|^2\, dt \; = \int_{-\infty}^{+\infty} |L_T(f)|^2\, df \tag{A.10}$$

To find the mean power contained in a frequency band Δf it is assumed that the excitation $l(t)$ is applied to a linear system with constant parameters whose weighting function is $h(t)$ and the transfer function is $H(f)$. The response $r_T(t)$ is given by Eq. A.11 where λ is an integration constant.

$$r_T(t) = \int_0^{\infty} h(\lambda) l_T(t-\lambda)\, d\lambda \tag{A.11}$$

The mean power of the response is written by Eq. A.20

$$P_m^{response} = \lim_{T\to\infty} \frac{2}{T} \int_0^T r_T^2(t)\, dt \; = \lim_{T\to\infty} \frac{2}{T} \int_0^T |R_T(f)|^2\, df \tag{A.12}$$

Fourier transform of the two members of Eq. A.11, we can show that Eq. A.13:

$$R_T(f) = H(f) L_t(f) \tag{A.13}$$

yielding to Eq. A.14

$$P_m^{response} = \lim_{T\to\infty} \frac{2}{T} \int_0^{\infty} |H(f)|^2 |L_T(f)|^2 \, df \tag{A.14}$$

If we consider $G_T(f) = \frac{2|L_T(f)|^2}{T}$, the mean power corresponding to the record $l_T(t)$, finite length T, in the band Δf centered on f, is written Eq. A.15 and total mean power through out the record Eq. A.16:

$$P_T(f, \Delta f) = \int_{f-\Delta f/2}^{f-\Delta f/2} G_T(f) \, df \tag{A.15}$$

$$P_T(f, \Delta f) = \lim_{T\to\infty} \int_{f-\Delta f/2}^{f-\Delta f/2} G_T(f) \, df \tag{A.16}$$

A.4 Wiener-Khinchine relations

It is shown that, for a stationary process Eq. A.17

$$G(f) = 2 \int_{-\infty}^{+\infty} R(\tau) e^{-2\pi i f \tau} \, d\tau \tag{A.17}$$

$R(\tau)$ being an even function of τ, we obtain Eq. A.18 :

$$G(f) = 4 \int_0^{+\infty} R(\tau) cos(-2\pi f \tau) \, d\tau \tag{A.18}$$

If we take the inverse transform of $G(f)$ the Eq. A.17 becomes Eq. A.19 and $R(0) = \overline{l^2(t)} = \int_0^{+\infty} G(f) \, df \ = (RMS \ value)^2$

$$R(\tau) = \frac{1}{2} \int_{-\infty}^{+\infty} G(f) e^{2\pi i f \tau} \, df \ = \int_0^{+\infty} G(f) cos(2\pi f \tau) \, df \tag{A.19}$$

These relations are called “Wiener-Khinchine relations”.

Considering one signal sample ${}^i l(t)$, the relation between the PSD of the excitation and the response of a linear system is:

$${}^i u(t) = \int_0^{\infty} h(\lambda) {}^i l(t - \lambda) \, d\lambda \tag{A.20}$$

yielding to Eq. A.21

$$^{i}u(t_1)^{i}u(t_2) = \int_0^\infty \int_0^\infty h(\lambda)h(\mu)^{i}l(t_1-\lambda)^{i}l(t_2-\mu)\,d\lambda d\mu \tag{A.21}$$

and hence Eq. A.22

$$R_u(t_1,t_2) = E[u(t_1)u(t_2)] = \int_0^\infty \int_0^\infty h(\lambda)h(\mu)R_l(t_1-\lambda,t_2-\mu)\,d\lambda d\mu \tag{A.22}$$

Example of a stationary process $R_u(t_1,t_2) = R_u(0,t_1-t_2) = R_u(t_1-t_2) = R_u(\tau)$ and $R_u(\tau) = \int_0^\infty \int_0^\infty h(\lambda)h(\mu)R_l(\tau,\lambda-\mu)\,d\lambda d\mu$

A.5 Transfer functions

Consider a stationary random vibration $s(t)$ applied to a linear mechanical system and its response $v(t)$. In the absence of noise on the input and on the response, measures $l(t)$ and $u(t)$ of these signals are identical to $s(t)$ and $v(t)$ respectively. Their Fourier transforms are linked by $U(f) = H(f)L(f)$ where $H(f)$ of the transfer function of the system. We will square each member of this equation: $U^*(f)U(f) = H(f)^*H(f)L^*(f)L(f)$ or according to the autospectrum definition, $G_{uu}(f) = |H(f)|^2 G_{ll}(f)$, a first expression of the transfer function, which we will call $H_1(f)$ defined by Eq. A.23, where $H_1(f)$ contains no information on the phase :

$$H_1(f) = \sqrt{\frac{G_{uu}(f)}{G_{ll}(f)}} \tag{A.23}$$

Going back and multiplying its two members by the conjugate Fourier transform of $L(f)$, $L^*(f)U(f) = H(f)L^*(f)L(f)$ or, according to the PSD definition (autospectrum and cross-power spectral density): $G_{lu}(f) = H(f)G_{ll}(f)$ yielding a second expression $H_2(f)$ of the transfer function Eq. A.24:

$$H_2(f) = \frac{G_{lu}(f)}{G_{ll}(f)} \tag{A.24}$$

Finally, multiply both sides of relation by the conjugate $U^*(f)$ of $U(f)$. It becomes $U^*(f)U(f) = H(f)U^*(f)L(f)$ and $G_{uu}(f) = H(f)G_{ul}(f)$.

Yielding the last expression of $H_3(f)$ Eq. A.25:

$$H_3(f) = \frac{G_{uu}(f)}{G_{ul}(f)} \tag{A.25}$$

These three conditions are theoretically similar as long as: (i) signals $l(t)$ and $u(t)$ have no noise; (ii) there is no other vibration source contributing to the response $u(t)$; (iii) PSDs are calculated with a very low statistical error.

The derivative of the auto-correlation function of a derivable process is: (i) continuous and derivable at any point; (ii) even. It is thus canceled for $\tau = 0$, yielding $E[l\dot{l}] = 0$ There is no correlation between a stationary process $l(t)$ and the derivative $\dot{l}(t)$ (whatever the distribution law). The auto-correlation functions of the derivative processes of $l(t)$ depend only on τ and the derivatives of a stationary process are stationary functions. However, the integral of a stationary function is not necessarily stationary. The result obtained shows the existence of a transfer function $H(\Omega)$ between $l(t)$ and its derivatives Eq.A.26 A.27 where $H(\Omega) = i\Omega$

$$S_{\dot{l}}(\Omega) = \mid H(\Omega) \mid^2 S_l(\Omega) \tag{A.26}$$

$$S_{\ddot{l}}(\Omega) = \mid H(\Omega) \mid^4 S_l(\Omega) \tag{A.27}$$